NEUROVIRULENCE VARIATION AMONG THE TWO GENOTYPES OF CHIKUNGUNYA VIRUS IN MALAYSIA

CHIAM CHUN WEI

FACULTY OF MEDICINE
UNIVERSITY OF MALAYA
KUALA LUMPUR

2015

NEUROVIRULENCE VARIATION AMONG THE TWO GENOTYPES OF CHIKUNGUNYA VIRUS IN MALAYSIA

CHIAM CHUN WEI

THESIS SUBMITTED IN FULFILMENT OF THE REQUIREMENTS FOR THE DEGREE OF DOCTOR OF PHILOSOPHY

FACULTY OF MEDICINE
UNIVERSITY OF MALAYA
KUALA LUMPUR

2015

UNIVERSITI MALAYA

ORIGINAL LITERARY WORK DECLARATION

Name of Candidate: **CHIAM CHUN WEI**

Registration/Matric No: **MHA110062**

Name of Degree: **Doctor of Philosophy**

Title of ~~Project Paper/Research Report/Dissertation/~~Thesis ("this Work"):

Neurovirulence variation among the two genotypes of chikungunya virus in Malaysia

Field of Study: **Medical Microbiology**

I do solemnly and sincerely declare that:

(1) I am the sole author/writer of this Work;
(2) This Work is original;
(3) Any use of any work in which copyright exists was done by way of fair dealing and for permitted purposes and any excerpt or extract from, or reference to or reproduction of any copyright work has been disclosed expressly and sufficiently and the title of the Work and its authorship have been acknowledged in this Work;
(4) I do not have any actual knowledge nor do I ought reasonably to know that the making of this Work constitutes an infringement of any copyright work;
(5) I hereby assign all and every rights in the copyright to this Work to the University of Malaya ("UM"), who henceforth shall be owner of the copyright in this Work and that any reproduction or use in any form or by any means whatsoever is prohibited without the written consent of UM having been first had and obtained;
(6) I am fully aware that if in the course of making this Work I have infringed any copyright whether intentionally or otherwise, I may be subject to legal action or any other action as may be determined by UM.

Candidate's Signature Date

Subscribed and solemnly declared before,

Witness's Signature Date

Name:
Designation:

ABSTRACT

Chikungunya virus (CHIKV), an alphavirus of the family *Togaviridae*, causes fever, polyarthritis, and rash. There are three genotypes: West African, Asian, and East, Central and South African (ECSA). The latter two genotypes have caused outbreaks in Malaysia. Recent ECSA CHIKV outbreaks have been associated with severe neurological disease including encephalitis, meningitis, and acute flaccid paralysis. It is not known if different CHIKV genotypes are associated with different severity of neurological disease. In this study, the neurovirulence of Asian (MY/06/37348) and ECSA (MY/08/065) strains of CHIKV were compared by intracerebral inoculation in suckling mice, followed by virus titration, quantitative real-time PCR, histopathology, and gene expression analysis of the harvested brains. Both genotypes of CHIKV replicated similarly in the brains, yet suckling mice infected with Asian CHIKV showed higher mortality compared to ECSA CHIKV-infected mice and control mice. Histopathologic analysis showed that both CHIKV genotypes were found to spread within the brain (where CHIKV antigen was localised to astrocytes and neurons) and beyond to skeletal muscle. In Asian CHIKV-infected suckling mice, apoptosis and necrosis were observed earlier in brains, and more extensive CHIKV spread and pathologic changes were seen in skeletal muscle. Gene expression analysis showed that pro-apoptotic genes (eIF2αK2) were upregulated at higher levels in Asian CHIKV-infected suckling mice, while genes involved in anti-apoptosis (BIRC3) and antiviral responses and CNS protection (CD40, IL-10RA, MyD88, and PYCARD) were upregulated more highly in ECSA CHIKV-infected suckling mice. In conclusion, these findings suggest that the higher mortality observed following Asian CHIKV infection in mice is not due to higher viral replication in the brain as there was more spread in muscle and due to differentially expressed genes involved in antiviral activity and CNS

protection. Further studies could focus on the differences in viral sequences encoding neurovirulence determinants. This information on important host responses may be used for development of therapeutic and prophylactic strategies against CHIKV infection, and identification of biomarkers for neurological CHIKV infections.

ABSTRAK

Virus chikungunya (CHIKV) adalah alphavirus daripada famili *Togaviridae* yang boleh menyebabkan demam, poliartritis, dan ruam. Terdapat tiga jenis genotip: "West African", "Asian", and "East, Central, dan South African (ECSA)". Dua genotip terakhir telah menyebabkan wabak di Malaysia. Wabak CHIKV baru-baru ini telah dikaitkan dengan komplikasi neurologikal seperti ensefalitis, meningitis, dan lumpuh. Ia belum dipastikan sama ada keterukan neurovirulen berkait rapat dengan genotip CHIKV yang berlainan. Dalam kajian ini, kesan neurovirulen CHIKV "Asian" (MY/06/37348) dan "ECSA" (MY/08/065) dibandingkan melalui inokulasi intraserebrum pada anak tikus, diikuti dengan pentitratan virus, kuantifikasi PCR segera, histopatologi, dan analisis ekspresi gen pada otak anak tikus. Replikasi kedua-dua genotip adalah sama di otak, tetapi anak tikus yang dijangkiti CHIKV "Asian" menunjukkan mortaliti yang tinggi berbanding anak tikus yang dijangkiti CHIKV "ECSA" dan yang tidak dijangkiti. Analisis histopatologi menunjukkan kedua-dua genotip CHIKV merebak di otak (antigen CHIKV dikesan di astrosit dan neuron) sehingga ke otot rangka. Tikus yang dijangkiti CHIKV "Asian" menunjukkan apoptosis dan nekrosis di otak dalam peringkat awal. CHIKV merebak dan perubahan patologi dikesan di otot rangka. Analisis gen ekspresi menunjukkan regulasi gen pro-apoptosis (eIF2αK2) meningkatkan regulasinya di tikus yang dijangkiti CHIKV "Asian" manakala gen yang terlibat dalam anti-apoptosis (BIRC3) dan proses antivirus dan perlindungan sistem saraf tunjang (CD40, IL-10RA, MyD88, dan PYCARD) meningkatkan regulasinya di tikus yang dijangkiti CHIKV "ECSA". Kesimpulannya, penemuan kajian ini menunjukkan bahawa mortaliti yang tinggi pada tikus yang dijangkiti CHIKV "Asian" bukan disebabkan oleh replikasi virus yang tinggi di otak, tetapi disebabkan oleh jangkitan di otot dan perbezaan ekspresi gen yang terlibat dalam aktiviti antivirus dan perlindungan sistem saraf tunjang

tikus. Kajian selanjutnya boleh ditumpukan pada kelainan urutan virus dalam pengekodan penentu neurovirulen. Maklumat ini penting untuk pembangunan terapi dan strategi profilaktik terhadap jangkitan CHIKV, dan mengenalpasti penanda bio untuk jangkitan neurologikal CHIKV.

ACKNOWLEDGEMENTS

I would like to express my sincere thanks and appreciation to the following people for their contributions during this study. First of all, I would like to thank Prof. Dr. Jamal I-Ching Sam and Assoc. Prof. Dr. Chan Yoke Fun for their supervision, advice, support, and guidance throughout the last five years.

I would like to extend my gratitude to lab members (Loong Shih Keng, Chan Shie Yien, Khor Chee Sieng, Chua Chong Long, Tan Chee Wah, Jeffrey Lai Kam Fatt, Jasmine Michael, Aw Yong Kam Leng, Nik Nadia bt. Nik Mohd. Nasir, Wong Hui Vern, Tee Han Kang) for their generosity and willingness in providing help and sharing of knowledge. Special thanks to other research team members, Prof. Dr. Wong Kum Thong and Dr. Ong Kien Chai as well as the staff of Department of Medical Microbiology and Medical Biotechnology Laboratory of Faculty of Medicine, INFRA Analysis Laboratory of Centre for Research Services, and Diagnostic Virology Laboratory of University Malaya Medical Centre for their technical assistance.

I would also like to thank the National Science Foundation, Ministry of Science, Technology and Innovation, and Institute of Graduate Studies, University Malaya for their financial support throughout the years of my candidature.

Finally, I also would like to mention credits to my family as well as fellow friends for their endless support and encouragement through this difficult and challenging period.

TABLE OF CONTENTS

LIST OF FIGURES

LIST OF TABLES

LIST OF SYMBOLS AND ABBREVIATIONS

ANOVA	analysis of variance
BBB	blood-brain barrier
BCL-2	B-cell lymphoma 2
BIRC3	baculoviral IAP repeat containing 3
Casp	caspase
CatS	cathepsin S
cDNA	complementary DNA
CHIKV	chikungunya virus
CNS	central nervous system
CPE	cytopathic effect
cRNA	complementary RNA
CSF1	colony-stimulating factor 1
DAPI	4’6-diamidino-2-phenylindole
DAVID	Database for Annotation,Visualization and Integrated Discovery
DENV	dengue virus
dNTP	deoxyribonucleotide triphosphate
dpi	days post-infection
ECSA	East, Central and South African
EEEV	Eastern equine encephalitis virus
Eff%	amplification efficiency
EMEM	Eagle’s minimal essential medium
eIF2αK2	eukaryotic translation initiation factor, alpha subunit kinase 2
FBS	foetal bovine serum
FITC	fluorescein isothiocynate
FOS	FBJ osteosarcoma oncogene
GFAP	glial fibrillary acidic protein
GM-CSF	granulocyte macrophage colony-stimulating factor
hpi	hours post-infection
HRP	horseradish peroxidase
IκB	I kappa B
IF	immunofluorescence
IFN	interferon

Ig	immunoglobulin
IL	interleukin
IPS-1	interferon promoter stimulator 1
IPTG	isopropyl β-D-1-thiogalactopyranoside
IRF	interferon regulatory factor
IRGM1	immune-related GTPase family M member 1
ISG	interferon-stimulated gene
Jak	Janus kinase
Jak-STAT	Janus kinase-signal transducers and activators of transcription
JEV	Japanese encephalitis virus
KEGG	Kyoto Encyclopedia of Genes and Genomes
LB	Luria-Bertani
LOQ	limit of quantification
MAP-2	microtubule-associated protein 2
MDA5	melanoma differentiation-associated gene 5
MHC	major histocompatibility complex
MyD88	myeloid differentiation primary response 88
NEAA	non-essential amino acids
NF-κB	nuclear factor kappa-light-chain-enhancer of activated B-cell
NHP	non-human primate
NLR	NOD-like receptor family protein
NLRP	NLR family pyrin domain-containing protein
NOD	nucleotide-binding oligomerization domain
OAS	2',5'-oligoadenylate synthetase
ONNV	O'nyong-nyong virus
ORF	open reading frame
PAMP	pathogen-associated molecular pattern
PBS	phosphate buffered saline
PCR	polymerase chain reaction
PI3K-Akt	phosphoinositide-3-kinase protein kinase B
PKR	protein kinase R
PYCARD	PYD and CARD domain containing
qRT-PCR	quantitative real-time polymerase chain reaction
R^2	correlation coefficient
RIG-I	retinoic acid-inducible gene I

RNase	ribonuclease
RRV	Ross River virus
RT-PCR	reverse transcriptase polymerase chain reaction
SFM	serum-free media
SFV	Semliki Forest virus
SINV	Sindbis virus
STAT	signal transducers and activators of transcription
TBS	tris-buffered saline
$TCID_{50}$	50% of tissue culture infectious dose
TLR	Toll-like receptor
TNF-α	tumor necrosis factor-α
TRAF	tumor necrosis factor receptor-associated factor
VEEV	Venezuelan equine encephalitis virus
WEEV	Western equine encephalitis virus
WNV	West Nile virus

LIST OF APPENDICES

CHAPTER 1

INTRODUCTION

Chikungunya fever was first described by Robinson (1955) after the 1952 viral epidemic in Tanzania (formerly Tanganyika). Chikungunya virus (CHIKV) was later isolated by Ross (1956). Chikungunya derives its name from the Makonde word kungunyala, which means "that which bends up" in reference to the stooped appearance of patients with debilitating and prolonged arthralgia that may persist for months (Robinson, 1955; de Ranitz *et al.*, 1965).

CHIKV, which is under the genus *Alphavirus* of the family *Togaviridae*, is transmitted to humans by *Aedes* mosquitoes. It is grouped antigenically within the Semliki Forest virus complex, and together with Sindbis virus (SINV) and Semliki Forest virus (SFV) are also known as Old World alphaviruses. CHIKV is an enveloped, single-stranded, linear, positive-sense RNA virus with a genome size of approximately 11.8 kb (Strauss and Strauss, 1994; Powers and Logue, 2007). There are three known genotypes: the West African, East, Central and South African (ECSA), and Asian genotypes.

The first two confirmed CHIKV outbreaks in Malaysia occurred in 1998 and 2006, and were due to the Asian genotype, while the third outbreak at the end of 2006 was caused by the ECSA genotype (Sam and AbuBakar, 2006; AbuBakar *et al.*, 2007). The recent 2008-2010 outbreak in Malaysia was of the ECSA genotype and affected over 10,000 people (Sam *et al.*, 2009). Compared to the limited nature of the first three outbreaks, this recent nationwide outbreak was postulated to be due to the presence of an A226V mutation in the E1 protein, which enhanced replication, infectivity, and dissemination efficiency of CHIKV in *Ae. albopictus* (Tsetsarkin *et al.*, 2007). This mutation has

independently arisen in Réunion and India since 2005 (Schuffenecker *et al*., 2006; de Lamballerie *et al*., 2008).

CHIKV produces dengue-like illness in humans, causing fever, polyarthritis, and rash (Robinson, 1955; de Ranitz *et al*., 1965). Recently, some studies have reported fatal CHIKV cases and neurological complications including encephalitis, encephalopathy, and meningitis (Rampal *et al.*, 2007; Robin *et al.*, 2008; Economopoulou *et al.*, 2009). Encephalopathy appears to be a common clinical manifestation in newborns infected through the mother-to-child route (Arpino *et al*., 2009; Couderc and Lecuit, 2009).

CHIKV infection is found to be age-dependent in mice, as adult mice are resistant, while neonates are particularly susceptible to severe infection (Couderc *et al.*, 2008). Ziegler *et al.* (2008) showed that in suckling mice, the virus entered the brain and replicated, and was cleared after ten days. In adult mice, the virus only replicated for a brief period of 1 to 2 days before clearance. Age-dependent susceptibility to severe central nervous system (CNS) infection has also been observed with other alphaviruses such as SFV, Ross River virus (RRV), and SINV (Fleming, 1977; Ryman *et al.*, 2007b).

In alphaviruses, variation of virulence due to different genotypes and within specific genotypes may result in different susceptibility, disease severity, and mortality in mice, similar to those observed in SFV (Fleming, 1977; Balluz *et al.*, 1993), SINV (Tucker *et al.*, 1993; Ubol *et al.*, 1994), Venezuelan equine encephalitis virus (VEEV) (Calisher and Maness, 1974), and Western equine encephalitis virus (WEEV) (Nagata *et al.*, 2006; Logue *et al*., 2009). Some alphaviruses such as SFV clearly show neurotropism for brain endothelium and neurons (Fazakerley, 2002).

An *in vitro* study in 1972 by Nakao found that there were few biological and immunological differences between African and Asian genotypes of CHIKV. This is of particular importance in Malaysia, where both Asian and ECSA genotypes are circulating, but differences in neurovirulence have not been determined.

The nature of CHIKV neurotropism in the CNS remains controversial. CHIKV was reported to infect the cerebral cortex and spinal cord of suckling mice, causing necrosis in the endoplasmic reticulum of neurons and glial cells (White, 1969). Couderc *et al*. (2008) showed that CHIKV spreads through the choroid plexus before infecting ependymal and leptomeningeal cells, but no infection was shown in brain microvessels and parenchyma. Das *et al.* (2010) reported CHIKV infection in glial cells, such as astrocytes and oligodendrocytes.

Neurological complications may be due to direct viral invasion or immunopathological damage resulting from cellular responses of the host. Little is known about the immune and cellular mechanisms involved in CNS pathology due to CHIKV infection of different genotypes. Thus, to address these uncertainties, different strains of CHIKV were used to infect mice, and to determine age-dependency, neurotropism, neurovirulence, and finally, to identify host neuronal immune responses that could lead to better understanding of neuropathogenesis.

CHAPTER 2

LITERATURE REVIEW

2.1 Alphaviruses

The genus *Alphavirus* belongs to the family of *Togaviridae*. Alphaviruses can be classified antigenically into eight complexes: Barmah Forest, Middelburg, Ndumu, Trocara, Semliki Forest, Eastern equine encephalitis, Venezuelan equine encephalitis, and Western equine encephalitis (Griffin, 2007).

CHIKV is classified under the Semliki Forest virus complex, which includes O'nyong-nyong virus (ONNV), RRV, SFV, Getah virus, Bebaru virus, and Mayaro virus. Generally, alphaviruses can also be classified into Old World or New World alphaviruses, depending on their geographic distribution. Old World alphaviruses, which include CHIKV, SFV, SINV, ONNV, and RRV predominantly cause polyarthralgia. The New World alphaviruses, such as VEEV and WEEV, often cause encephalitis (Solignat *et al.*, 2009).

2.2 Chikungunya virus

CHIKV is a spherical, enveloped, linear, plus-sense single-stranded RNA virus with icosahedral symmetry, and diameter of 60-70 nm. The virion, containing an RNA genome of approximately 11.8 kb, is arranged as an icosahedron with a triangulation number of four (T = 4 symmetry) (Simizu *et al.*, 1984). To date, three genotypes have been identified: West African, ECSA, and Asian.

The genome is encapsulated in an icosahedral protein shell, forming a nucleocapsid. The icosahedral protein shell is composed of the capsid protein, followed by the outer lipid bilayer, known as the virion envelope. The virion envelope is derived from host-cell plasma membrane which is augmented with cholesterol and sphingolipid. The molecules are essential for viral entry and budding. The virion envelope also consists of 240 copies of E1-E2 glycoprotein heterodimers that are grouped as trimers, forming 80 transmembrane "knobs" of trimers.

The RNA has two open reading frames (ORF) encoding four non-structural proteins (nsP1, nsP2, nsP3, and nsP4), and five structural proteins (capsid (C), E3, E2, 6K, and E1). The ORF is flanked by a non-translated region with a 7-methylguanosine cap at the 5' end and a polyadenylated non-translated region at the 3' end. The genomic organization is: 5' C-nsP1-nsP2-nsP3-nsP4-(junction region)-C-E3-E2-6K-E1-poly(A) 3' (Khan *et al.*, 2002).

2.3 CHIKV proteins

The CHIKV structural protein genes form the virion, while the non-structural proteins are involved in virus replication and pathogenesis (Figure 2.1).

2.3.1 Structural proteins

The structural ORF encodes for capsid protein and envelope glycoproteins in the cytoplasm of the host cell. The capsid protein is assembled with viral nucleic acid to form the nucleocapsid, which is divided into the outer capsid protein region, and the inner region consisting of protein and RNA. The capsid protein of the New World alphaviruses enters the nucleus to interfere with host cell gene transcription (Aguilar *et al.*, 2007; Garmashova *et al.*, 2007).

Furin cleavage of pE2 produces E2 glycoprotein, a long, glycosylated thin molecule that extends into the nucleocapsid and is involved in receptor binding. Attachment is followed by receptor-mediated endocytosis, forming an endosome during virion entry into the host cell.

E1 is also glycosylated and is anchored at the base of each surface spike, forming a lattice on the virus surface. During early viral infection, E1 glycoprotein is responsible for fusion of viral envelope and host plasma membrane. Surface proteins of the endosome convert into ion-permeable fusion pores during the late endosome stage, allowing the release of nucleocapsid into host cell cytoplasm.

The E3 glycoprotein is also cleaved out from pE2 by furin. E3 glycoprotein can be found between the petals of the E1-E2 spike resulting in a dual-lobed petal. During viral

replication, E3 stabilizes the pE2-E1 complex as it moves from the mildly acidic environment of the Golgi to the site of budding.

6K is a small polypeptide cleaved by signalase from the translated p130 polyprotein and then incorporated into virions in small numbers (7 to 30 copies). This protein interacts with E2 and E1 glycoproteins, and has been associated with the budding process and virion formation. The importance of the 6K protein in transport and assembly remains unclear, though it may have an essential role in the structure of alphavirus particles.

2.3.2 Non-structural proteins

The non-structural ORF encodes proteins for viral RNA transcription and replication, polyprotein cleavage, and RNA capping in the cytoplasm of the host cell.

The nsP1 protein possesses guanine-7-methyltransferase and guanyltransferase enzymatic activities which are essential in capping and cap methylation of newly synthesized viral genomic and subgenomic RNA. Due to the mediation of cysteine palmitoylation and a distinct patch of basic and hydrophobic residues within the nsP1, it has been suggested to anchor replication complexes to cellular membranes and specifically initiate or maintain minus-strand replicative intermediates.

The N-terminal domain of nsP2 protein has a helicase activity required for RNA duplex unwinding during RNA replication and transcription. This N-terminal domain also has RNA triphosphatase and nucleoside triphosphatase activity. The C-terminal domain of nsP2 acts as a cysteine protease that cleaves non-structural polyprotein; the enzymatically non-functional methyltransferase domain may be involved in regulation of minus-strand synthesis and development of cellular cytopathic effects. The nsP2

polyprotein is also responsible for *in cis*- and *in trans*-cleavage of nsP3/nsP4 and P123 junctions. In addition, Old World alphaviruses use the nsP2 protein to interfere with host cell gene transcription in the nucleus (Garmashova *et al.*, 2007).

The nsP3 protein is composed of two domains: an N-terminal domain that is highly conserved, and a C-terminal domain that varies in sequence and length according to virus species. The phosphorylated nsP3 protein may play a role in minus-strand and subgenomic RNA synthesis, pathogenesis modulation in mice, and apoptosis induction in infected cells.

The nsP4 protein consists of two domains: a C-terminal domain that maintains the homology of viral RNA-dependent RNA polymerases, and an N-terminal domain that contains a small region which is not conserved. NsP4 has adenylytransferase activity that may aid in maintenance of the viral genomic poly(A) tail.

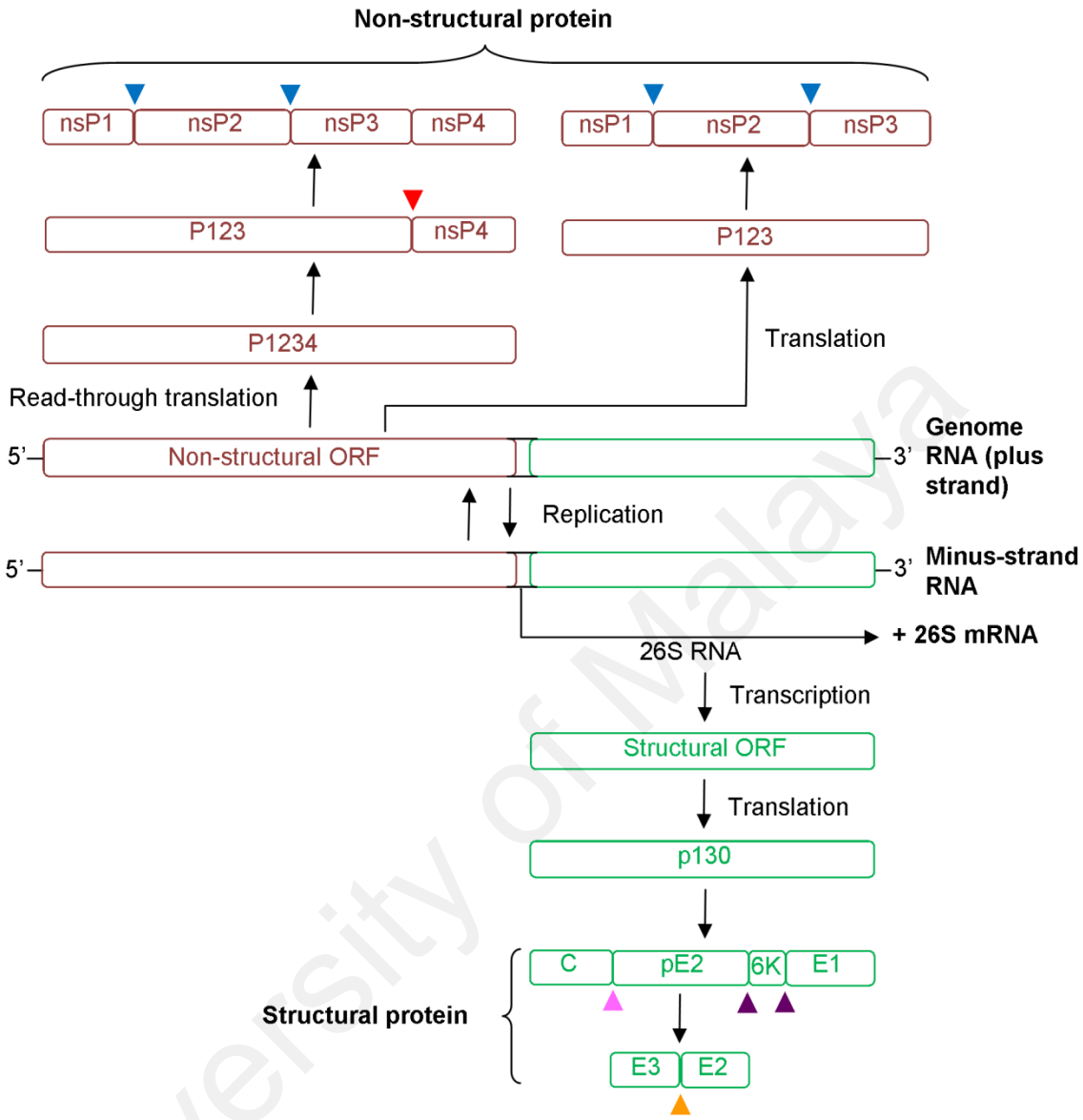

Figure 2.1: CHIKV genome replication and production of viral proteins. A subgenomic positive-strand mRNA referred to as 26S RNA, is transcribed from a negative-strand RNA intermediate and serves as the mRNA for the synthesis of viral structural proteins. The different non-structural proteins (nsP1–nsP4) and structural proteins (C, E1, E2, E3, 6K) are generated after proteolytic cleavage of polyprotein precursors (nsP2 *in cis* cleavage, ▼; nsP2 *in trans* cleavage, ▼; capsid *in trans* cleavage, ▲; signalase cleavage, ▲; furin cleavage, ▲). Figure adapted and modified from Strauss and Strauss (1994) and Solignat *et al.* (2009).

2.4 Replication cycle of chikungunya virus

The CHIKV replication cycle is very similar to that of other alphaviruses, of which SINV and SFV have been the most extensively studied (Figure 2.2; Strauss and Strauss, 1994; Jose *et al.*, 2009). The entry of CHIKV into susceptible cells begins when E2 glycoprotein attaches to host receptors. This causes rearrangement of glycoproteins, and induces receptor-mediated endocytosis and formation of an endosome. When the endosome migrates into the host cell, the internal pH of the vesicle drops, and this destabilizes the E1-E2 heterodimer and exposes the E1 glycoprotein hidden fusion loop at the distal tip. These fusion domains trimerize, and create a fusion pore which combines the viral and phospholipid membranes of the late endosome. This causes the release of the nucleocapsid into host cell cytoplasm. The genomic RNA is released after the nucleocapsid disassembles, following binding to the large ribosomal subunit. Changes of environmental pH during entry may also lead to nucleocapsid disassembly.

The positive genomic RNA first undergoes multiple replications. The non-structural protein ORF either translates into P123 or reads through to translate into P1234. The nsP3/nsP4 junction of read-through translated polyprotein P1234 is cleaved *in cis* by nsP2, producing P123 and nsP4 proteins which form the minus-strand replication complex. As infection proceeds, polyprotein P123 is cleaved *in trans* by nsP2 at the nsP1/nsP2/nsP3 junctions. As a result, the plus-strand replication complex is formed from nsP1, nsP2, and nsP3 proteins, which is involved in synthesis of plus-strand and subgenomic RNA at a later stage of infection (Figure 2.1).

During early infection, minus-strand RNA synthesis predominates as a result of replication of genomic RNA and an effective P123 and nsP4 complex synthesized earlier. This complex is more efficient in synthesis of minus-strand RNA than genomic

RNA. The abundance of P123 is reduced by its cleavage by nsP2, resulting in reduction of minus-strand RNA synthesis as the infection proceeds (Figure 2.1).

Some of the replicated minus-strand RNA is transcribed into subgenomic RNA, which contains the structural protein ORF. This is followed by translation into capsid, pE2, 6K, and E1 proteins. The capsid protein is first cleaved *in trans* and is assembled with viral genomic RNA to form the nucleocapsid, before being transported to the budding site near the plasma membrane. Meanwhile, signalase cleaves at pE2/6K and 6K/E1, the junction of pE2-6K-E1. E1 and pE2 proteins are transported into endoplasmic reticulum to form the pE2-E1 complex, followed by the cleavage of pE2 by furin to form E3 and E2 proteins at the Golgi apparatus. After the glycoproteins undergo processing and maturation, the resultant E1-E2 heterodimer is transported to the phospholipid bilayer membrane of the host cell to form a trimer of heterodimers (Figure 2.1).

Finally, the virion is released when the nucleocapsid buds out, incorporating part of the phospholipid host membrane with the E1-E2 glycoproteins. The phospholipid bilayer membrane of the host cell becomes the CHIKV virion envelope, while the E1-E2 trimers form the 80 transmembrane glycoproteins spikes (Jose *et al.*, 2009; Solignat *et al.*, 2009).

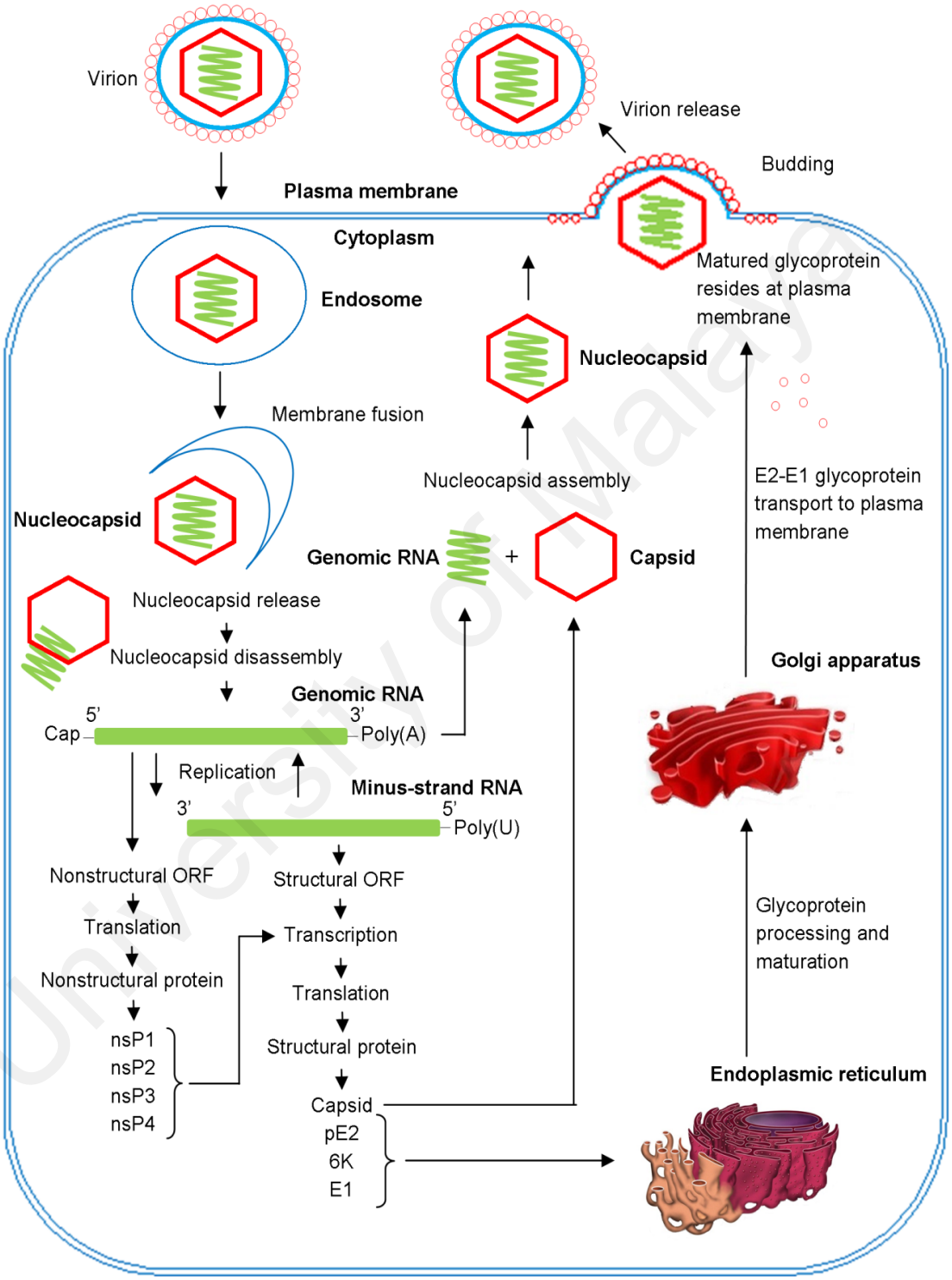

Figure 2.2, continued: The replication cycle of CHIKV. CHIKV first attaches to the cellular receptor before receptor-mediated endocytosis. This is followed by membrane fusion of the endosome, nucleocapsid release and disassembly, and genomic RNA release. The genomic RNA undergoes replication and translation. The translated proteins except capsid are translocated across the endoplasmic reticulum and Golgi apparatus for processing and maturation before transport to the plasma membrane. The replicated genomic RNA and translated capsid are assembled to produce nucleocapsid, which later incorporates glycoproteins at the plasma membrane, before budding as a complete virion. Figure adapted and modified from Jose *et al.* (2009) and Solignat *et al.* (2009).

2.5 Epidemiology

After the first epidemiological study of a CHIKV epidemic in 1952 by Lumsden (1955), sporadic epidemics took place in Africa and Asia over the following few decades. The period between outbreaks can range from several years to a few decades. In Africa, CHIKV epidemics occurred in Tanzania, Uganda, and Zimbabwe in the 1950s. The Asian genotype was isolated in Bangkok, Thailand in 1958 (Hammon *et al.*, 1960). Before the 2005 outbreak, transmission of the Asian genotype was seen in Asian countries, including India, the Philippines, Cambodia, Vietnam, Laos, Myanmar, Malaysia, and Indonesia. The worldwide CHIKV epidemics in 2005 were caused by the ECSA genotype, started in East Africa, and spread quickly across the Indian Ocean islands, India, and Southeast Asian countries over the next few years (Figure 2.3; Pulmanausahakul *et al.*, 2011; Thiberville *et al.*, 2013; Weaver, 2014). CHIKV cases were also reported in Europe (Parola *et al.*, 2006; Panning *et al.*, 2008), Taiwan (Huang *et al.*, 2009), and USA (Lanciotti *et al.*, 2007) due to travellers returning from outbreak regions. Autochthonous transmission was also reported for the first time in Europe in Italy (Rezza *et al.*, 2007).

An A226V mutation in the E1 glycoprotein likely made a major contribution to the widespread outbreaks from 2005. This mutation arose independently in La Réunion Island and India (Schuffenecker *et al.*, 2006; de Lamballerie *et al.*, 2008). The mutation enhances replication, infectivity, and dissemination efficiency of CHIKV in the vector *Ae. albopictus* (Tsetsarkin *et al.*, 2007). However, the recent 2013 outbreaks in the Americas were found to be due to the Asian genotype (Leparc-Goffart *et al*., 2014). Although both *Ae.* species are present in the Americas, *Ae. aegypti* may play the major role in transmission because the Asian genotype more efficiently infects *Ae. aegypti* than *Ae. albopictus* (Das *et al.*, 2010; Weaver, 2014).

CHIKV transmission in Africa circulates in natural sylvatic cycles between mosquitoes (*Ae. africanus, Ae. furcifer-taylori, Ae. luteocephalus, Mansonia sp.* and *Culex. sp*.) and non-human primates (NHPs; baboons and *Cercopithecus* monkeys) which act as reservoirs (Diallo *et al.*, 2012). CHIKV transmission in Asia is believed to be mainly due to an urban cycle between humans and mosquitoes (*Ae. aegypti* and *Ae. albopictus*). However, CHIKV was recently detected in Malaysian primates, indicating that NHPs may also act as a reservoir in Asia (Apandi *et al.*, 2009).

In Malaysia, prior to 2008, only small outbreaks had been reported. Outbreaks in Klang, Selangor and Bagan Panchor, Perak in 1998 and 2006, respectively (Lam *et al.*, 2001; Kumarasamy *et al.*, 2006) were caused by the Asian genotype. The third outbreak in Ipoh, Perak at the end of 2006 was caused by the ECSA genotype which lacked the A226V mutation. The recent 2008-2010 outbreak in Malaysia was of the ECSA genotype, likely imported from India, and has caused over 10,000 cases throughout Malaysia (Figure 2.4; Sam and AbuBakar, 2006; AbuBakar *et al.*, 2007). The nationwide spread of the recent outbreak, compared to the limited nature of the first three outbreaks, was postulated to be due to the presence of the A226V mutation in the E1 protein.

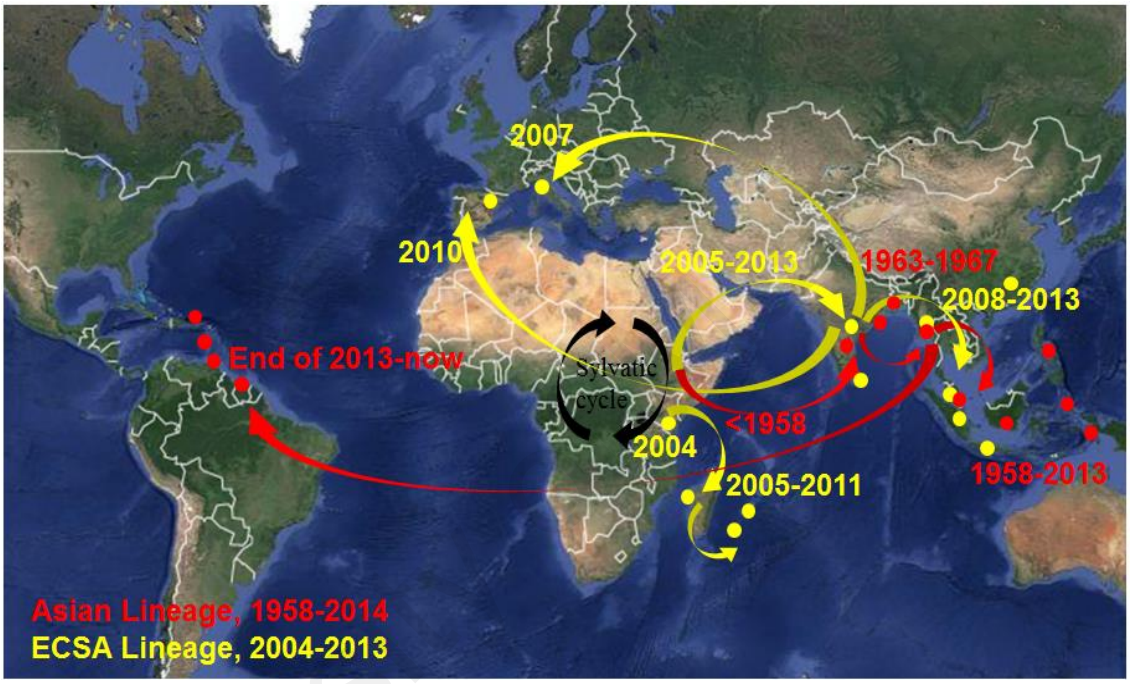

Figure 2.3: Map showing the global spread of CHIKV. Spread of the Asian lineage (red arrows and dots) and the Indian Ocean lineage (yellow arrows and dots) are shown. Figure adapted and modified from de Lamballerie *et al.* (2008), Das *et al.* (2010), and Weaver (2014), using Google Maps.

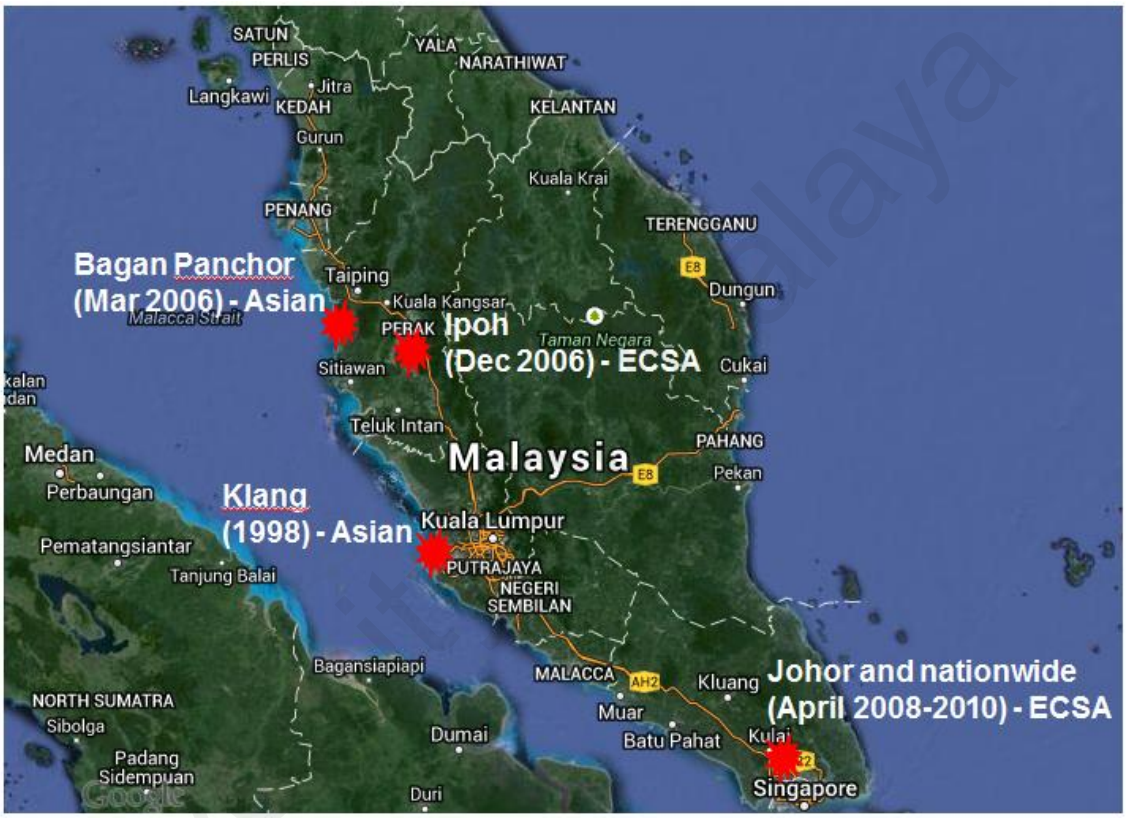

Figure 2.4: Map showing the outbreaks of CHIKV in Peninsular Malaysia. Figure drawn using Google Maps.

2.6 Clinical manifestations

CHIKV has drawn global attention due to its rapid spread, high morbidity, and neurological complications that had only been rarely reported previously (Mohan *et al.*, 2010).

2.6.1 General clinical manifestations

The CHIKV incubation period is estimated to be between 2 to 10 days (Thiberville *et al.*, 2013). Clinical manifestations are variable, ranging from asymptomatic to multi-organ failure and death (Economopoulou *et al.*, 2009). During the acute stage, infected patients suffer from abrupt onset of high fever, rash, and arthralgia. Fever usually presents in a single spike pattern (Sebastian *et al.*, 2009). Acute symptoms other than arthralgia usually last 7 to 10 days. Severe arthralgia with visible and/or palpable swelling which limit motion usually happens at peripheral joints (wrists, ankles, and phalanges), and proximal joints (shoulder, hips, and knees) (Robinson, 1955; de Ranitz *et al.*, 1965; Taubitz *et al.*, 2007; Sebastian *et al.*, 2009; Staikowsky *et al.*, 2009).

Arthralgia usually lasts for several weeks, but can persist for months or years. Patients with persistent arthralgia may experience general discomfort, impaired quality of life due to early exacerbations or inflammatory relapses at joints, and long-lasting rheumatism (Simon *et al.*, 2011). Joint erosions and/or joint space narrowing were also observed in chronically affected patients (Bouquillard and Combe, 2009; Chaaithanya *et al.*, 2014).

Other common acute symptoms include rash, intense fatigue, throat discomfort, abdominal pain, nausea, vomiting, constipation, myalgia, and headache. Transient confusion has also been reported in elderly patients. Conjunctival suffusion, persistent

conjunctivitis, swelling of eyelids, pharyngitis, and lymphadenopathy have also been reported (Robinson, 1955; de Ranitz *et al.*, 1965; Taubitz *et al.*, 2007; Mohan *et al.*, 2010). Non-severe bleeding has also been reported but is less severe compared to dengue and rarely causes shock (Sebastian *et al.*, 2009).

CHIKV infection needs to be differentiated from dengue infection, which is endemic in Malaysia. In comparing the two diseases, CHIKV infection is significantly associated with arthralgia and rash with a normal white blood cell count, while dengue virus (DENV) infection is associated with myalgia, bleeding, raised aspartate transaminase, and leucopaenia (Laoprasopwattana *et al.*, 2012; Lee *et al.*, 2012; Mohd Zim *et al.*, 2013).

2.6.2 Neurological manifestations

Unlike West Nile virus (WNV), Japanese encephalitis virus (JEV), and New World alphaviruses such as Eastern equine encephalitis virus (EEEV), VEEV, and WEEV, CHIKV is not considered a "true" neurotropic virus that causes encephalitis. However, fatal CHIKV cases and serious neurological complications have been reported recently during the ECSA outbreaks. Neurological complications had only been rarely described before in past outbreaks of Asian CHIKV in India in 1964 (Singh *et al.*, 2008) and Cambodia in 1970 (Arpino *et al.*, 2009). The unusual neurological manifestations seen in the recent ECSA outbreaks include altered level of consciousness, seizures, myoclonus, cerebral ataxia, encephalitis, encephalopathy, meningitis, and acute flaccid paralysis, (Rampal *et al.*, 2007; Robin *et al.*, 2008; Economopoulou *et al.*, 2009; Chusri *et al.*, 2011; Gauri *et al.*, 2012; Kalita *et al.*, 2013). Encephalopathy appears to be the most common clinical manifestation among elderly adults, children, and newborns

infected through the mother-to-child route (Gérardin *et al.*, 2008; Couderc and Lecuit, 2009).

Possible reasons for the increased reports of neurological involvement are a huge increase in CHIKV cases, infection of an immunologically naïve population, viral mutations leading to increased neurovirulence, and increased awareness and interest leading to increased diagnosis of CHIKV infection (Taubitz *et al.*, 2007; Rampal *et al.*, 2007).

2.7 Pathogenesis

2.7.1 Pathology in humans

CHIKV infects human epithelial and endothelial cells, primary fibroblasts, and monocyte-derived macrophages (Sourisseau *et al.*, 2007). In humans, CHIKV replicates in fibroblasts of the skin after a mosquito bite before spreading to liver (endothelial cells), joints, muscle (satellite cells and fibroblasts), stromal cells of lymphoid tissues, and the CNS (epithelial and endothelial cells) through lymph nodes and microvasculature (Sourisseau *et al.*, 2007; Schwartz and Albert, 2010). Severe arthralgia was due to local inflammation and often incapacitating with visible or palpable swelling that limits motion (Taubitz *et al.*, 2007; Schilte *et al.*, 2013). Prolonged arthralgia may persist for months with bony erosions, joint effusion, synovial thickening and erosions, and tendinitis (de Ranitz *et al.*, 1965; Chaaithanya *et al.*, 2014). Histopathological reports on tissue other than joints are scarce. Autopsy of a CHIKV-infected adult showed a swollen brain and haemorrhage during gross examination; microscopic examination showed oedema, focal ischemic changes, demyelination of white matter, lymphocyte infiltration, and gitter cells (Ganesan *et al.*, 2008).

2.7.2 Pathology in non-human primates

Detection of CHIKV has been reported previously in NHPs from Africa and Malaysia (Peiris *et al*., 1993; Inoue *et al.*, 2003; Apandi *et al*. 2009). NHPs can be used to study virus-induced pathophysiological mechanisms, and for evaluation of drug and vaccine efficacy. Infection of *Macaca fascicularis* through saphenous vein inoculation or the intradermal route mimics CHIKV infection in humans, with intermediate doses (10^2-10^6 PFU) causes fever and rash, and at higher doses (>10^7 PFU) causing wrist and ankle joint swelling, meningoencephalitis, and mortality (Labadie *et al.*, 2010). Pathology findings include mild multifocal necrosis of muscle fibres and severe, persistent

histiocytosis in the spleen. CHIKV mainly infects macrophages, dendritic cells, and endothelial cells in muscle, spleen, and liver. During acute infection, CHIKV is detectable in cerebrospinal fluid; during acute and late infection, CHIKV infects lymphoid tissues, liver, joints and muscle. High viral titres were also present in spleen, lymph nodes, joints, muscle, and liver of infected pregnant monkeys, but not in foetal tissue (Chen *et al.*, 2010).

2.7.3 Pathology in mice

After intracerebral inoculation of CHIKV, infected mice had heart hypertrophy, cyanosis, clammy skin, and necrotic bowel, and microscopic evidence of blood vessel dilation and congestion (Halstead and Buescher, 1961). CHIKV infection in ICR, OF1, C57BL/6 and 129s/v mice causes pathological changes in skin, muscles, joints, liver, spleen, and central nervous system (Ziegler *et al.*, 2008; Couderc *et al.*, 2008). Microscopic findings include pronounced CHIKV tropism for fibroblasts, focal individual muscle fibre wavy changes, necrotic myositis, muscle atrophy, and multifocal inflammation with lymphocyte and macrophage infiltration. Examination of skin tissue also showed the presence of viral antigen with infiltration of inflammatory cells, and muscle necrosis and calcification. CHIKV injection in C57BL/6J mice in the footpad caused local swelling and oedema, with pathological findings of arthritis, tenosynovitis, myositis, inflammation with histiocytes, neutrophils, and lymphocytes, and rare plasma cells in the foot joint (Morrison *et al.*, 2011).

The nature of CHIKV neurotropism in the mouse CNS is unclear. Following intradermal inoculation, CHIKV spread through the choroid plexus route before infecting the subventricular zone, involving ependymal and leptomeningeal cells, but not brain microvessels, parenchyma, microglial, and astrocytes (Couderc *et al.*, 2008).

Griffin (2005) reported vascular lesions with congestion of cerebral capillaries, pericapillary haemorrhages at the lateral ventricles, glial reaction, and neuronal lesions in the hippocampus, cortex, and midbrain nuclei. Ziegler *et al.* (2008) did not observe CHIKV antigen in the brain of suckling mice although the virus was shown to have entered and replicated initially. However, White (1969) reported CHIKV infection in the cerebral cortex and spinal cord of suckling mice with necrosis clearly seen in the endoplasmic reticulum of neurons. This is in contrast with other studies where CHIKV was reported to infect glial cells such as astrocytes and oligodendrocytes, but not microglial cells (Chatterjee and Sarkar, 1965; Das *et al.*, 2010; Das *et al.*, 2015).

Other alphaviruses such as SFV showed neurotropism for brain endothelium and neurons (Fazakerley, 2002). Labrada *et al.* (2002) observed high viral titres in CNS and extensive apoptosis in one-day-old mice infected with SINV, while four-week-old mice showed asymptomatic infection with low viral titres and absence of apoptosis, indicating that neurotropism may be age-dependent. VEEV, WEEV, and EEEV were also reported to induce high viral titre viremia, invade the CNS and cause encephalitis in mice (Atkins, 2013).

2.8 Host responses

Host cellular responses to CHIKV infection have been described previously, and include innate and adaptive immune responses, apoptosis, autophagy, and necrosis.

2.8.1 Cell death

There are three main types of cell death observed in CHIKV infection: apoptosis, autophagy, and necrosis.

2.8.1.1 Apoptosis

Apoptosis is an energy-dependent type of programmed cell death under the genetic and functional control of cells (Krejbich-Trotot *et al.*, 2011a). This causes the cell to shrink and segment into membrane-bound apoptotic bodies (Griffin, 2005). Apoptosis occurs by intrinsic and/or extrinsic pathways. The intrinsic apoptotic pathway is mediated by mitochondrial outer membrane permeabilization (MOMPS) that may be dependent or independent of activation of caspase (Casp). The extrinsic apoptotic pathway is either initiated by specific transmembrane receptors or binding of lethal ligands. This extrinsic apoptotic pathway is caspase-dependent, involves activation of Casp8, Casp9 or Casp10 that leads to Casp3 cascade, and is also mediated by MOMPS (Galluzzi *et al.*, 2012).

Alphaviruses such as SFV (Glasgow *et al.*, 1997), SINV (Ubol *et al.*, 1994; Lewis *et al.*, 1996), VEEV (Steele and Twenhafel, 2010), and EEEV (Steele and Twenhafel, 2010) cause apoptosis in cell lines and mice. Apoptosis was identified after CHIKV infection in RAW264.7 mouse macrophages (Kumar *et al.*, 2012b), CHME-5 human embryonic foetal microglia (Abere *et al.*, 2012), human cervical adenocarcinoma (HeLa) cells (Krejbich-Trotot *et al.*, 2011a), human primary fibroblasts (Krejbich-Trotot *et al.*,

2011a), and C57BL/6 and newborn Swiss albino mice (Wang *et al.*, 2008; Dhanwani *et al.*, 2011).

2.8.1.2 Autophagy

Autophagy or autophagic cell death is an intracellular recycling pathway in response to stress and during development that delivers components to lysosomes for degradation (Galluzzi *et al.*, 2012). This provides energy and anabolic building blocks for the cells. It is characterized by formation of double-membrane vesicles known as autophagosomes that fuse and are degraded by lysosomes (Griffin, 2005; Walsh and Edinger, 2010).

Autophagy was triggered after CHIKV infection in HeLa cells (Judith *et al.*, 2013), HEK293 cells (Krejbich-Trotot *et al.*, 2011b), and mouse embryonic fibroblasts (Joubert *et al.*, 2012). CHIKV-induced autophagy is mediated by endoplasmic reticulum and oxidative stress pathways (Joubert *et al.*, 2012). Judith *et al.* (2013) found that the autophagy receptor p62 has an antiviral role protecting cells from death by binding to CHIKV capsid while autophagy receptor NDP52 binds to nsP2 to limit nsP2-induced cell death. This is consistent with studies by Krejbich-Trotot *et al.* (2011b) and Joubert *et al.* (2012) which found that autophagy promoted CHIKV replication and delayed caspase-dependent cell death.

2.8.1.3 Necrosis

Necrosis is an energy-independent type of cell death due to injury, malfunction, or metabolic insufficiency. Necrosis is usually engaged when apoptosis and autophagy are not activated for cell death. It is characterized by cell swelling and plasma membrane rupture (White, 2008). Alphaviruses such as SFV (Balluz *et al.*, 1993; Galbraith *et al.*,

2006), SINV (Nargi-Aizenman and Griffin, 2001; Griffin, 2005), VEEV, EEEV, and WEEV (Steele and Twenhafel, 2010) cause necrosis in cerebellar neurons, humans, mice, and NHPs. CHIKV-infected C57BL/6 and BALB/c mice exhibit necrosis in the cerebral cortex, hippocampus, olfactory lobe, and spinal cord (White, 1969; Wang *et al.*, 2008). Necrotic features were observed in CHIKV-infected adult muscles (Ozden *et al.*, 2007). Necrosis was also observed in mouse skeletal muscle, cardiac muscle, cartilage, and skin (Ziegler *et al.*, 2008; Clavarino *et al.*, 2012; Rudd *et al.*, 2012). Vascular wall fibronoid necrosis, pulpar necrosis, and coagulative necrosis that did not involve blood vessels were also observed in mice (Oliver *et al.*, 2009; Morrison *et al.*, 2011; Rudd *et al.*, 2012).

2.8.2 Immune control of CHIKV

Cytokines and chemokines modulate CHIKV infection. IFN plays a major role as an antiviral cytokine as observed in clinical, *in vitro*, and *in vivo* studies. CHIKV, which is a single-stranded RNA virus, may engage the Toll-like receptor (TLR) signalling pathway through TLR7 and TLR8, while the intermediate double-stranded RNA may activate TLR3. The pattern-recognition receptors recognize pathogen-associated molecular motifs (PAMPs) of CHIKV, which are the ssRNA and dsRNA. This leads to activation of TNF receptor-associated factor 3 (TRAF3) and TRAF6, followed by activation of interferon regulatory factor 3 (IRF3) and IRF7 which produce type I IFN (IFN-α/β) essential for antiviral responses (Schwartz and Albert, 2010; Wang *et al.*, 2014).

CHIKV infection also seems to engage retinoic acid-inducible gene I (RIG-I)-like receptor and nucleotide-binding oligomerization domain (NOD)-like receptor signalling pathways. In the RIG-I-like receptor signalling pathway, the PAMPs also activate

melanoma differentiation-associated gene 5 (MDA5) and/or RIG-I which are translocated to mitochondria. This is followed by association with mitochondrial antiviral signalling protein, 2'-5' oligoadenylate synthetase 2 (OAS2), and NOD2, forming a complex which activates TRAF3 and leads to type I IFN production. In addition, mitochondrial antiviral signalling protein also activates I kappa B (IκB) which is essential for the release of nuclear factor kappa-light-chain-enhancer of activated B cell (NF-κB) (Schwartz and Albert, 2010; Ting *et al*., 2010; Lazear *et al.*, 2013). NF-κB later translocates to the nucleus to synthesise pro-inflammatory cytokines (pro-IL-1β and pro-IL-18) and survival genes such as BCL-2, c-IAP1/2, and XIAP. The survival genes inhibit Casp3, 7, and 9 which inhibit apoptosis (Bertrand *et al.*, 2009; Wang *et al*., 2014). In the NOD-like receptor signalling pathway, NOD2 also activates Casp1 through NOD-like receptor family (NLR) protein (Ting *et al*., 2010). Then, the activated Casp1 cleaves pro-IL-1β and pro-IL-18 into IL-1β and IL-18, respectively (Pang and Iwasaki, 2011; van de Veerdonk *et al*., 2011). OAS2 also activates endogenous ribonuclease (RNase L) which degrades viral RNA, thus inhibiting viral replication (Ting *et al*., 2010). The IL-1β synthesized from infected cells further induces production of type I IFN and pro-inflammatory cytokines from non-infected cells such as dendritic cells, macrophages, and microglia through the NF-κB signalling pathway. The IL-1β associates with myeloid differentiation primary response 88 (MyD88) through IL-1R and Toll-IL-1 receptor domain-containing protein. MyD88 and TRAF6 from the TLR signalling pathway also activates I kappa B kinase complex, followed by activation of IκB and further release of NF-κB (Schwartz and Albert, 2010; Wang *et al*., 2014).

2.8.2.1 CHIKV immune responses in humans

IFN-α and IFN-γ were found to be higher in infants than adult patients, which correlates with higher viral load and increased susceptibility to CHIKV infection in infants

(Werneke *et al.*, 2011). Secretion of IFN-β and translation of interferon-stimulated genes (ISGs) in CHIKV-infected human fibroblasts is activated through IRF3 (White *et al.*, 2011).

IL-6, MCP-1 (CCL2), CCL4 (MIP-1β), MIG (CXCL9), and IP-10 (CXCL10) were generally found upregulated in CHIKV-infected patients. Studies of CHIKV-infected patients in Singapore detected higher levels of IL-2R, IL-5, IL-6, IL-7, IL-8, IL-10, IL-12, IL-15, granulocyte macrophage colony-stimulating factor (GM-CSF), IP-10, MCP-1, and IFN-α, but lower levels of IL-8, eotaxin, and EGF compared to controls (Ng *et al.*, 2009; Chow *et al.*, 2011). Infants mount a robust acute response against CHIKV infection by expressing MCP-1, CCL4, MIG, IP-10, IL-1Rα, and IL-12p40/p70. Apart from MIG, these were at higher levels than adult patients. IL-4, IL-5, IL-13, IL-15, and IL-17 were elevated similarly in both infected infants and adults when compared to healthy individuals (Werneke *et al.*, 2011).

Studies have showed that IL-1β, IL-6, IL-10, MCP-1, MIG, and IP-10 increased in serum of the patients during the acute phase of infection (Ng *et al.*, 2009; Chaaithanya *et al.*, 2011; Kelvin *et al.*, 2011). MIGand IP-10 have also been associated with the early phase of disease resolution (Kelvin *et al.*, 2011). Low RANTES (CCL5) was observed in patients with higher severity (Ng *et al.*, 2009). Studies also showed that IL-1β, IL-5, IL-6, IL-8, IL-10, IL-12, tumor necrosis factor-α (TNF-α), MCP-1, and CCL4 were increased in serum of chronically-affected patients (Chaaithanya *et al.*, 2011; Kelvin *et al.*, 2011). Synovial fluid of CHIKV-infected patient also showed high expression of MCP-1, IL-6, and IL-8 (Hoarau *et al.*, 2010).

CHIKV infection in humans also elicits robust and rapid adaptive immune responses (Hoarau *et al.*, 2010, Wauquier *et al.*, 2011). Robust production of IgM and IgG has been observed within the first week of infection (Hoarau *et al.*, 2010). Dendritic cells, macrophages, natural killer cells, and T_H1/T_H2 cells are activated to produce specific chemokines and cytokines during recovered or persistent CHIKV infection, including IL-12, IL-1Ra, IL-6, IFN-α, IP-10 (CXCL10), MCP-1 (CCL2), and CCL4 (MIP-1β) (Ng *et al.*, 2009; Her *et al.*, 2010; Hoarau *et al.*, 2010). In addition, more than 50% of chronic CHIKV patients have natural killer and T ($CD4^+$ and $CD8^+$) cells circulating (Hoarau *et al.*, 2010). Maternal transfer of CHIKV antibody to infants has also been found to protect infants from CHIKV disease (Watanaveeradej *et al.*, 2006).

2.8.2.2 CHIKV immune responses in animal models

OF1, μMT, C57BL/6J, CD-1, Swiss albino, and BALB/c mice have been used to study immune responses to CHIKV infection. NHPs such as *M. mulatta* and *M. fascicularis* have also been studied.

Astrogliosis, dendritic cells, and leukocytes were observed in brains of newborn OF1 mice, suggesting an innate immune response although choroid plexus was not stained with CHIKV (Das *et al.*, 2015). CHIKV-infected mice showed activation of type I IFN, antiviral genes, TLRs, and pro-inflammatory cytokines, leading to clearance of CHIKV from infected organs (Lum *et al.*, 2013; Priya *et al.*, 2014). Mice deficient in type I IFN (Couderc *et al.*, 2008) and viperin (Teng *et al.*, 2012), a product of ISGs, were more susceptible to CHIKV infection, virus dissemination, and severe joint inflammation. This suggests that type I IFN and viperin are essential in protecting mice. A higher viral load enhanced expression by patient PBMCs of type I IFN expression and type I IFN signalling pathways genes such as IRF3, IRF7, and RSAD2 (viperin-encoding genes).

Other studies also showed involvement of IRF3, IRF7, and ISGs in protecting mice from CHIKV infection (White *et al.*, 2011; Rudd *et al.*, 2012). Alphaviruses such as SINV (Esen *et al.*, 2014), ONNV (Seymour *et al.*, 2013), RRV (Morrison *et al.*, 2006), and VEEV (Sharma *et al.*, 2009) were also found to induce type I IFN, natural killer cells, and macrophages in mice. These involved upregulation of TLRs, chemokines, inflammatory cytokines, IFN, IRFs, and signal transduction genes in infected mouse brains.

Type I IFN, IL-6, IL-15, TNF-α, MCP-1, CCL4, and IP-10 were generally found to be upregulated in CHIKV-infected animal models. CHIKV disease severity and persistent infection in mice and NHPs have been linked to pro-inflammatory cytokines such as IL-6, TNF-α, and IFN-α/β/γ, while increase of MCP-1, RANTES, CCL4, and IP-10 are correlated with increased CHIKV viremia (Labadie *et al.*, 2010; Patil *et al.*, 2012). Pro-inflammatory cytokines were induced by increased replication and higher neurovirulence of SFV in the CNS of mice (Tuittila *et al.*, 2004). Gene expression profiles of CHIKV-infected and rheumatoid arthritis-induced mouse models were found to be similar, with IFNs, IL-4, IL-10, IL-8, IL-15, TNF-α, GM-CSF, and lymphotoxin B increasing with disease severity (Nakaya *et al.*, 2012). Significant elevation of IL-6, IL-1β, TNF-α, and OAS was also seen in mouse lymphocytes (Dhanwani *et al.*, 2011; Werneke *et al.*, 2011).

$CD4^+$ but not $CD8^+$ T cells (Gardner *et al.*, 2012) and deficiency of type I IFN (IFN-α/β) (Teo *et al.*, 2013) were involved in joint swelling in infected mice. This suggests the involvement of adaptive and innate immune responses in CHIKV disease. Similarly, RRV infection in CD-1 and C57BL/6J mice induces adaptive immune cells such as $CD4^+$ and $CD8^+$ T lymphocytes (Morrison *et al.*, 2006). Antibodies have been observed

to control and eliminate CHIKV infection in µMT and C57BL/6J mice (Hawman *et al.*, 2013; Lum *et al.*, 2013), as well as alphaviruses SFV and SINV from mouse brains (Levine *et al.*, 1991; Fragkoudis *et al.*, 2008). The persistence of CHIKV infection in specific tissue especially joint-associated tissues seems to be controlled by adaptive and innate immune responses (Hawman *et al.*, 2013; Teo *et al.*, 2013). A live CHIKV/IRES vaccine was able to elicit adaptive immune responses to protect 129/Sv mice (Chu *et al.*, 2013).

2.8.2.3 CHIKV immune responses in cell lines

CHIKV infection has been studied in mouse cell lines such as RAW264.7 macrophages (Kumar *et al.*, 2012b), BV2 microglia (Das *et al.*, 2015), CLTT astrocytes (Das *et al.*, 2015), and N2a neuroblastoma (Priya *et al.*, 2013). Human cell lines such as primary fibroblasts, HeLa, HEK293 embryonic kidney cells (Krejbich-Trotot *et al.*, 2011b), primary osteoblasts (Noret *et al.*, 2012), and CHME-5 human embryonic foetal microglia (Abere *et al.*, 2012) have also been studied.

Innate immune responses were regulated in CNS-related cells such as CHME-5 human embryonic foetal microglia, N2a mouse neuroblastoma, CLTT mouse astrocytes, and BV2 mouse microglial cells. Although Abere *et al.* (2012) showed that CHME-5 human embryonic foetal microglia downregulated innate immune responses, Das *et al.* (2015) demonstrated otherwise with robust innate immune responses, apoptosis, and inflammation in mouse brain cells.

In CHIKV-infected cell lines, autophagy and upregulation of TNF-α, IL-6, GM-CSF, and interferon promoter stimulator 1 (IPS-1) resulted in activation of IRF3, followed by IFN-β production (Krejbich-Trotot *et al.*, 2011b; White *et al.*, 2011; Kumar *et al.*,

2012b). CHIKV infection of RAW264.7 mouse macrophages led to upregulated TNF-α, IL-6, and GM-CSF (Kumar *et al.*, 2012b), while infection of primary human osteoblasts induced IL-6 and RANKL (Noret *et al.*, 2012). In infected osteoblasts, IL-6 reduced osteoprotegrin secretion to cause bone loss and finally occurrence of arthralgia and arthritis. This is in agreement with previous studies which implicated IL-6 in persistent arthralgia, especially in elderly patients (Hoarau *et al.*, 2010; Schaible *et al.*, 2010; Chow *et al.*, 2011).

A study of non-hematopoietic fibroblasts found that RIG-I-like receptor and TLR trigger a type I IFN response to control CHIKV and prevent virus dissemination (Schilte *et al.*, 2010). The nsP2 protein of SINV has been linked to IFN suppression (Frolova *et al.*, 2002). Fros *et al.* (2010) showed that CHIKV replication suppressed IFN production upon production of nsP2. This blocked signal transducers and activators of transcription 1 (STAT1) phosphorylation and nuclear translocation in mammalian cells induced by either type I or type II IFN. CHIKV suppresses the antiviral IFN response by preventing expression of ISGs, which inhibits phosphorylation of Janus kinase 1 (Jak1), tyrosine kinase 2, and STAT1 and STAT2. The reduction of STAT prevents nuclear translocation of STAT1/STAT2 heterodimers from cytoplasm into nucleus, which in turn stops secretion of antiviral IFN-α (White *et al.*, 2011). Another study suggested that Jak2 rather than STAT was inhibited by CHIKV nsP2, thus inhibiting IFN-stimulated Jak-STAT signalling (Abere *et al.*, 2012). Other antiviral proteins include protein kinase R (PKR) (Randall and Goodbourn, 2008), OAS (Bréhin *et al.*, 2009), Mx proteins (Randall and Goodbourn, 2008), and IFN-γ by natural killer cells (Gardner *et al.*, 2010).

2.9 Treatment and prophylaxis

There are no known proven antiviral treatments effective against CHIKV infection, so the mainstay of treatment is supportive management of the patient's symptoms. Analgesics and anti-pyretics such as paracetamol/acetaminophen and non-steroidal anti-inflammatory drugs may be prescribed, while encouraging bed rest and fluid intake. Disease-modifying anti-rheumatic drugs such as methotrexate, hydroxychloroquine or sulphasalazine, and anti-tumour necrosis factor-α (anti-TNF-α) antibodies for severe chronic arthritis have been suggested (Bouquillard and Combe, 2009). Immunotherapy using human CHIKV immune serum has been reported to protect CHIKV-infected mice (Couderc *et al.*, 2009).

There are no licensed human vaccines currently available. Prior to the CHIKV reemergence in 2005, early vaccine candidates included a formalin-inactivated CHIKV vaccine prepared in chick embryos and green monkey kidney tissue culture (Harrison *et al.*, 1967; White *et al.*, 1972), and the CHIK 181/clone 25 prepared from CHIKV strain 15561 passaged in MRC-5 cells (Levitt *et al.*, 1986). Tween 80 and ether-inactivated CHIKV vaccine prepared in green monkey kidney tissue culture (Eckels *et al.*, 1970) and TSI-GSD-218 (Edelman *et al.*, 2000) vaccines showed immunogenicity and satisfactory seroconversion rates in healthy volunteers, but with unacceptable side effects, such as transient arthralgia.

Since 2005, there has been renewed interest in development of vaccines. These include a recombinant CHIKV vaccine comprising an adenovirus or alphavirus (EEEV or SINV) as a backbone encoding the structural polyprotein of CHIKV (Wang *et al.*, 2008; Wang *et al.*, 2011); a DNA vaccine based on CHIKV capsid, envelope E1, and E2 (Muthumani *et al.*, 2008; Mallilankaraman *et al.*, 2011); a formalin-inactivated ECSA

genotype CHIKV vaccine prepared in green monkey kidney tissue culture (Tiwari *et al.*, 2009); a viral-like particle vaccine (Akahata *et al.*, 2010; Chang *et al.*, 2014); a DNA replicon and protein (Hallengärd *et al.*, 2014); and a recombinant modified vaccinia Ankara or IRES-based attenuation (Plante *et al.*, 2011; van den Doel *et al.*, 2014; Weger-Lucarelli *et al.*, 2014). Kumar *et al.* (2012a) and Khan *et al.* (2012) also tested a recombinant protein vaccine and a formalin-inactivated whole virus vaccine. Recently, codon re-encoding was used to introduce random mutations into the LR2006 CHIKV strain, resulting in modification of nucleic acid sequences without changing the amino acid sequences for a cheap and safe attenuated virus vaccine (Nougairede *et al.*, 2013).

2.10 Hypothesis

Based on the host immune and cellular responses to CHIKV and other alphaviruses, neurological diseases may be due to immunopathological damage as well as direct viral invasion. It would be of great interest to compare neurovirulence variation among different CHIKV isolates, as inter-strain differences have been observed in other alphaviruses such as SFV and WEEV (Logue *et al*., 2009). This is of particular relevance to Malaysia, where both Asian and ECSA genotypes of CHIKV circulate. Therefore in this study, it is hypothesised that infection with different genotypes of CHIKV has different neurovirulence effects in a mouse model.

2.11 Main objective

To compare the neurovirulence due to CHIKV strains of different genotypes in mice by studying the replication, brain histopathology and transcriptomic changes.

2.12 Specific aims

1) To compare the replication kinetics of Asian and ECSA genotypes of CHIKV in ICR mice
2) To describe and compare the histopathology of ICR mice infected with Asian or ECSA genotypes of CHIKV
3) To examine and validate the significant transcriptomic changes in the brains of ICR suckling mice infected with Asian or ECSA genotypes of CHIKV

CHAPTER 3

METHODOLOGY

3.1 Tissue culture

3.1.1 Techniques

Media and solution for tissue culture were prepared using ultrapure (type 1) water through Milli-Q Integral 5 Water Purification System (Millipore, USA). The chemicals used were ultrapure grade. Glass bottles with screw-capped lids with non-toxic plastic blue washers were used for storage of the media. All cell culture and media preparations were done with aseptic procedures in a Class II, type A2 biological safety cabinet (ESCO, USA). Cells used in this study were grown in sterile 25 cm^2 tissue culture flasks (Nunc, Denmark), 75 cm^2 tissue culture flasks (TPP, Switzerland), 24-well tissue culture plates and 96-well tissue culture plates (BD, USA).

3.1.2 Cell lines

Vero cells (African green monkey kidney, ATCC CCL-81, passage number 10 to 30) and SK-N-MC cells (human neuroblastoma, ATCC HTB-10, passage number 65 to 85) were used in this study.

3.1.3 Media for tissue culture

Eagle's minimal essential medium (EMEM) was used as the growth and maintenance media for both Vero and SK-N-MC cells. For Vero cells, the growth media was supplemented with 10% foetal bovine serum (FBS) while maintenance media was supplemented with 2% FBS. 1× non-essential amino acids (NEAA), 100 units/mL and 100 µg/mL penicillin-streptomycin, and 2 mM L-glutamine were added for both media. For SK-N-MC cells, the growth media was supplemented with 20% FBS while

maintenance media was supplemented with 2% FBS. In addition to 1× NEAA, 100 units/mL and 100 µg/mL penicillin-streptomycin, and 2 mM L-glutamine, sodium pyruvate was also added. Sodium bicarbonate was added as a buffering agent, and the pH of the media was adjusted to 7.2.

3.1.4 Reestablishment, propagation, and freezing of cell lines

To revive frozen cell lines, cryovials containing the desired cell lines were retrieved from liquid nitrogen storage and immediately thawed in a 37°C water bath. When almost thawed, the cells were transferred immediately into pre-incubated re-establishment media (20% FBS growth media) in 75 cm^2 tissue culture flasks. The media dilutes the toxic effects of dimethyl sulphoxide, which is present in the cryopreservation media. The cells were incubated in a humidified chamber at 37°C, in the presence of 5% CO_2. The re-establishment media was discarded after 1 hour incubation and replaced with fresh media. The monolayer reached confluency in 1 to 2 days.

Upon reaching 70% confluency, the cells were passaged. The growth media was first discarded and the cell monolayer was rinsed twice with phosphate buffered saline (PBS) (OXOID, England). One mL of 0.12% trypsin-EDTA (0.12% trypsin, 1× EDTA, 1× PBS, and 100 units/mL and 100 µg/mL penicillin-streptomycin) for Vero cells and 0.01% trypsin-EDTA (0.01% trypsin, 1× EDTA, 1× PBS, and 100 units/mL and 100 µg/mL penicillin-streptomycin) for SK-N-MC cells was added, and cells were incubated at 37°C for 5 minutes. When cells appeared rounded, the flasks were gently tapped to detach the cell monolayer from the flask surface. One mL of growth media was added to inactivate the enzymatic effect of trypsin.

The cells were gently mixed without generating bubbles. For propagation, the cell suspension was split into a ratio of 1:3 to 1:6 for seeding into 75 cm^2 tissue culture flasks, and topped up with 10 mL of growth media. The cells were incubated at 37°C, in the presence of humidified 5% CO_2. The monolayer reached confluency in 3 to 4 days and could then be used for subsequent experiments.

For long-term storage, 1×10^5 cells were mixed in 5% DMSO cryopreservation media with 20% FBS growth media in cryovials. The vials were immediately placed in a freezing container containing isopropanol overnight before transfer to liquid nitrogen storage.

3.2 Virus

3.2.1 Virus isolates

The Malaysian CHIKV isolates used in this study were MY/06/37348, of the Asian genotype, isolated from a patient from Bagan Panchor in 2006 (GenBank accession number FN295483), and MY/08/065, of the ECSA genotype, isolated from a patient from Johor in 2008 (GenBank accession number FN295485). Both patients had uncomplicated CHIKV disease. Both isolates had been passaged three times in Vero cells. DENV strain New Guinea C (ATCC VR-1584) and SINV strain Ar-339 (ATCC VR-1248) that had been passaged two times in Vero cells were also used to test specificity of the quantitative real-time PCR (qRT-PCR), as these are viruses present in Malaysia which cause similar clinical illness to CHIKV.

3.2.2 Virus stock

The virus stock was propagated in Vero cells with aseptic procedures and at different times to minimise cross-contamination of virus isolates. Once the cells reached 70% confluency in 75 cm^2 tissue culture flasks, the cells were infected with virus isolates. Growth media was removed and 100 µL virus inoculum was added. The flask was rocked gently for 1 hour at room temperature to ensure even infection of the cell monolayer. After 1 hour of virus adsorption, the inoculum was removed and replaced with 10 mL of maintenance media. The infected cells were incubated at 37°C, in the presence of humidified 5% CO_2. Cytopathic effect (CPE) was observed daily. Upon reaching 70% CPE, the infected cells were freeze-thawed once before centrifuging the suspension at 40,000 × g for 20 minutes at 4ºC. Supernatant was then filtered using a 0.20 µm filter (Sartorius, USA), and stored in aliquots at -80°C until further use.

3.3 Confirmation of *in vitro* virus infection

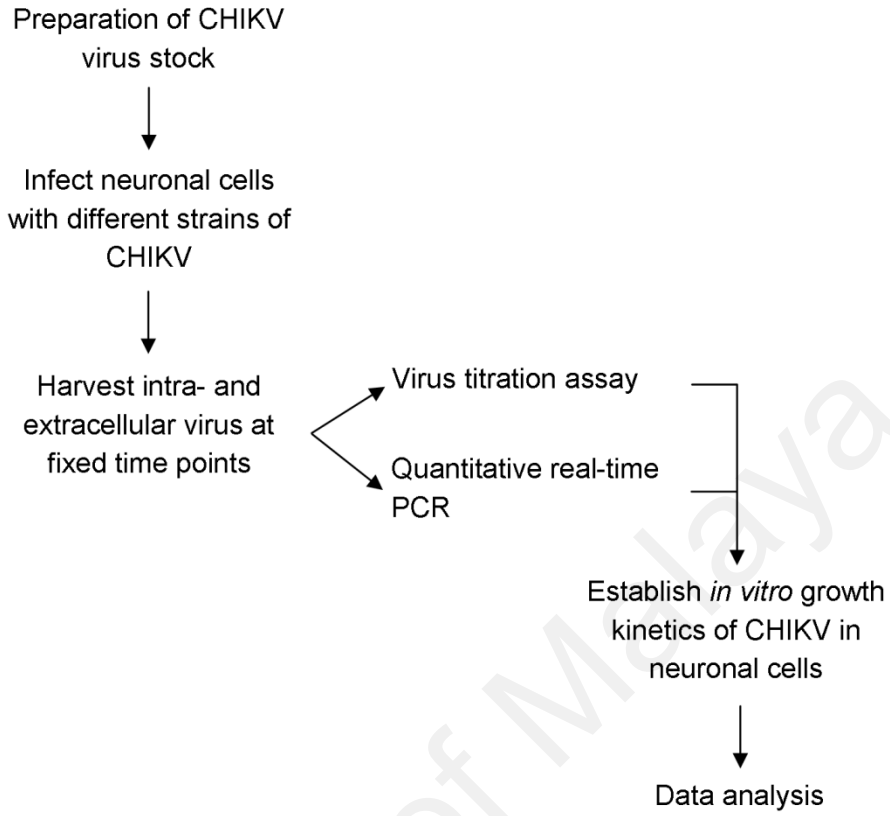

Figure 3.1: Flow chart confirming *in vitro* virus infection.

To compare the viral replication kinetics of different CHIKV genotypes in neuronal cells, SK-N-MC cells were infected with CHIKV, and virus and RNA were harvested for viral titration assay and qRT-PCR, respectively.

3.3.1 Virus growth kinetics

A 70% confluent cell monolayer of 3 to 4 days from a 75 cm^2 culture flask was used for infection. The cells were passaged and seeded in 24-well tissue culture plates. Vero cells were seeded at a density of 1×10^5 cells/well while SK-N-MC cells were seeded at 2×10^5 cells/well with 0.5 mL growth media. After overnight incubation at 37°C in the presence of humidified 5% CO_2, cells were infected with CHIKV at multiplicity of infection (MOI) of 1, and rocked gently at room temperature for 1 hour. To determine the volume of virus needed to achieve an MOI of 1, the $TCID_{50}$/mL of the virus stock was first obtained through virus titration assay (see section 3.3.3). According to the

Poisson distribution, the $TCID_{50}$/mL was multiplied by 0.69 to convert to PFU/mL. This was followed by multiplying the number of seeded cells by 1 for an MOI of 1 to obtain the total PFU. Finally, the total PFU was divided by PFU/mL to obtain the total volume of virus needed to achieve MOI of 1. Virus inoculum were then removed and the cell monolayer was rinsed twice with serum-free media (SFM; 1× EMEM, 1× NEAA, 100 units/mL and 100 µg/mL penicillin-streptomycin, and 2 mM L-glutamine). Then, 1 mL of maintenance media was added before incubation at 37°C in the presence of humidified 5% CO_2. Mock-infected control Vero and SK-N-MC cells were prepared as above, with SFM in place of the virus inoculum.

Extracellular virus was collected at 8-hourly time-points from 0 to 72 hours, and at 96 hours. The supernatant was centrifuged at 500 × g for 5 minutes at 4°C to remove cell debris. Then, 140 µL of supernatant was collected for viral RNA extraction for the positive-strand qRT-PCR assay. Finally, 500 µL supernatant was collected for the virus titration assay.

Intracellular virus was collected for the negative-strand qRT-PCR assay. Cell lysates were scraped gently with pipette tips and subjected to centrifugation at 500 × g for 5 minutes at 4°C. Supernatant was discarded and 0.5 mL TRIzol reagent (Invitrogen, USA) was added to the pellet, which was stored at -80°C for total RNA extraction.

3.3.2 Microscopic observation

Tissue culture flasks, 24-well plates and 96-well plates were visualised under an inverted microscope, Olympus CKX41 (Olympus, Japan). Pictures of virus- and mock-infected cells were captured under phase-contrast at magnifications of ×20 using a microscope with an attached digital camera (Nikon, Japan).

3.3.3 Virus titration assay

A 75 cm^2 culture flask of 70% confluent Vero cells at 3 to 4 days was used for infection. The cells were passaged and seeded in 96-well tissue culture plates at a density of 1×10^4 cells/well with 100 µL growth media. After overnight incubation at 37°C in the presence of humidified 5% CO_2, cells were infected with 100 µL 10-fold serially diluted virus suspension, and rocked gently at room temperature for 1 hour. Virus inoculum was then removed, and maintenance media was added before incubation at 37°C in the presence of humidified 5% CO_2. Plates were read every day until 5 days post-incubation to determine the end-point titer, defined as the amount of virus that produces CPE in 50% of cell cultures tested. The $TCID_{50}$/mL values were calculated according to the formula by Reed and Muench (Reed and Muench, 1938).

3.3.4 Viral RNA and total RNA extraction

For the positive-strand RNA qRT-PCR assay, viral RNA was extracted from 140 µL of supernatant with the QIAamp Viral Mini Kit (Qiagen, USA), following the manufacturer's protocol. For the negative-strand RNA qRT-PCR assay, total RNA was extracted from the cell lysates as per the TRIzol reagent protocol until phase separation. The mixture was separated into the lower red phenol-chloroform phase, an interphase and a colourless upper aqueous phase which contained total RNA. The harvested aqueous phase was followed with RNA isolation using the RNeasy Mini Kit (Qiagen) with the DNase I (Qiagen) for RNA cleanup following manufacturers' protocols. The extracted total RNA was then eluted by adding 40 µL of RNA Storage Solution (Ambion, USA) and stored at -80°C.

3.3.5 Molecular cloning

A strand-specific *in vitro* RNA transcript which acts as RNA standard control for qRT-PCR standard curve was generated to assess the synthesis of CHIKV positive- and negative-strand RNA. The chosen target was the nsP3 gene positions 5026 to 5161 based on the CHIKV prototype S27 sequence (GenBank accession number AF369024). NsP3 was used as it is involved in negative-strand and subgenomic RNA synthesis.

3.3.5.1 Primer design

For the positive-strand qRT-PCR assay, primers targeting the CHIKV nsP3 region with an expected product size of 136 bp were designed (Table 3.1). For the negative-strand nsP3 assay, a tagged forward primer was designed, containing a 24 nucleotide "tag" sequence unrelated to CHIKV at the 5'-end of the nsP3 sense primer. This "tag" sequence improved the specificity of negative qRT-PCR assays (Komurian-Pradel *et al.*, 2004; Plaskon *et al.*, 2009). All primers were designed based on alignments of publicly-available CHIKV sequences using Geneious version 5.0.3 (Biomatters, New Zealand) and Primer Express version 3.0 (Applied Biosystems, USA).

3.3.5.2 Generation of cDNA

Positive-strand RNA was synthesised with nsP3-R primer added during cDNA synthesis. The 5' tagged sense primer Tag nsP3-F was used to transcribe cDNA from negative-strand RNA. Later, sense and antisense primers as well as 5' tag sequence and antisense primers were then used in subsequent qRT-PCR assays to generate positive-strand-specific and negative-strand-specific dsRNA, respectively (Richardson *et al.*, 2006). A mixture of 500 nM antisense primers, 50 nM dNTP mix (Promega, USA), and 1 µL of RNA were incubated at 65°C for 5 minutes in a BioRad MyCycler thermal cycler (Bio-Rad, USA) and then placed on ice for 4 minutes. The cDNA was

synthesized with 200 U Superscript III Reverse Transcriptase (Invitrogen), 0.1 M DTT (Invitrogen), 40 U RNaseOUT (Invitrogen), and 1× first strand buffer (Invitrogen). Reactions were incubated at 50°C for 60 minutes, then the room temperature enzyme was inactivated at 70°C for 15 minutes. Unincorporated primers were subsequently digested with 20 U of Exonuclease I (New England Biolabs, USA) by incubating at 37°C for 30 minutes followed by 80°C for 20 minutes. The cDNA were stored at -80°C until further use.

3.3.5.3 A-tailing of cDNA fragments

Conventional PCR was performed using GoTaq Flexi DNA Polymerase Kit (Promega) to add a single deoxyadenosine to the 3'-terminus of the blunt-end cDNA fragments to improve the efficiency of ligation to the vector insertion site 3' T overhangs. The reaction included 1.25 U GoTaq DNA polymerase, 1× reaction buffer with 1 mM $MgCl_2$, 0.2 mM of each dNTP (Promega), 0.2 µM of sense and antisense primers (Table 3.1), 0.5 µL cDNA, and nuclease-free water to a final volume of 50 µL. The thermal cycling program was 95ºC for 4 minutes, followed by 30 cycles of 95ºC for 1 minute, 55ºC for 1 minute and 72ºC for 1 minute, and 5 minutes extension at 72ºC.

PCR products were subjected to agarose gel electrophoresis with 6× loading dye and loaded into 1.5% agarose gel in 0.5× Tris-acetate-EDTA buffer with added GelRed (Biotium, USA). The gel was then electrophoresed at 90V for 30 minutes in 0.5× Tris-acetate-EDTA buffer (20 mM Tris base, 9.5 mM glacial acetic acid, 9.5 mM EDTA). The gel was viewed under ultraviolet illumination using a BioSpectrum AC Imaging System with a Biochemi HR Camera (UVP, USA). The expected A-tailing PCR product was excised and gel-purified with Expin GEL SV (GeneAll, Korea). The purified PCR product was confirmed again with 1.5% agarose gel electrophoresis and stored at -20°C.

3.3.5.4 Preparation of competent TOP10F' *Escherichia coli* cells

TOP10F' *E. coli* (Invitrogen) was chosen as the cloning host for the pGEM-T vector (Promega, Appendix 1) with its insert. Prior to transformation, the frozen non-competent TOP10F' *E. coli* was streaked on Luria-Bertani (LB) (BD) plate with 15 µg/mL tetracycline and incubated overnight at 37ºC. A single colony was then inoculated into 5 mL LB broth with 15 µg/mL tetracycline and incubated for 4 to 5 hours at 37ºC with continuous orbital shaking until the OD_{600} reached 0.6 to 0.8. The absorbance was determined with a nanospectrophotometer (IMPLEN, Germany). Then, 1 mL of culture was transferred into a 1.5 mL tube and centrifuged at 1,000 × g for 3 minutes at room temperature. The supernatant was discarded, and the pellet resuspended in 500 µL of cold 100 mM $CaCl_2$ with gentle flicking. Another 1 mL of 100 mM $CaCl_2$ was added to the tube and mixed by inversion. The tube was incubated on ice for approximately 2 hours to achieve maximum competency which increases the ability of TOP10F' *E. coli* to incorporate plasmid DNA during transformation.

3.3.5.5 Ligation of cDNA fragments

The amplified gene of interest was ligated into the pGEM-T vector. A mixture of 1× rapid ligation buffer, 50 ng pGEM-T vector, 3 µL purified PCR product and 3 Weiss units T4 DNA ligase were incubated overnight to maximise the ligation success rate of the gene of interest into the vector insertion site.

3.3.5.6 Transformation

The competent TOP10F' *E. coli* from section 3.3.5.4 was centrifuged at 1,000 × g for 3 minutes at 4ºC. The supernatant was discarded, and the pellet was resuspended in 80 µL of 100 mM $CaCl_2$ with cut off tips. Next, 4 µL of ligation mix (pGEM-T + gene of interest) was added and gently mixed with cut-off tips before incubation on ice for 45

minutes. The transformation mix was gently mixed again before incubation at 42ºC for 1 minute for heat shock without shaking. The mixture was incubated on ice for 5 minutes. Then, 900 µL Super Optimal Broth with Catabolite Repression medium was added at room temperature and mixed by gentle inversion to aid recovery from the heat shock process. Next, the mixture was incubated and shaken at 37ºC for 75 minutes. At the end of incubation, the transformation mix was centrifuged at 1,000 × g for 3 minutes at room temperature to avoid overgrowth of satellite colonies. The supernatant was discarded, except for 50 µL which was used for plating the pellet on a prepared LB/ampicillin plate overlaid with 100 µL of 0.1 M IPTG and 50 µL of 50 mg/mL X-Gal. The plate was incubated overnight at 37ºC.

3.3.5.7 Screening of transformants

Generally, recombinant white colonies will contain the gene of interest. After overnight incubation, white colonies were transferred with a sterile toothpick to a new LB/ampicillin/IPTG/X-Gal plate with drawn grids. Each of the recombinant colonies was streaked on each grid and incubated overnight at 37ºC. The next day, colony PCR was performed. A few randomly chosen recombinant colonies were transferred, resuspended with 50 µL milli-Q water, and boiled for 15 minutes to lyse the bacteria. Then, 5 µL of supernatant was obtained after centrifugation at 10,000 × g for 5 minutes, and the presence of the gene of interest plus the T7 promoter sequence was confirmed by conventional PCR (see section 3.3.6.1) using T7 and specific antisense primers. The thermal cycling program was 95ºC for 4 minutes, followed by 30 cycles of 95ºC for 1 minute, 55ºC for 1 minute and 72ºC for 1 minute, and 5 minutes extension at 72ºC. The PCR product was subjected to 1.5% agarose gel electrophoresis, viewed under ultraviolet illumination and products of the expected size were excised. The gel was purified with Expin GEL SV and reconfirmed again with 1.5% agarose gel

electrophoresis with added GelRed. The gel was then electrophoresed at 90V for 30 minutes in 0.5× Tris-acetate-EDTA buffer. The gel was viewed under ultraviolet illumination using a BioSpectrum AC Imaging System with Biochemi HR Camera. PCR products for DNA sequencing were sent to First BASE Laboratory Sdn Bhd (Selangor, Malaysia). The sequence results were assembled into contigs using Geneious version 5.0.3.

3.3.5.8 Subculture of recombinant colonies

The final confirmed recombinant colony with the gene of interest was streaked again onto a new LB/ampicillin plate. A single recombinant colony was first inoculated in 5 mL LB broth with 0.1 µg/mL ampicillin. The culture was incubated at 37ºC with vigorous shaking until the OD_{600} reached 0.6 to 0.8. Then, 1 mL of the culture was subsequently aliquoted into a 2 mL screw cap tube with autoclaved 80% glycerol and mixed well to final 15% glycerol. The recombinant colony culture stock was stored at -80ºC.

Table 3.1: Primers used in this study.

Primer	Sequence (5'-3')	T_m (°C)	Genome position*	Polarity
nsP3-F	GCGCGTAAGTCCAAGGGAAT	48.7	5,026 – 5,045	Sense
nsP3-R	AGCATCCAGGTCTGACGGG	50.3	5,143 – 5,161	Antisense
Tag	CCTCCGCGGCCGTCATGGTGG CGA	62.5	-	Sense
Tag nsP3-F	CCTCCGCGGCCGTCATGGTGG CGAGCGCGTAAGTCCAAGGG AAT	71.6	-	Sense
T7	TAATACGACTCACTATAGGG	56.3	-	Sense

* Numbering based on CHIKV prototype S27 sequence (GenBank accession number AF369024).

3.3.6 Molecular assays

3.3.6.1 Reverse transcriptase PCR (RT-PCR)

RT-PCR was performed using the Access RT-PCR System (Promega) to confirm CHIKV infection, following the manufacturer's protocol. Viral RNA was extracted as above from section 3.3.4 and used as template for RT-PCR. The reaction included 0.1 U AMV reverse transcriptase, 0.1 U *Tfl* DNA polymerase, 1× AMV/*Tfl* reaction buffer, 1 mM $MgSO_4$, 0.2 mM of each dNTP (Promega), 0.6 µM of sense and antisense primers (Table 3.1), 1 µL RNA template, and nuclease-free water to a final volume of 50 µL. The thermal cycling program was 42ºC for 60 minutes, 94ºC for 5 minutes, followed by 30 cycles of 94ºC for 1 minute, 55ºC for 1 minute and 72ºC for 1 minute, and 5 minutes extension at 72ºC.

PCR products were subjected to 1.5% agarose gel electrophoresis with 6× loading dye and GelRed. The gel was then electrophoresed at 90V for 30 minutes in 0.5× Tris-acetate-EDTA buffer. The gel was viewed under ultraviolet illumination using the BioSpectrum AC Imaging System with Biochemi HR Camera.

3.3.6.2 Generation of external standards

Following confirmation of the gene of interest from section 3.3.5.7, the selected recombinant colony was cultured again in LB broth supplemented with ampicillin. Purification of plasmid was performed using QIAprep Spin Miniprep Kit (Qiagen), following the manufacturer's instructions. Finally, plasmid was eluted with 50 µL of Buffer EB and stored at -20°C.

The gene of interest plus T7 promoter sequence was amplified through conventional PCR and gel purified with Expin GEL SV. Following purification, PCR product was *in*

vitro transcribed using MEGAshortscript Kit (Ambion) and purified with MEGAclear Kit (Ambion). The *in vitro* RNA transcripts were finally eluted in 100 µL of elution buffer preheated to 95°C. Concentrations of *in vitro* RNA transcripts were determined with a nanospectrophotometer and stored at -80°C**.**

For external standards for each assay**,** cDNA was synthesized from *in vitro* RNA transcripts as templates as described above in section 3.3.5.2. After quantifying, the cDNA was serially diluted 10-fold with PCR water and stored at -80°C.

3.3.6.3 Quantitative real-time PCR (qRT-PCR)

The positive-strand RNA qRT-PCR assay was used to measure viral load, while the negative-strand RNA qRT-PCR assay was used to quantify replicative intermediate RNA. The viral RNA and total RNA was extracted as above from section 3.3.4 and used as template for positive- and negative-strand RNA qRT-PCR, respectively. The qRT-PCR was performed in the StepOne Plus Real-Time PCR System (Applied Biosystems). Serially diluted standard cDNA and test sample cDNA, synthesized from viral RNA and total RNA, were assayed in a 10 µL reaction volume containing 1× Power SYBR Green PCR Master Mix, 1 µM sense and antisense primers, 1 µL of cDNA, and 3.8 µL of nuclease-free water. Non-template control was also included by replacing the cDNA with PCR water. Cycling parameters were 95ºC for 10 minutes, then 40 cycles of 95ºC for 15 seconds and 60ºC for 1 minute. Following amplification, melting curve analysis was used to verify the amplified product by its specific melting temperature. Experiments were repeated thrice with a triplicate sample each time to increase the statistical power.

The resulting number of RNA copies per reaction was multiplied by 5,714 to obtain a final viral RNA copy number per mL of initial sample. PCR amplification efficiency was calculated using the formula $E = 100(10^{-1/slope}-1)$.

3.3.6.4 Specificity and precision of strand-specific assays

DENV strain New Guinea C (ATCC VR-1584) and SINV strain Ar-339 (ATCC VR-1248) were used to test specificity, as these are viruses present in Malaysia which cause similar clinical illness to CHIKV.

Serial dilutions of nsP3 cDNA generated from *in vitro* transcribed CHIKV RNAs were used to confirm strand-specificity. Various concentrations of cDNA derived from the positive-strand primer set were tested using the nsP3 negative-strand qRT-PCR protocol, while cDNA derived from the negative-strand primer set was tested using the nsP3 positive-strand qRT-PCR protocol.

Precision was determined by calculating intra- and inter-assay coefficient of variation, dividing the respective standard deviation with its mean value. Intra-assay variability was determined by testing technical triplicates of standards diluted across 5 $\log_{10}$ units. Inter-assay variability was determined by calculating the coefficient of variation of diluted standards from three different experiment runs.

3.3.7 Indirect immunofluorescence (IF) detection

IF staining was performed to confirm CHIKV infection in Vero and SK-N-MC cells. A 70% confluent cell monolayer at 3 to 4 day-old from a 75 cm^2 culture flask was used for infection. The cells were passaged and seeded in poly-D-lysine coated growth chamber slides (Thermo Scientific, USA). Vero cells were seeded at a density of 1×10^4

cells/well, while SK-N-MC cells were seeded at 2×10^4 cells/well with 100 µL growth media. After overnight incubation at 37°C in the presence of humidified 5% CO_2, cells were infected with CHIKV, and rocked gently at room temperature for 1 hour. Virus inoculum was then removed and 100 µL of maintenance media was added, before incubation at 37°C in the presence of humidified 5% CO_2. Mock-infected control Vero and SK-N-MC cells were prepared with SFM in place of the virus inoculum.

The maintenance media was discarded and the coated cells were fixed with fresh 4% paraformaldehyde (Merck, Germany) in PBS for 30 minutes on ice. After washing the slide twice with PBS for 5 minutes, the growth chamber slide gasket was removed and cells were incubated with 0.25% of Triton-X in PBS for 7 minutes before being washed twice with PBS for 5 minutes. Cells were incubated for 1 hour with Image IT FX Signal Enhancer (Sigma, USA) at 37ºC in a moist chamber and subsequently washed twice with PBS for 5 minutes. This was followed with 1 hour incubation of 1:100 dilution of the primary antibody, in-house polyclonal rabbit anti-CHIKV, at 37ºC in a moist chamber. The polyclonal rabbit anti-CHIKV was previously prepared by inoculating heat-inactivated CHIKV strain MY/06/37348 premixed with Freund's complete adjuvant into a New Zealand white rabbit. This was followed by booster injections at days 7, 21, 35 and 49, and serum was collected 1 week after the final booster injection. The slide was washed twice with PBS for 5 minutes and subsequently incubated for 1 hour with 1:50 dilution of secondary antibody, goat anti-rabbit IgG fluorescein isothiocyanate (FITC) conjugate (Thermo Scientific), at 37ºC in a moist chamber. The slide was washed twice with PBS for 5 minutes before being counterstained with 300 nM of 4'6-diamidino-2-phenylindole (DAPI) (Invitrogen) for 5 minutes at room temperature. Finally, the slide was washed with milli-Q water for 5 minutes, air dried and then mounted with anti-fade mounting fluid (Molecular Probes, USA) and a cover

slip. The slide was observed under an inverted fluorescence microscope (Nikon) at a magnification of ×60.

3.4 Determination of virus neurovirulence in mice

Animal ethical approval MP/14/07/2010/JICS(R) was obtained from the University Malaya Animal Care and Use Committee. Neurovirulence of the two CHIKV genotypes was compared in Institute for Cancer Research (ICR) mice, obtained from University Malaya Laboratory Animal Centre. One-day-old suckling mice and six-week-old adult female mice were used for this study.

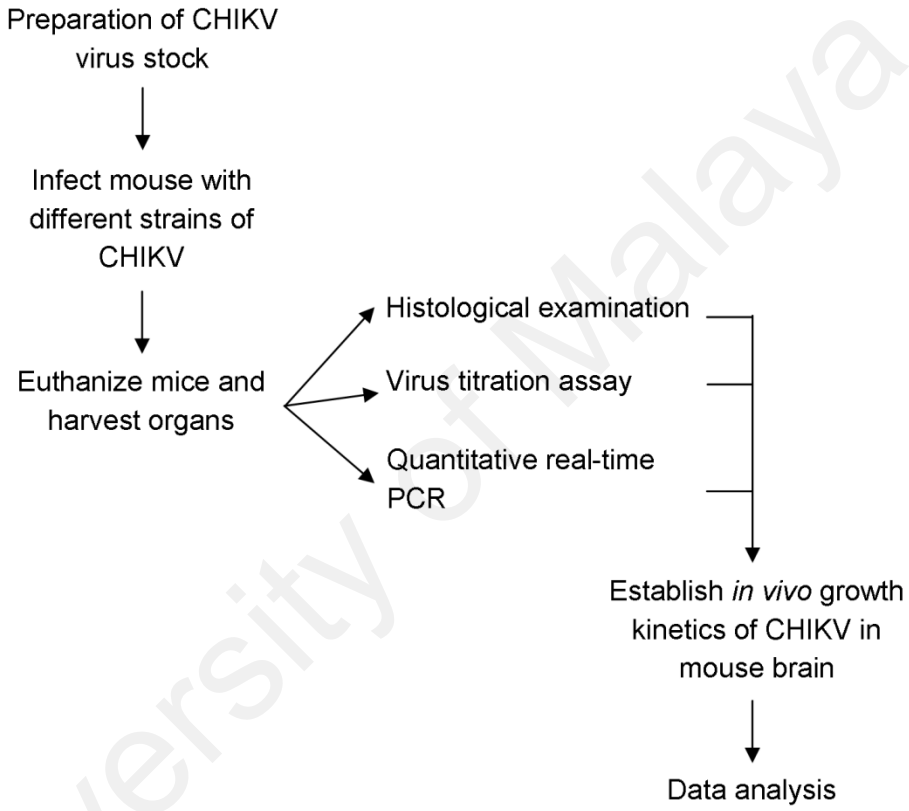

Figure 3.2: Flow chart determining virus neurovirulence in mice.

To compare the neurovirulence of different CHIKV genotypes in mice, CHIKV was intracerebrally inoculated, and the mouse brains were harvested at set time points for viral titration assay, qRT-PCR, and histopathologic analysis.

3.4.1 Intracerebral inoculation of virus into mice

Virus inoculation was performed in a Class II, type A2 biological safety cabinet. A 100 µL virus suspension of 5.5 $\log_{10}$ $TCID_{50}$/mL was first loaded in a 1 mL syringe with a 26G needle. Each mouse was anaesthetised with CO_2 in an anaesthesia chamber, before

the left side of its head was decontaminated with 70% ethanol. The syringe with loaded virus suspension was inserted 2 to 3 mm into the left parietal area by turning the needle slowly through the skull. Each suckling mouse was inoculated with 20 µL of virus suspension over 10 seconds, while each adult female mouse was inoculated with 50 µL of virus suspension, before slow removal of the needle. The mock-infected mice which act as negative controls were inoculated with SFM instead of virus suspension. Suckling mice were observed daily for signs of illness, weight gain, and survival for up to 14 days. The day that a moribund mouse was euthanized or found dead was considered the day of death, which was used for calculation of mean time to death. Four independent experiments were performed, with 9 to 13 suckling mice per group. Another group of mice was inoculated as described above for *in vivo* virus growth kinetics; three suckling and adult female mice were euthanized on days 0, 1, 2, 4, 6, and 8 post-infection, respectively.

3.4.2 Dissection of mouse brains

Each mouse was first anaesthetised with CO_2 in an anaesthesia chamber and euthanized by cardiac puncture. The head was decontaminated with 70% ethanol and the fur was removed to reveal the cranial bone. The mouse neck was flexed and bone scissors was inserted into the foramen magnum at the base of the skull. The cranium was cut away with small snips along the sides all the way forward to the snout and the skull was removed. The brain was carefully lifted out after cutting the blood vessels and cranial nerves connected to the base of the skull.

The harvested brain was either immersed immediately in fixative 10% neutral buffered formalin (10% paraformaldehyde, 28 mM Na_2HPO_4, 40 mM NaH_2PO_4) for subsequent histology, or weighed for subsequent virus and viral RNA isolation. For the latter, the

brain was loaded into a 2 mL homogenizing tube with 1.4 mm ceramic beads (Omni, USA), and homogenized with a Precellys 24 homogenizer (Bertin Technologies, French). SFM was added to half of the homogenised brains to the final 10% of the harvested mouse brain weight. The resulting supernatant was collected for virus titration assay or qRT-PCR. TRIzol reagent was added to the other half of the homogenized brain to the final 10% of the harvested mouse brain weight for total RNA extraction.

3.4.3 Mouse brain viral RNA and total RNA

The homogenized brain viral RNA and total RNA were extracted as described in section 3.3.4.

3.4.4 Tissue processing for histology

The harvested brain was fixed in 10% neutral buffered formalin for a week before being sectioned according to the desired plane of section and placed in an embedding cassette. The tissue sample was processed overnight in the reagents below with a LEICA TP1020 automated tissue processor (Leica, Germany).

	Reagent	**Time (minutes)**
Fixation	10% neutral buffered formalin	-
Dehydration	70% ethanol	60
	95% ethanol I	60
	95% ethanol II	60
	95% ethanol III	60
	100% ethanol I	60
	100% ethanol II	60
	100% ethanol III	60
Clearing	Xylene I	60
	Xylene II	60
Embedding	65ºC paraffin I	30
	65ºC paraffin I with vacuum to remove small air bubbles	30

The sample was transferred from a 10% neutral buffered formalin bath into a series of increasing concentrations of ethanol solution for dehydration for 60 minutes each. During clearing, the sample was soaked in xylene solution for removal of ethanol for 60

minutes each before hot paraffin was used for embedding. For a paraffin block, hot paraffin was first preloaded into a base mold before the desired plane section was placed facing downwards into the base mold. The base mold was cooled briefly before being closed with the embedding cassette and more hot paraffin was loaded. The cooled paraffin block was sectioned at 4 µm thickness with a LEICA RM2235 rotary microtome (Leica). The tissue sections in ribbons were floated and separated individually in a 40ºC water bath. The tissue section was placed onto dried silanized glass slides that were pre-washed with 2% silane solution (Sigma) in acetone. The slides were placed on a 60ºC hot plate for 20 to 30 minutes and left at room temperature to allow tissue bonding to the slides.

In addition, supernatant from CHIKV-infected Vero cells with 70% CPE were mixed with finely cut non-infected mouse lungs to act as a staining control. The staining control was centrifuged at 10,000 × g for 5 minutes before being fixed in 10% neutral buffered formalin for a week and processed as described above. Under microscopic observation, the CHIKV-infected Vero cells could be found attached to the mouse lungs.

3.4.5 Haematoxylin and eosin staining

This general staining was performed to observe the morphological and histological changes of the tissue section. Haematoxylin stains nuclei blue while eosin stains cytoplasm pink. The slides containing the tissue sections were placed in a slide holder and first deparaffinised with the following protocol:

	Reagent	Time (minutes)
Deparaffinisation	Xylene I	3
	Xylene II	3
	Xylene III	3
Rehydration	Absolute ethanol	2
	95% ethanol I	2
	95% ethanol II	2
	95% ethanol III	2
	Running tap water	2-3

After deparaffinising the tissue section with a series of xylene solutions for 3 minutes each, the tissue section was rehydrated with decreasing concentrations of ethanol solution for 2 minutes each and a final wash with tap water. The rehydrated tissue section was soaked in haematoxylin for 10 minutes and washed with running tap water for 3 minutes. Tissue slides were dipped in 5% acid alcohol 3 times before being washed in running tap water for 3 minutes. Next, slides were dipped in 2% potassium acetate 3 times before being washed in running tap water for 3 minutes. This was followed by dipping in 80% ethanol 5 times before immersion in eosin for 45s. The slides were rehydrated by dipping 5 times each in 95% ethanol I, 95% ethanol II, and absolute ethanol I before being dipped in absolute ethanol II 10 times. Finally, the slides were dried with a hair dryer or at 60ºC in an oven before being dipped in xylene and mounted with DPX mountant (Sigma) and cover slips. The slides were examined under a light microscope (Nikon).

3.4.6 Immunohistochemistry

Specific staining was performed to stain the antigen of interest with an antibody which was then revealed by a coloured chromogen. The slides containing the tissue sections were placed in a slide holder and first deparaffinised with the following protocol:

	Reagent	Time (minutes)
Deparaffinisation	Xylene I	5
	Xylene II	5
	Xylene III	5
Rehydration	Absolute ethanol	2
	95% ethanol I	2
	95% ethanol II	1
	95% ethanol III	1
	Running tap water	2-3

After deparaffinising the tissue section with a series of xylene solutions for 5 minutes each, the tissue section was rehydrated with decreasing concentrations of ethanol solution for 1 to 2 minutes each and a final wash with tap water. The rehydrated tissue section first underwent heat-induced epitope retrieval by soaking in boiled Tris-EDTA buffer, pH 9.0 (10 mM Tris Base, 1 mM EDTA) for 30 minutes. After heating, the slide holder was removed and allowed to cool down for another 15 minutes at room temperature before being washed in running tap water for 5 minutes. The peroxidase activity was blocked by incubating with 3% H_2O_2 (Ajax Finechem, Australia) in methanol for 20 minutes before the slides were washed in Tris-buffered saline (TBS), pH 7.6 (49 mM Tris Base, 1.37 M NaCl) for 5 minutes. The slides were blocked with 1:20 dilution of goat serum (Dako, Denmark) for 20 minutes at room temperature in a moist chamber to stop non-specific background staining by the secondary antibody. The slides were then incubated overnight with primary antibody, rabbit anti-CHIKV capsid (kindly provided by Professor Andres Merits, University of Tartu, Estonia), diluted 1:5,000 in antibody diluent (Dako) at 4ºC in a moist chamber. Positive staining control and negative staining control sections were incubated with and without primary antibody, respectively.

The slides were washed thrice in TBS for 5 minutes and subsequently incubated for 30 minutes with secondary antibody, EnVision/HRP Rabbit/Mouse (Dako), at room temperature in a moist chamber. This was followed by washing twice in TBS for 5

minutes before 1:50 dilution of DAB reagent (Dako) was added. The slides were immediately immersed in tap water when the sections turned brown and washed in running tap water for 5 minutes. Slides were counterstained with haematoxylin for 1 minute and washed twice again in running tap water for 5 minutes. Finally, the slides were dried with a hair dryer or at 60ºC in an oven before being dipped into xylene and mounted with DPX mountant and cover slips. The slides were examined under an upright brightfield microscope, Olympus BX51 (Olympus).

3.4.7 Double immunofluorescence staining

This was performed to specifically stain and observe the presence of more than one antigen or biomarker of interest. Each antigen or biomarker of interest will be revealed by specific antibody conjugated with different fluorescein molecules.

The tissue section was processed as described in section 3.4.6 until overnight incubation with the primary antibody, the rabbit anti-CHIKV capsid diluted 1:5,000 in antibody diluent, at 4ºC in a moist chamber. The slides were washed thrice in TBS for 5 minutes and subsequently incubated for 30 minutes with 1:500 dilution of secondary antibody, the goat anti-rabbit IgG alkaline phosphatase, at room temperature in a moist chamber. Slides were washed twice in TBS for 5 minutes before incubation in Liquid Permanent Red chromogen (Dako) in a moist dark chamber. The slides were incubated for 30 minutes before being washed in running tap water for 5 minutes.

The slides were soaked again in boiled Tris-EDTA buffer for 10 minutes for heat-induced epitope retrieval as described in section 3.4.6. Slides were incubated overnight at 4ºC in a moist dark chamber with one of the second primary antibodies, either rabbit anti-cleaved Casp3 (Asp175) diluted 1:200 (Cell Signaling, USA), mouse anti-glial

fibrillary acidic protein (GFAP, GA5) diluted 1:1,000 (Cell Signaling), or rabbit anti-microtubule-associated protein-2 (MAP-2, H-300) diluted 1:2,500 (Santa Cruz, USA) diluted in antibody diluent. The slides were washed thrice in TBS for 5 minutes and subsequently incubated for 30 minutes with 1:500 dilution of the second secondary antibody, goat anti-rabbit or goat anti-mouse Alexa Fluor-488 conjugate (Invitrogen), at room temperature in a moist dark chamber. Slides were washed twice in TBS for 5 minutes before counterstaining for 30 minutes with 300 nM of DAPI in a moist dark chamber at room temperature. The slides were washed twice in running tap water for 5 minutes. Finally, the slides were dried with a hair dryer or at 60ºC in an oven before mounting with anti-fade mounting fluid and cover slips. The slides were stored at 4ºC in the dark, and later examined with a confocal microscope (Leica).

3.5 Transcriptomics of CHIKV-infected mouse brains

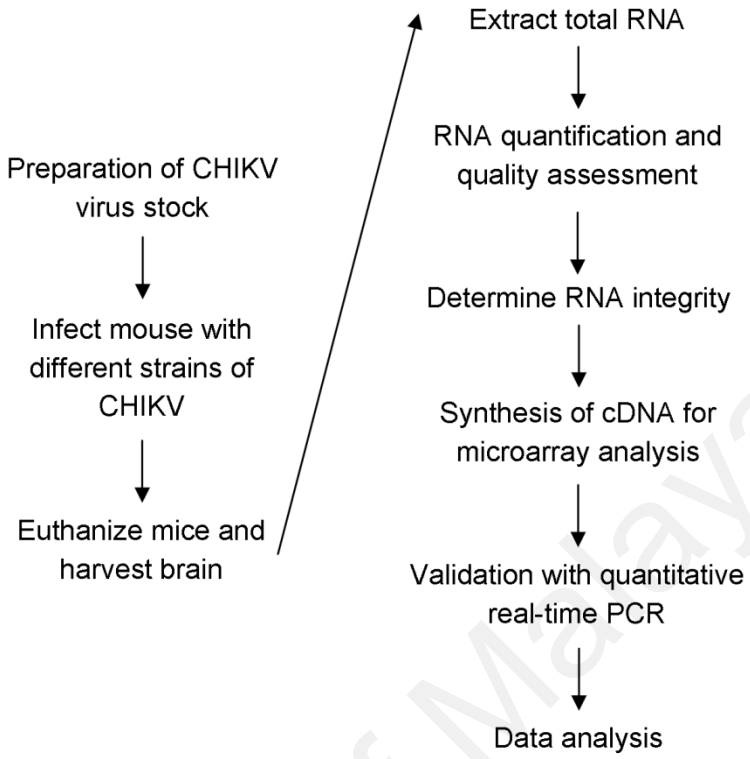

Figure 3.3: Flow chart determining gene expression of CHIKV-infected mouse brains.

To examine the gene expression changes upon infection of different CHIKV genotypes in mouse brains, total RNA was harvested and hybridized on a microarray slide. Thousands of genes can be studied simultaneously to generate a snapshot of the entire transcriptome of the mouse brains. Bioinformatic analysis was performed with Genespring (Agilent, USA) and Database for Annotation, Visualization and Integrated Discovery (DAVID) to determine the significantly regulated genes in host cellular responses. About 45 genes of interest were selected for qRT-PCR to validate the significantly differentially expressed genes.

3.5.1 RNA quantification and quality assessment

Mouse brains were harvested as described from section 3.4.2, and later total RNA was extracted as described in section 3.3.4. The total RNA was used as the input for transcriptomic study of gene expression or regulation.

Total RNA concentration was first determined by measuring the absorbance at 260 nm (A_{260}) using an Epoch Microplate Spectrophotometer (Bio-Tek, USA). The purity of total RNA with A_{260}/A_{280} ratio of 1.9 to 2.1 indicates the absence of protein contamination. An A_{260}/A_{230} ratio of more than 2.0 indicates absence of other organic compounds, such as guanidium isothiocyanate, alcohol, and phenol as well as cellular contaminants such as carbohydrates. Samples that passed the quality assessment were selected for the RNA integrity test.

3.5.2 Determination of RNA integrity

Total RNA integrity was determined with an Agilent 2100 bioanalyzer (Agilent, USA) using the RNA 6000 Nano LabChip kit (Agilent) following manufacturer's instructions. For quality control, the ratio of 28S rRNA to 18S rRNA should be approximately 2:1. In addition, the ribosomal bands or peaks should be sharp without smearing towards smaller-sized RNA. Samples with the highest RNA integrity number that fulfilled the above quality control criteria were selected for downstream applications.

3.5.3 Microarray

Following the manufacturer's protocol (One-Color Microarray-Based Gene Expression Analysis - Low Input Quick Amp Labeling), total RNA from two biological replicates was hybridized onto SurePrint G3 Mouse GE 8 × 60K microarray (Agilent), scanned with a microarray scanner (Agilent), and finally extracted with Feature Extraction

(Agilent). Data analysis was performed with Genespring (Agilent), followed by functional annotation and cluster analysis.

3.5.3.1 Probe labelling

The Low Input Quick Amp Labeling Kit generates fluorescent complementary RNA (cRNA) with a sample input RNA of 200 ng of total RNA for one-colour processing. The method uses T7 RNA polymerase, which simultaneously amplifies the target material as well as incorporating cyanine 3-labelled CTP. Amplification is typically at least 100-fold from total RNA to cRNA with this kit.

A volume of 2 µL of prediluted 1:5,000 RNA spike-in controls was added to 1.5 µL of 200 ng of total RNA. Then, 1.8 µL of T7 promoter primer mix was added. The T7 promoter primer mix was composed of 0.8 µL of T7 promoter primer and 1 µL of nuclease-free water. The final 5.3 µL of mixture was incubated at 65ºC for 10 minutes before cooling on ice for 5 minutes.

The 5× first strand buffer was first prewarmed at 80ºC for 3 to 4 minutes before it was briefly vortexed and spun down to be kept at room temperature. The cDNA was synthesized with 2 µL 5× first strand buffer, 1 µL 0.3 M DTT, 0.5 µL 10 mM dNTP mix, 1.2 µL AffinityScript RNase block mix, and the previously prepared 5.3 µL template mixture. The 10 µL cDNA reaction was incubated at 40ºC for 2 hours, and at 70ºC for 15 minutes to inactivate the enzyme before being placed on ice for 5 minutes.

The cRNA was transcribed with 0.75 µL nuclease-free water, 3.2 µL 5× transcription buffer, 0.6 µL 0.1 M DTT, 1 µL NTP mix, 0.21 µL T7 RNA polymerase blend, 0.24 µL

cyanine 3-CTP, and 10 µL cDNA template. The 16 µL cRNA reaction was incubated at 40ºC for 2 hours.

A volume of 84 µL of nuclease-free water was added to the cRNA reaction above to make a final volume of 100 µL. The cRNA was purified with RNeasy mini kit according to the manufacturer's protocol. Then, 30 µL of nuclease-free water was added to the column before the final centrifugation to elute the purified cRNA sample. The cRNA sample was kept on ice.

3.5.3.2 cRNA quantification and integrity determination

The cRNA was quantitated with a nanospectrophotometer. Cyanine 3 dye concentration (pmol/µL), RNA absorbance ratio (260 nm/280 nm), and cRNA concentration (ng/µL) were recorded. The cRNA yield and specific activity were determined as follows:

a) cRNA yield = (Concentration of cRNA) × 30 µL /1000

= µg of cRNA

b) Specific activity = (Concentration of Cy3)/(Concentration of cRNA) × 1000

= pmol Cy3 per µg cRNA

For the 8 × 60K microarray, the labelled cRNA sample must fulfil the quality control criteria of more than 0.825 µg cRNA yield and 6 pmol Cy3 per µg cRNA specific activity. The labelled cRNA integrity was also determined with an Agilent 2100 bioanalyzer using the RNA 6000 Nano LabChip kit following manufacturer's instructions. The electropherogram has to range between 200 and 2000 nucleotides, and have a high RNA integrity number before proceeding to hybridization.

3.5.3.3 Hybridization

The cRNA was fragmented with 5 µL 10× blocking agent, 1 µL 25× fragmentation buffer, 600 ng labelled cRNA, and nuclease-free water in a final volume of 24 µL. The reactions were incubated at 60ºC for 30 minutes before being placed on ice for 1 minute.

After the incubation time, an equal volume of 2× hybridization buffer was added to stop the fragmentation reaction. After centrifugation for 1 minute at room temperature at 16,000 × g, 40 µL of sample was loaded onto the array before assembly with a SureHyb slide chamber. The chamber was later placed in a hybridization oven for 17 hours at 65ºC with 10 rpm rotation.

The hybridized array slide was disassembled by submerging in a first dish filled with gene expression wash buffer 1. The slide was washed in a second dish filled with gene expression wash buffer 1 for 1 minute, and then a final dish with overnight prewarmed gene expression wash buffer 2 for 1 minute. The slide was removed slowly from the final dish to remove droplets on the slides before it was placed in a slide holder.

3.5.3.4 Scanning and data analysis

The assembled slide holder was immediately scanned with the Agilent microarray scanner. The scanned images were exported as TIFF files to Feature Extraction for image analysis before it was analysed with Genespring software.

Normalization and filtering of the data were performed with the Genespring software. The data was first logarithmic (base 2) transformed before normalization by scaling the 75th percentile of the housekeeping probes in each chip, and also normalization with

baseline transformation to the medians of all samples for each gene. This will reduce variability in the data due to the differences in the signal intensity across slides and genes. This was followed with probe set quality control by flag filtering and expression filtering. One-way analysis of variance (ANOVA) was performed to compare expression infected brains (MY/06/37348, MY/08/065, and mock) at 1 day post-infection (dpi) and 6 dpi. Genes with downregulation (≤ -2.0 fold change) or upregulation (≥ 2.0 fold change) were filtered with Microsoft Excel SQL (Microsoft, USA) to select genes which showed differences present in both CHIKV genotypes, Asian genotype (MY/06/37348) only, or ECSA genotype (MY/08/065) only, when compared to mock-infected mouse brains. To identify the genes involved in host immune-related responses, the filtered genes were uploaded to DAVID - Bioinformatics Resources 6.7 (https://david.ncifcrf.gov/tools.jsp) for functional annotation and cluster analysis.

3.5.4 TaqMan array microfluidic card validation

A total of 45 immune-related genes were selected for confirmation of expression based on previous gene expression and proteomic studies on SINV (Ryman and Klimstra, 2008; Johnston *et al.*, 2001), SFV (McKimmie *et al.*, 2006), VEEV (Koterski *et al.*, 2007; Sharma *et al.*, 2008; Sharma and Maheshwari, 2009), JEV (Saha and Rangarajan, 2003; Gupta and Rao, 2011; Yang *et al.*, 2011), WNV (Venter *et al.*, 2005), rabies (Prosniak *et al.*, 2001; Saha and Rangarajan, 2003; Wang *et al.*, 2005), prions (Sorensen *et al.*, 2008), and DENV (Fink *et al.*, 2007; Bordignon *et al.*, 2008; de Kruif *et al.*, 2008). The selected genes chosen were functional annotated genes involved in apoptosis, autophagy, necrosis, inflammation, innate and adaptive immune responses, and signalling pathways such as TLR, NF-κB, Jak-STAT, NOD-like receptor, T cell

receptor, RIG-I-like receptor, and TNF signalling pathways. The 18S, GAPDH, GUSB, and HPRT1 genes were used as reference genes.

The generated gene lists of interest were fabricated on the TaqMan array microfluidic card (Applied Biosystems). Each well which represents a gene of interest was prefabricated with primers. Following the manufacturer's protocol, 400 ng of total RNA from each of three biological replicates were selected for synthesis of single-stranded cDNA using High Capacity RNA-to-cDNA Kit (Applied Biosystems). The cDNA was mixed with TaqMan Fast Advanced Master Mix (Applied Biosystems) before being loaded into the TaqMan array microfluidic card. Validation was performed with the Quant Studio 12K Flex Real-Time PCR System (Applied Biosystems). Cycling parameters were 50ºC for 2 minutes, 92ºC for 10 minutes, then 40 cycles of 97ºC for 1 second and 62ºC for 20 seconds. The data was extracted and analyzed with Expression Suite Software 1.0.3 (Applied Biosystems) with the Benjamini-Hochberg false discovery rate test. Expression of selected immune-related genes with relative quantification ≥ 1.5 or ≤ 1.5 in either MY/06/37348- or MY/08/065-infected mice were compared between MY/06/37348- and MY/08/065-infected mice using the independent t-test ($P < 0.01$). The significantly regulated genes were uploaded to STRING (http://string-db.org) for network analysis to determine gene interaction.

3.6 Statistical analysis

The Mann-Whitney test was used to compare medians of non-parametric experiment results for *in vitro* and *in vivo* replication assays. Survival of mice was analysed using the Kaplan-Meier survival curve. One-way ANOVA was performed on gene expression study while the independent t-test was performed for qRT-PCR comparison between virus isolates MY/06/37348 and MY/08/065. All statistical analyses were performed using SPSS 20 (IBM) and P value < 0.05 or P value < 0.01 were considered as statistically significant as stated.

CHAPTER 4

RESULTS

4.1 *In vitro* replication of chikungunya virus

The replication kinetics of the MY/06/37348 (Asian genotype) and MY/08/065 (ECSA genotype) isolates in Vero and SK-N-MC neuronal cells were compared.

4.1.1 Microscopic observation

Vero and SK-N-MC cells were infected with the two virus isolates MY/06/37348 and MY/08/065, and observed daily for CPE. The infection led to rounded cells, granulation and disintegration of cell bodies, detachment, and lysis, followed by death. Vero cells appeared healthy before 24 hours post-infection (hpi) (Figure 4.1), while SK-N-MC cells appeared healthy before 48 hpi (Figure 4.2).

Microscopic observation of Vero cells showed that MY/08/065 caused more CPE than MY/06/37348 at 24 hpi (Figures 4.1d and f). However, Vero cells infected with either virus began to detach from the growth surface and showed similar CPE at 48 hpi (Figures 4.1e and g). In SK-N-MC cells, MY/08/065 caused more than 70% CPE at 72 hpi, 24 hours earlier than MY/06/37348 (Figures 4.2i and l). Mock-infected cells, which act as the negative control, appeared healthy up to seven days post-infection (dpi) for Vero cells and 14 dpi for SK-N-MC cells, before cells died due to over-confluency. Microscopic results suggest that MY/08/065 replicates at a greater rate than MY/06/37348 in Vero and SK-N-MC cells.

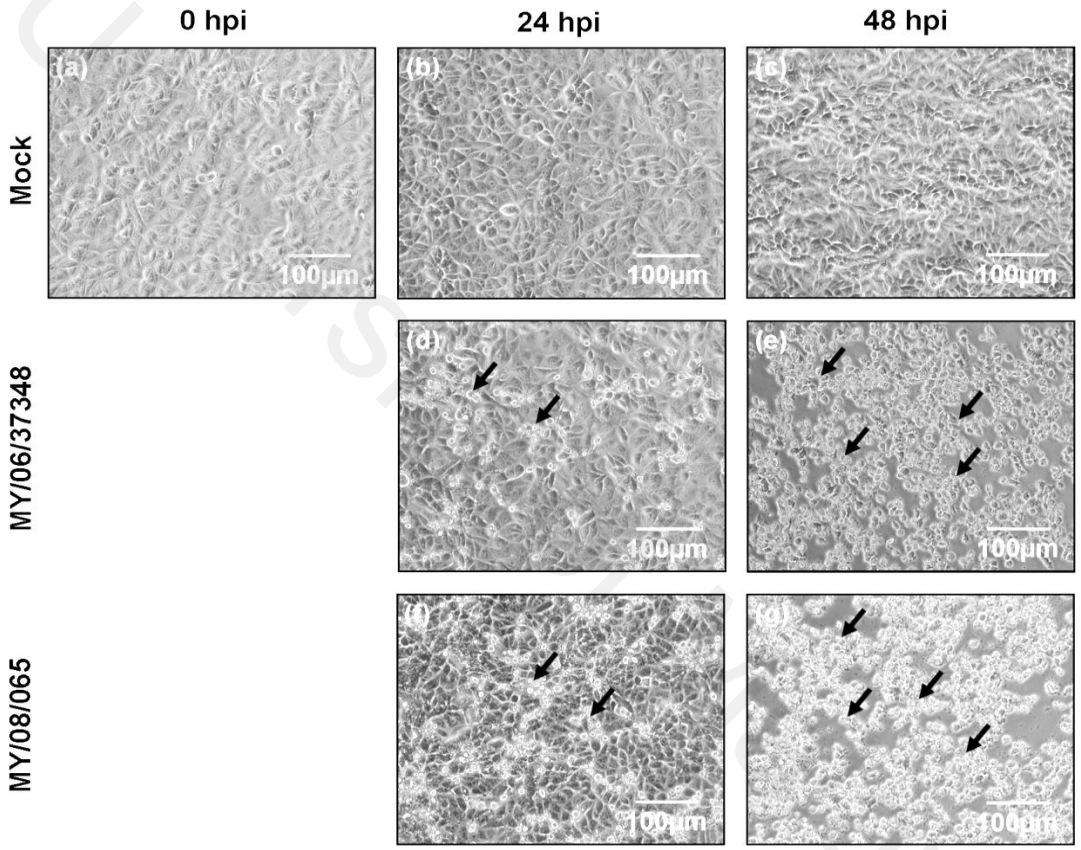

Figure 4.1: Daily observation of CPE in CHIKV-infected Vero cells. At 0, 24 and 48 hpi, the mock-infected cells appeared as a monolayer of cuboidal cells (a-c). Vero cells were infected with either virus isolate MY/06/37348 (d, e) or MY/08/065 (f, g). Infected cells started to become distorted at 24 hpi, an indication of CPE (d, f; arrows). By 48 hpi, 70% of the cells showed CPE with rounded and refractive cells, and had detached from the growth surface (e, g). Magnification: ×20.

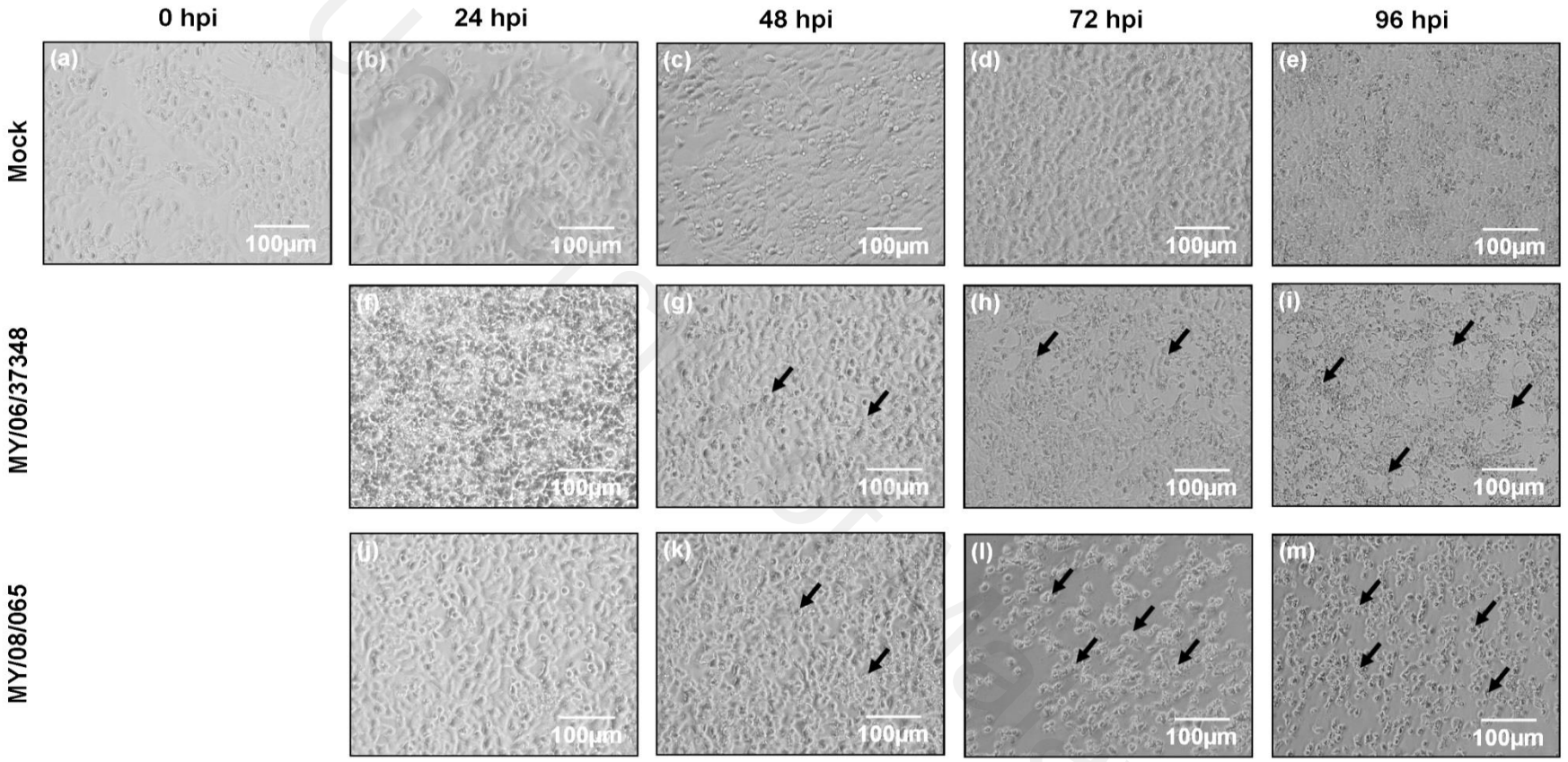

Figure 4.2: Daily observation of CPE in CHIKV-infected SK-N-MC cells. From 0 to 96 hpi, the mock-infected cells appeared as a monolayer of cells (a-e). SK-N-MC cells were infected with either virus isolate MY/06/37348 (f, i) or MY/08/065 (j, m). Infected cells started to become distorted at 48 hpi, an indication of CPE (g-i, k-m; arrows). At 72 and 96 hpi, 70% of the cells showed CPE with rounded and refractive cells, and had detached from the growth surface (i, l). Magnification: ×20.

4.1.2 Confirmation of CHIKV infection using immunofluorescence staining

Immunofluorescence staining was performed to confirm CHIKV infection of Vero and SK-N-MC cells at 24 hpi (Figures 4.3 and 4.4). The previously prepared primary antibody, in-house polyclonal rabbit anti-CHIKV was bound to secondary antibody, goat anti-rabbit IgG conjugated with FITC. Positive-infected cells stained as green fluorescence. DAPI was used to stain the nuclei dark blue. The mock-infected cells did not show green fluorescence. Immunostaining of CHIKV antigen confirmed that MY/06/37348 and MY/08/065 infected both Vero and SK-N-MC cells.

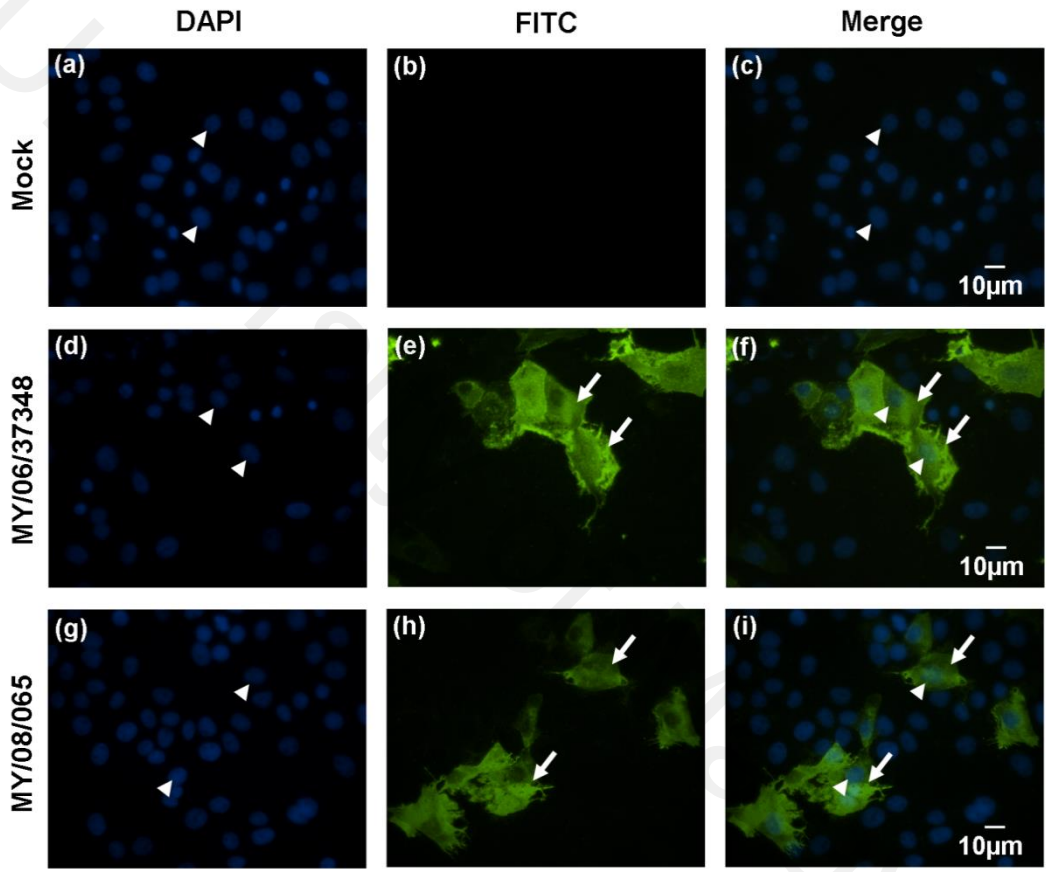

Figure 4.3: Confirmation of CHIKV infection in Vero cells by IF. Vero cells were mock-infected (a-c), or infected with either virus isolate MY/06/37348 (d-f) or MY/08/065 (g-i). At 24 hpi, CHIKV-infected cells were stained with FITC (green; arrows, ➞) (e, h). DAPI was used as counterstaining for nuclei (dark blue, arrowheads, ►). Magnification: ×60.

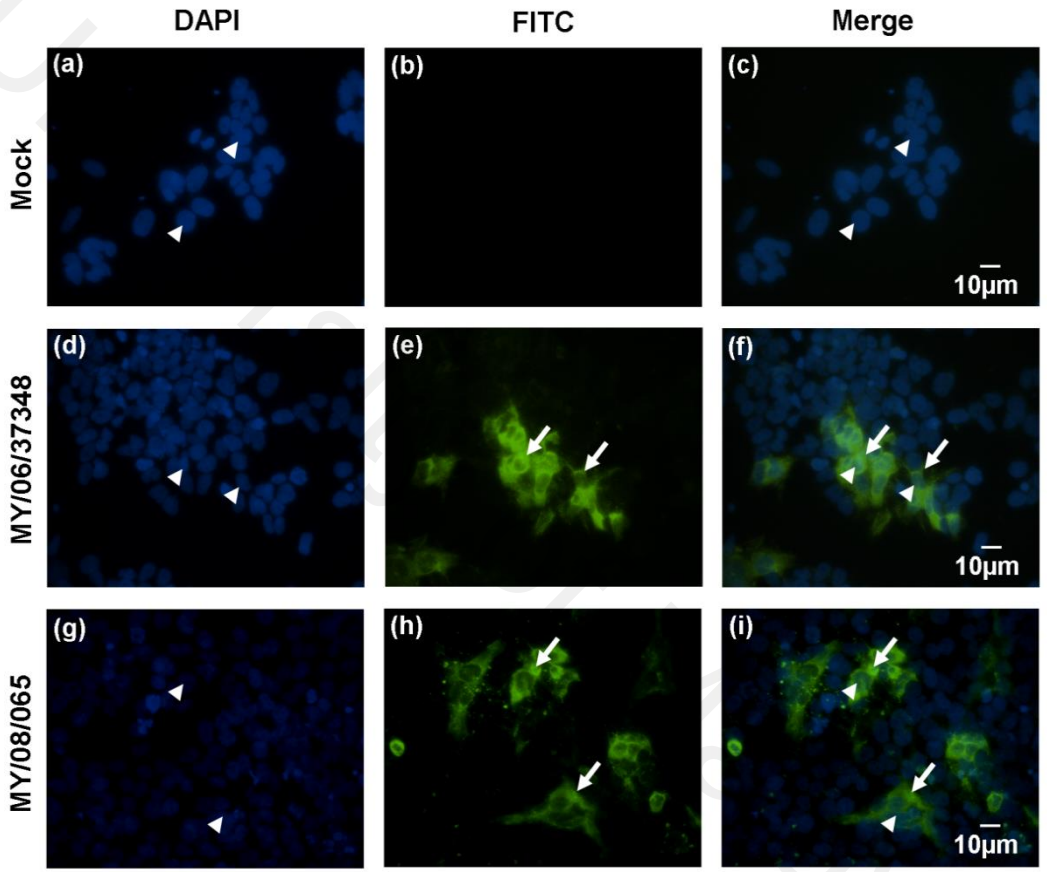

Figure 4.4: Confirmation of CHIKV infection in SK-N-MC cells by IF. SK-N-MC cells were mock-infected (a-c), or infected with either virus isolate MY/06/37348 (d-f) or MY/08/065 (g-i). At 24 hpi, CHIKV-infected cells were stained with FITC (green; arrows, ➞) (e, h). DAPI was used as counterstaining for nuclei (dark blue, arrowheads, ►). Magnification: ×60.

4.1.3 Validation of qRT-PCR

In-house strand-specific qRT-PCR assays for CHIKV were previously designed (Chiam *et al.*, 2013, see section 3.3.6.3). The positive-strand RNA qRT-PCR assay was used to measure CHIKV RNA in Vero and SK-N-MC cells, and mouse brains. The negative-strand RNA qRT-PCR assay was used to quantify replicative intermediate RNA in Vero and SK-N-MC cells, which is an indicator of active viral replication.

In order to validate the qRT-PCR assays before use, the limit of quantification (LOQ), amplification efficiency (Eff%) and specificity were determined in this study. The nsP3 positive-strand assay had an LOQ of 1 $\log_{10}$ RNA copies/reaction and 100.58% efficiency (Table 4.1, Figure 4.5a). The nsP3 negative-strand assay had an LOQ of 3 $\log_{10}$ RNA copies/reaction and 95.7% efficiency (Table 4.1, Figure 4.5b). To facilitate comparison between different rounds of experiments for each qRT-PCR assay, an ideal standard curve was achieved, with a regression coefficient (slope) between -3.2 to -3.4, and a correlation coefficient (R^2) between 0.9 to 1.1 during determination of LOQ and Eff%.

As a comparison, the strand-specific conventional PCR assays were found to be less sensitive with LOQs of 4 $\log_{10}$ RNA copies/reaction (Figure 4.6). The qRT-PCR assays did not detect DENV RNA (at 163.6 ng/µL) and SINV RNA (at 114.5 ng/µL), and were specific for both virus isolates MY/06/37348 and MY/08/065. When previously tested by others on templates containing both positive- and negative-strands of RNA, the nsP3 strand-specific assays were found to be highly specific, and did not detect the presence of the opposite strand RNA at concentrations of up to 9 $\log_{10}$ RNA copies/reaction (Chiam *et al.*, 2013).

Table 4.1: Performance characteristics of positive-strand and negative-strand RNA qRT-PCR assays.

Assay (strand)	LOQ (copies per reaction)	Slope	R^2	Efficiency (%)	Dynamic range (log_{10} copies)
nsP3 (+)	1 log_{10}	-3.31	0.999	100.6	1-9
nsP3 (-)	3 log_{10}	-3.42	1.000	95.7	3-9

LOQ: limit of quantification

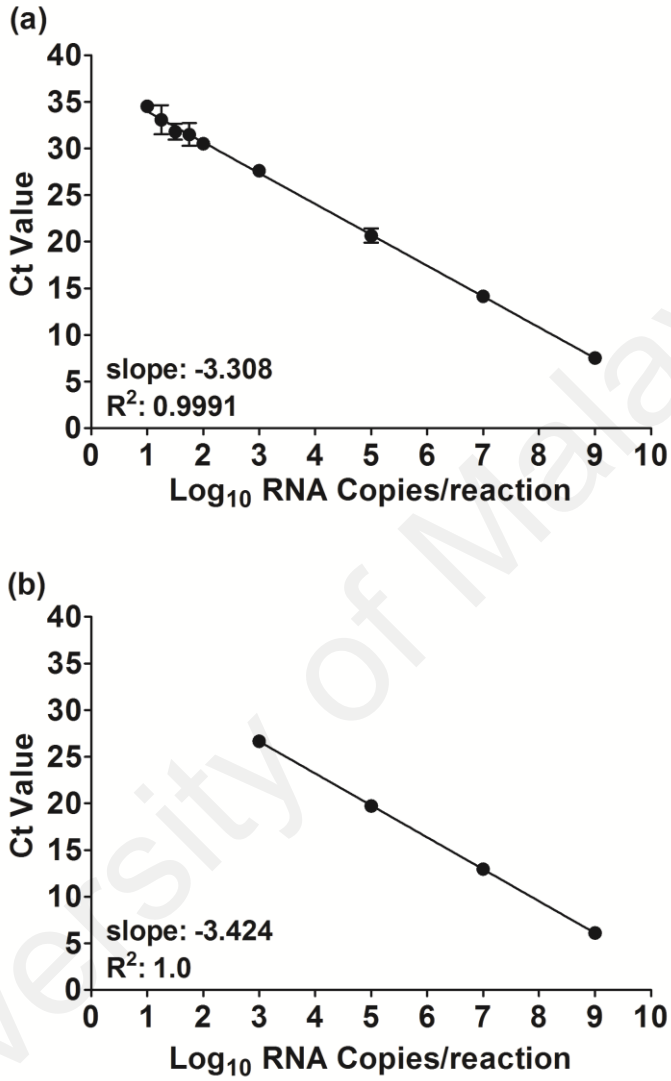

Figure 4.5: CHIKV strand-specific qRT-PCR standard curves. Strand-specific priming was performed during cDNA synthesis and qRT-PCR was performed using primers amplifying nsP3 regions. The qRT-PCR standard curves for nsP3 positive-strand RNA (a) and nsP3 negative-strand RNA (b) are shown.

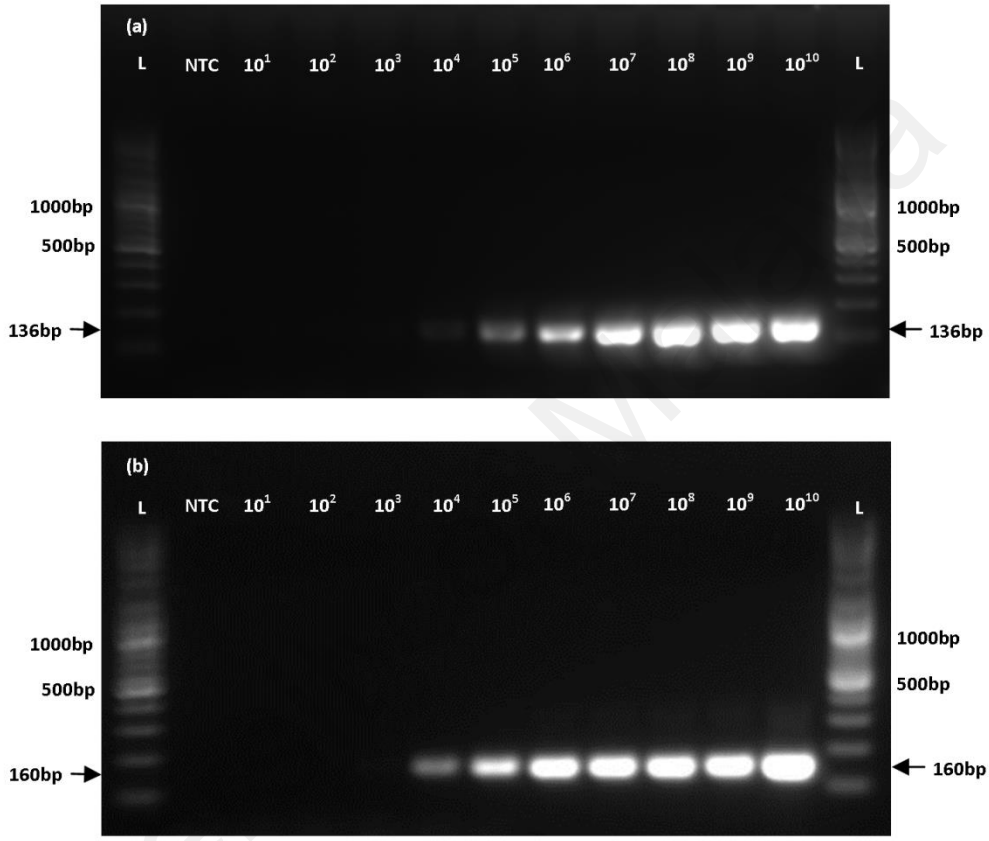

Figure 4.6: Conventional PCR detection. Serially-diluted cDNA was amplified, and PCR products were visualized by 1.5% agarose gel analysis and GelRed staining for nsP3 positive-strand RNA (a) and nsP3 negative-strand RNA (b). NTC: no template control; lane L: ladder (100 bp).

4.1.4 Virus replication *in vitro*

The replication kinetics of CHIKV in Vero and SK-N-MC cells were determined by titration and qRT-PCR. In Vero cells, MY/06/37348 reached peak mean virus titres of approximately 10^7 $TCID_{50}$/mL at 32 hpi (Figure 4.7ai) and RNA copies of approximately 10^{12} RNA copies/mL at 40 hpi (Figure 4.7aii). MY/08/065 reached peak mean virus titres of approximately 10^7 $TCID_{50}$/mL at 32 hpi and RNA copies of approximately 10^{10} RNA copies/mL at 24 hpi. The nsP3 negative-strand RNA copies of both virus isolates increased exponentially in the first 16 to 24 hours in Vero cells (Figure 4.7aiii).

In SK-N-MC cells, MY/06/37348 reached peak mean viral titres of approximately 10^4 $TCID_{50}$/mL and RNA copies of approximately 10^{12} RNA copies/mL at 32 hpi, while MY/08/065 reached peak mean viral titres of approximately 10^6 $TCID_{50}$/mL and RNA copies of approximately 10^{12} RNA copies/mL later at 64 hpi (Figures 4.7bi and bii). The nsP3 negative-strand RNA copies of both virus isolates increased exponentially in the first 32 hours in SK-N-MC cells (Figure 4.7biii).

MY/08/065 reached significantly higher viral titres than MY/06/37348 in both Vero and SK-N-MC cells. This was seen during most of the SK-N-MC infection, but only in the post-peak timepoints in Vero cells. However, MY/06/37348 had significantly higher positive-strand RNA copies in Vero cells. Analysis of negative-strand RNA copies, which indicate viral genomic replication of positive-strand viruses, showed little difference between the two viruses in each cell line, except for a higher level of MY/08/065 at a single timepoint.

In summary, both virus isolates were found to infect Vero and SK-N-MC cells. However, MY/08/065 was able to cause more CPE at early stages and reached higher viral titres when compared to MY/06/37348. This suggests that MY/08/065 replicated more effectively to produce infectious virus than MY/06/37348 in cells, despite the higher amounts of viral RNA detected in MY/06/37348-infected Vero cells.

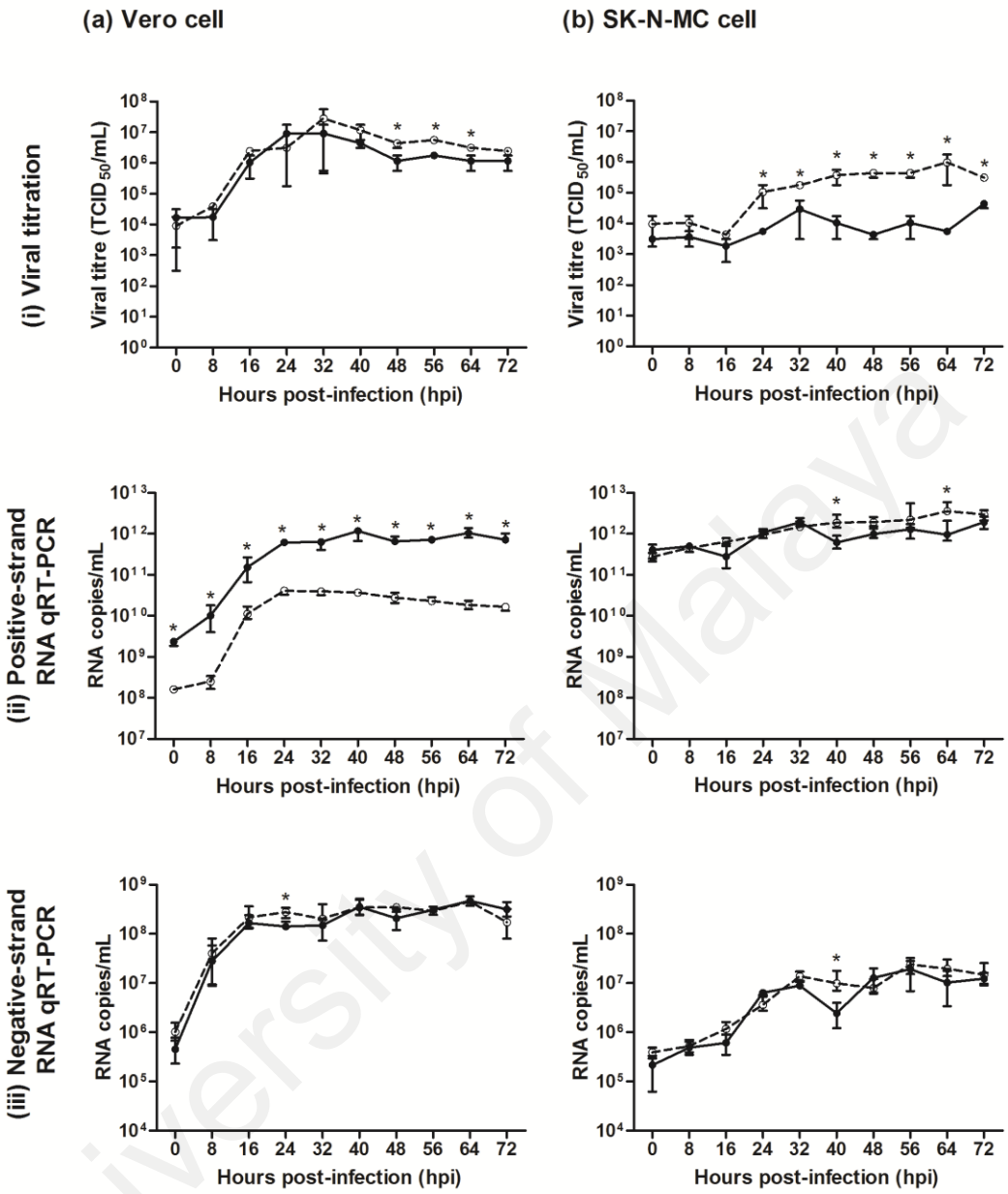

Figure 4.7: *In vitro* comparative replication kinetics of Malaysian CHIKV strains. Vero cells (a) and SK-N-MC cells (b) were infected with either virus isolate MY/06/37348 (●), or MY/08/065 (○). Replication was measured by virus titration (i), and RNA quantification for positive-strand RNA (ii) and negative-strand RNA (iii). Median ± interquartile ranges of 3 independent experiments are plotted. Asterisks (*) indicate *P* values < 0.05.

4.2 CHIKV neurovirulence in mice

As CHIKV was found to infect SK-N-MC human neuroepithelioma cells, the objective of this part of the study was to compare the neurovirulence of MY/06/37348 and MY/08/065 following intracranial inoculation in adult and suckling mice.

4.2.1 Signs of illness and survival

Lower weight gain was observed among suckling mice inoculated with either virus isolate MY/06/37348 or MY/08/065 compared to control mice inoculated with serum-free medium (Figure 4.8a). Mice infected with MY/06/37348 gained significantly less weight compared to control mice from 2 to 11 dpi, while mice infected with MY/08/065 gained less weight than control mice at 3 and 4 dpi. Suckling mice inoculated with CHIKV showed lethargy, hair loss around the inoculation site on the head, and hind limb paralysis compared to control mice. Suckling mice inoculated with MY/06/37348 showed 90.5% mortality and mean time to death of 7.2 days, which was significantly different from suckling mice inoculated with MY/08/065, which showed 60.0% mortality and mean time to death of 9.0 days (Figure 4.8b).

The first death in suckling mice inoculated with MY/06/37348 was recorded at 4 dpi, with the highest number of deaths recorded at 4 and 6 dpi. Meanwhile, the first death in suckling mice inoculated with MY/08/065 was recorded at 2 dpi, with the highest number of deaths recorded at 5 dpi. Infection with either virus isolate led to similar survival rates in the first 5 dpi, after which the mortality of MY/06/37348-infected suckling mice increased at a faster rate. Only two mock-infected suckling mice (6.1%) were found dead at 2 and 9 dpi, and the rest survived throughout the experiments. Analysis with the log-rank test showed that total survival of MY/06/37348-, MY/08/065-, and mock-infected suckling mice was significantly different ($\chi^2 = 49.2$, *P*

< 0.05). Overall, suckling mice inoculated with MY/06/37348 had higher mortality than mice inoculated with MY/08/065.

The adult female mice inoculated intracerebrally with CHIKV did not show any signs of illness and did not die (results not shown). The higher mortality and severe clinical signs observed in suckling mice show that the outcome of CHIKV infection in mice is age-dependent.

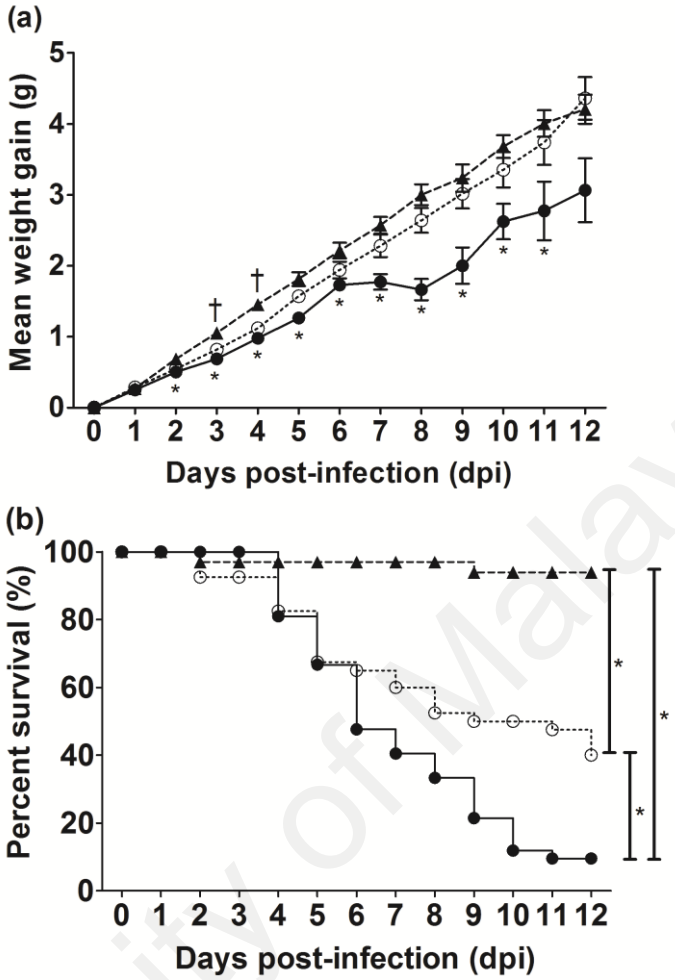

Figure 4.8: Weight and survival of suckling mice inoculated intracerebrally with Malaysian CHIKV strains. Suckling mice were intracerebrally inoculated with either virus isolate MY/06/37348 (●, n = 42), MY/08/065 (○, n = 40), or serum-free medium (▲, n = 33). Compared to control suckling mice, mice inoculated with MY/08/065 († shows significant differences), or MY/06/37348 (* shows significant differences) had reduced weight gain. Mean ± SEM of 3 independent experiments are shown (a). The survival of suckling mice inoculated with MY/06/37348 was significantly reduced ($P < 0.05$) compared to mice inoculated with MY/08/065 or control mice (b). Significantly different comparisons are indicated by * ($P < 0.05$).

4.2.2 Virus replication *in vivo*

The replication of CHIKV in brains of suckling and adult mice was determined by using titration and qRT-PCR. In suckling mice, both virus isolates reached peak mean virus titres at 2 dpi (Figure 4.9ai) and peak RNA copies at 1 dpi (Figure 4.9aii). There was a significant difference in titres at only one timepoint, with MY/08/065 having higher virus titres than MY/06/37348 at 8 dpi. At 8 dpi, viral RNA remained detectable at 10^7 to 10^8 RNA copies/g, while viral titres were approximately 10^1 $TCID_{50}$/g.

In adult female mice, MY/06/37348 and MY/08/065 reached peak virus titres at 2 and 4 dpi, respectively (Figures 4.9bi and bii). Both virus isolates reached peak RNA copies at 4 dpi and remained detectable at approximately 10^9 to 10^{10} RNA copies/g from 6 dpi onwards, when the viral titre was no longer detectable. Compared to MY/08/065, MY/06/37348 reached a significantly higher virus titre at 1 dpi, and significantly greater RNA copies at 1 and 2 dpi.

In suckling mice, the similar viral loads seen with each virus isolate suggests that viral replication alone does not explain the higher mortality and more severe disease following infection with MY/06/37348. This is also supported by the findings in adult mice infected with either virus isolate, which did not show differences in disease or mortality despite greater replication of MY/06/37348 in the first 1 to 2 dpi.

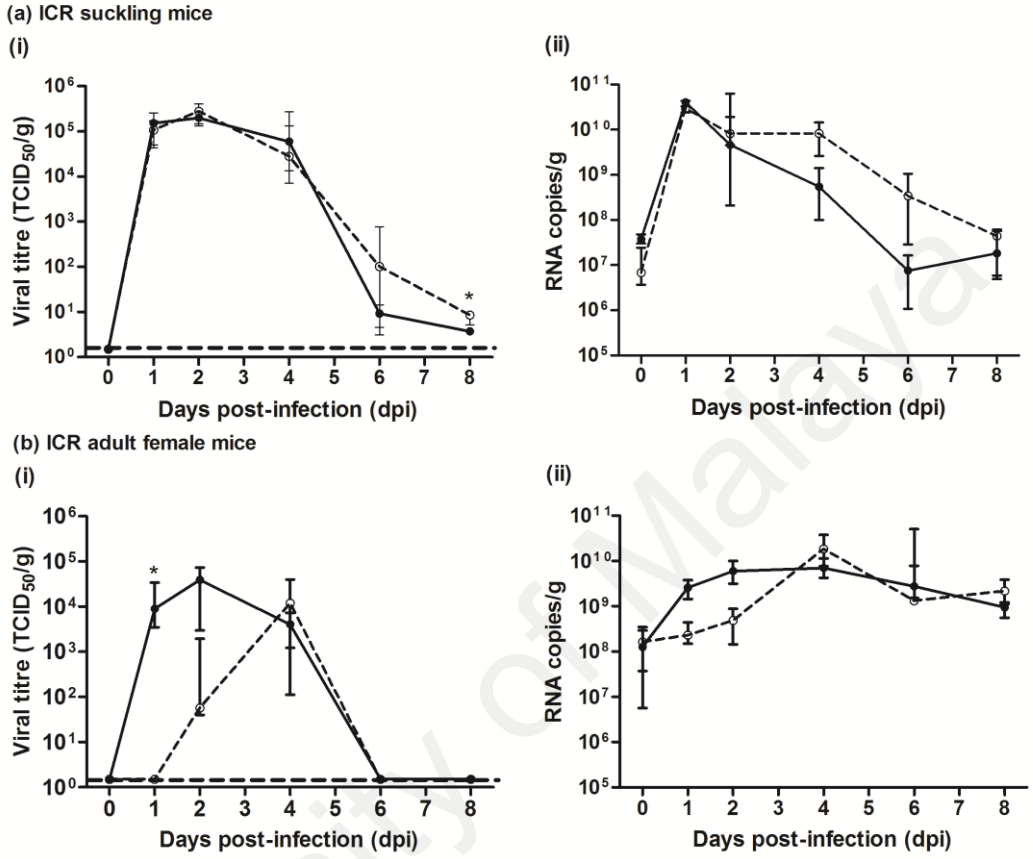

Figure 4.9: *In vivo* comparative replication kinetics of Malaysian CHIKV strains. (a) ICR suckling mice were inoculated with either virus isolate MY/06/37348 (●, n = 16), or MY/08/065 (○, n = 17), and (b) ICR adult mice were inoculated with either virus isolate MY/06/37348 (●, n = 22), or MY/08/065 (○, n = 21). Replication was measured by using virus titration (i) and RNA quantification (ii). Median ± interquartile ranges of 3 independent experiments are plotted. * indicates *P* values < 0.05. The dashed line indicates the limit of detection of the virus titration assay at 1.5 $TCID_{50}$/g.

4.2.3 Histopathology of infected mice

Histopathological changes in both infected suckling mice and adult mice were examined. The adult six-week-old female mice did not show any notable pathologic findings attributable to intracranial inoculation of CHIKV (data not shown). In suckling mice infected with either virus isolate MY/06/37348 or MY/08/065, the presence of apoptotic bodies, necrosis, inflammatory cells, and perivascular cuffing was mainly observed in the olfactory bulb, thalamus, cerebral cortex, cerebellum, and hippocampus (Figure 4.10). Apoptosis was observed earlier at 2 to 4 dpi for MY/06/37348-infected suckling mice than in MY/08/065-infected suckling mice, in which apoptosis was evident at 4 to 6 dpi. Necrosis, another type of cell death, was also observable at 2 to 4 dpi for MY/06/37348-infected suckling mice, while in MY/08/065-infected suckling mice necrosis was present for longer, up to 6 dpi. Meanwhile, inflammatory cells were found to be more abundant and consistent until 6 dpi in MY/08/065-infected suckling mice than in MY/06/37348-infected suckling mice, which only showed presence of inflammation at 2 dpi. Overall, in MY/06/37348-infected suckling mice, in which mortality was 90.5%, apoptosis and necrosis were seen during early stages of infection, while there was a shorter inflammatory response. MY/08/065-infected suckling mice showed similar mortality in the first 5 dpi but ultimately lower total mortality, and a longer and more profound inflammatory response, while apoptosis was seen later, and necrosis was present for longer.

Double immunofluorescence staining was carried out in brain tissue (Figure 4.11). CHIKV was found to localize in cells that had apoptosis activation as indicated by staining of cleaved caspase 3. CHIKV was also detected in astrocytes using GFAP staining and neuronal cells using MAP-2 staining.

To determine the distribution of CHIKV over time, the presence of CHIKV capsid in infected suckling mice brains was observed by immunohistochemical staining (summarised in Table 4.2). After MY/06/37348 inoculation into the left parietal area, CHIKV antigen was first seen at the left and right alveus, choroid plexus, and dorsal and ventral aspects of the third ventricle at 1 dpi (Figure 4.12). Other sites involved included the olfactory bulb and hippocampus. At 2 dpi, MY/06/37348 had spread to the left and right lateral ventricles, fourth ventricle, and the dorsal aspect of the cerebellum, and continued to be detectable in the left and right alveus, choroid plexus, the ventral aspect of third ventricle, and olfactory bulb. At 4 dpi, MY/06/37348 was still detectable in the same areas, and in addition, had spread to the cerebral aqueduct. By 6 dpi, CHIKV antigen was only detectable in the ventral aspects of the third and fourth ventricles, and olfactory bulb. At 8 dpi, no antigen was detected in the brain.

The spread of CHIKV was also determined following infection with MY/08/065 (Figure 4.13). CHIKV antigen was first found at the left and right alveus, right lateral ventricle, choroid plexus, dorsal and ventral aspect of the third ventricle, fourth ventricle, cerebral aqueduct, and thalamus at 1 and 2 dpi. Other sites involved included the olfactory bulb and cerebellum. The hippocampus only showed presence of MY/08/065 at 1 dpi. At 4 dpi, the olfactory bulb, left and right alveus, left lateral ventricle, ventral aspect of the third ventricle, fourth ventricle, cerebral aqueduct, and thalamus remained infected by MY/08/065. At 6 dpi, CHIKV antigen was only detected at the lateral ventricle, the ventral aspect of the third ventricle, left and right alveus, and left thalamus; by 8 dpi, CHIKV antigen was only present in the lateral and third ventricles.

Other non-CNS organs such as skeletal muscle, liver, and spleen were also stained to examine the extent of viral spread following intracerebral infection. Skeletal muscles of

the head at 6 dpi (Figures 4.14b) and thigh (Figures 4.14c and d), and liver (Figures 4.14f) at 8 dpi showed histopathological changes in both MY/06/37348- and MY/08/065-infected suckling mice. At 8 dpi, vacuolization and apoptotic bodies were seen in the liver, and abundant infiltrates, fragmented myocytes, and oedema were observed in thigh skeletal muscle, more so in MY/06/37348-infected suckling mice than MY/08/065-infected suckling mice. However, in skeletal muscle of the head, more inflammation was observed in MY/08/065-infected suckling mice than MY/06/37348-infected suckling mice, although no apoptotic bodies were observed. No pathological changes were seen at earlier timepoints. CHIKV antigen was also seen at non-CNS sites such as oral mucosal membranes, brown fat cells in the head, and head and thigh skeletal muscle, particularly following MY/06/37348 infection (Figure 4.15). MY/08/065 was only found to infect thigh skeletal muscle from 4 to 8 dpi. There were no pathological changes observed in the spleen and no CHIKV antigen staining observed in the spleen and liver. Overall, this suggests that inoculation of CHIKV into the mouse brain leads to both viral spread and induction of an immune response at distant sites outside the CNS after a few days.

Taken together, intracerebral inoculation of CHIKV in the left parietal area of mice led to spread of infection in the the brain ipsilaterally and contralaterally from the injection site to the cerebral cortex, cerebellum, hippocampus, thalamus, and olfactory bulb as well as the choroid plexus and lining of ependymal cells. CHIKV localised in astrocytes and neurons. Intracerebral inoculation of CHIKV also led to pathological changes and CHIKV spread to other non-CNS sites in the head such as brown fat cells, oral mucosal membranes, and skeletal muscle, as well as distant sites such as thigh skeletal muscle.

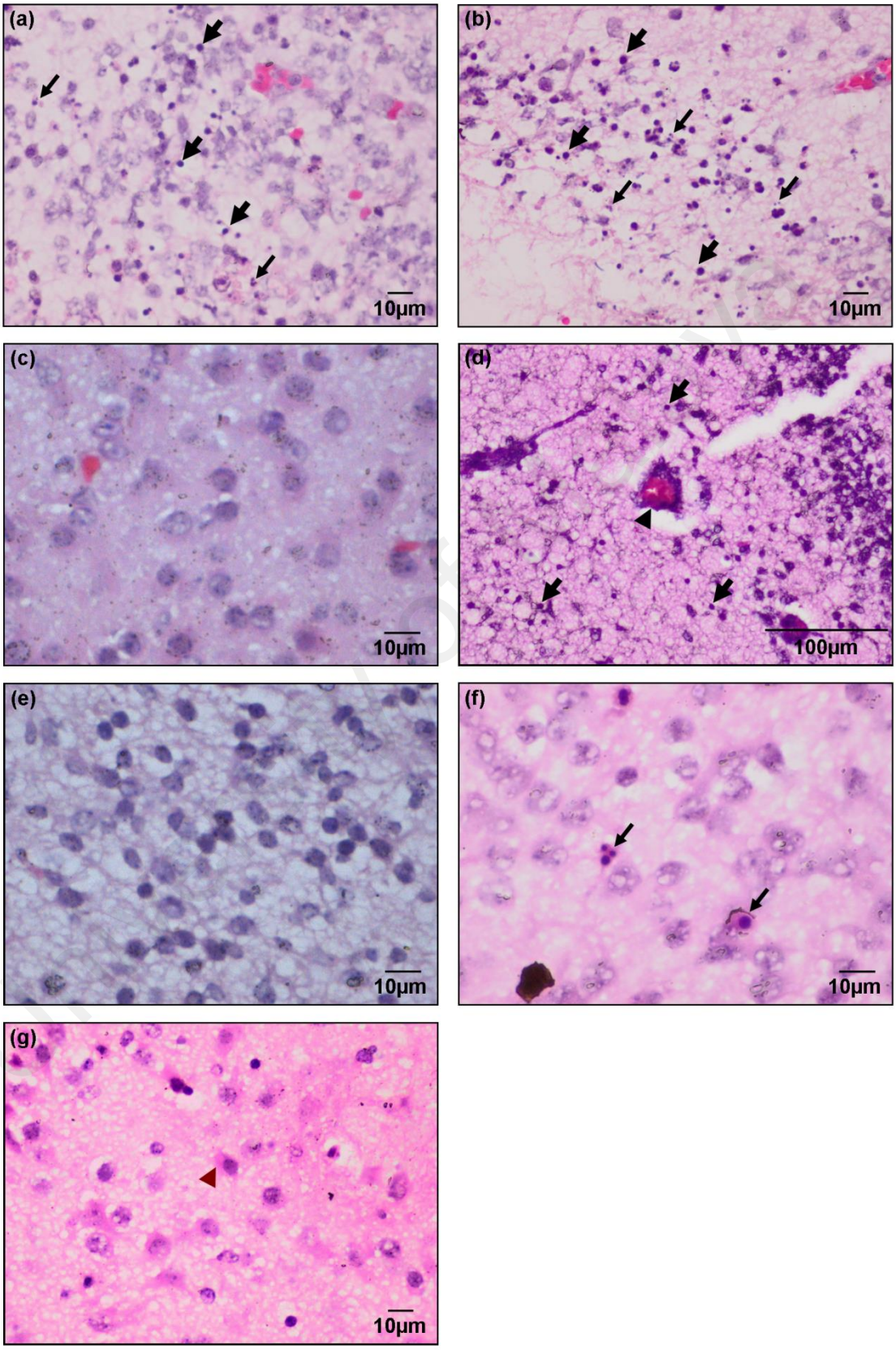
(a)
10µm
(b)
10µm
(c)
10µm
(d)
100µm
(e)
10µm
(f)
10µm
(g)
10µm

Figure 4.10, continued: Histopathological changes in brains of CHIKV-infected suckling mice. Haematoxylin and eosin sections of the cerebral cortex at 1 dpi (c) and cerebellum at 6 dpi (e) of the mock-infected mice are also shown. As histopathological appearances were similar for mice intracerebrally inoculated with either virus isolate MY/06/37348 or MY/08/065, representative sections are shown. For infected mice, stains of the olfactory bulb at 4 dpi (a), the thalamus at 4 dpi (b), the cerebral cortex at 6 dpi (d), the cerebellum at 6 dpi (f), and the hippocampus at 6 dpi (g) are shown. Focal haemorrhage (a) with presence of apoptotic bodies (thin arrows, ➞), inflammatory cells (thick arrows, ➡), perivascular cuffing (arrowheads, ►), and necrosis (maroon arrowheads, ►) can be seen. Magnification: ×20 (d); ×40 (a, b, g); ×60 (c, e, f).

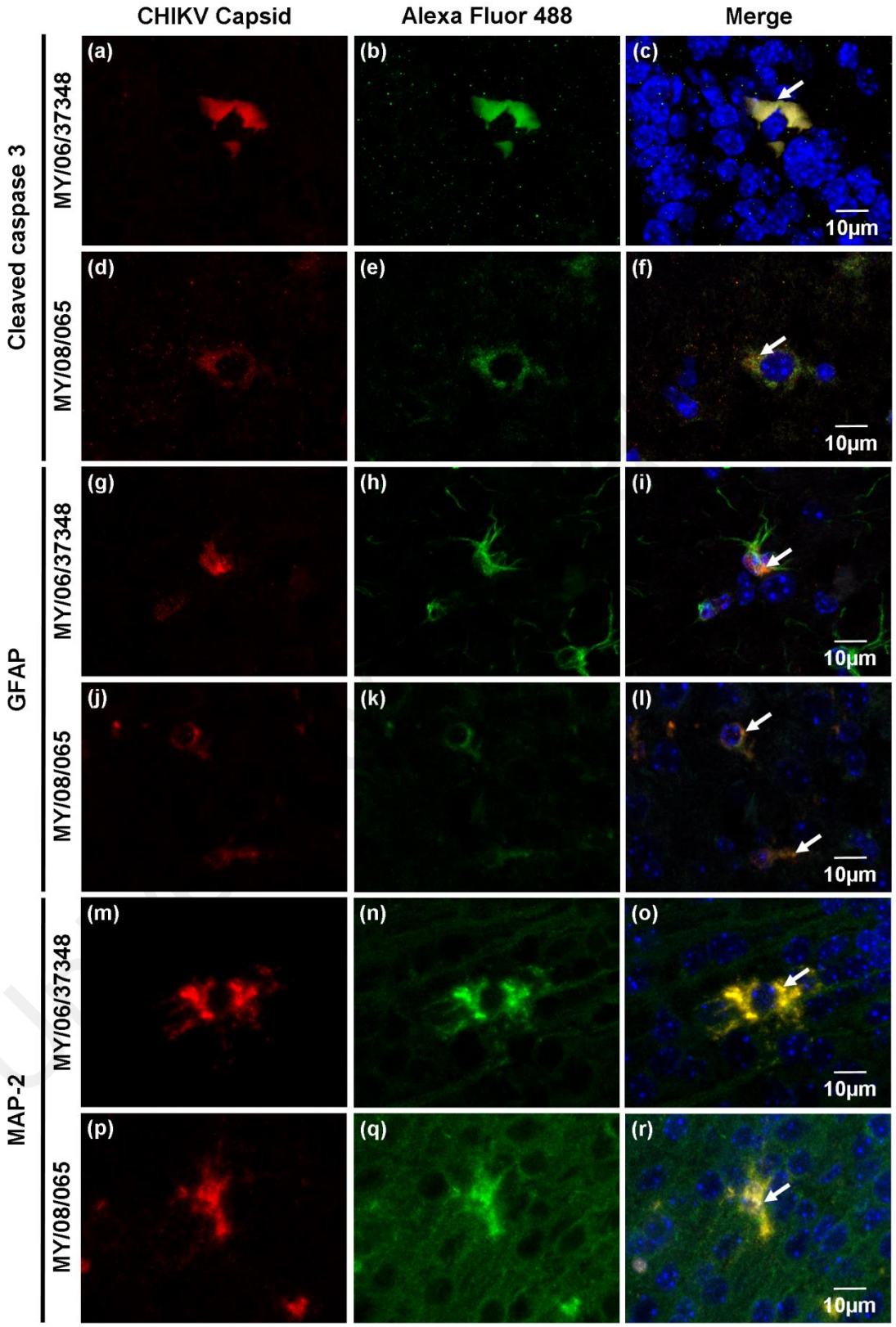
CHIKV Capsid
Alexa Fluor 488
Merge
Cleaved caspase 3
GFAP
MAP-2
MY/06/37348
MY/08/065
MY/06/37348
MY/08/065
MY/06/37348
MY/08/065
(a)
(b)
(c)
(d)
(e)
(f)
(g)
(h)
(i)
(j)
(k)
(l)
(m)
(n)
(o)
(p)
(q)
(r)
10µm

Figure 4.11, continued: Double immunofluorescence staining of the CHIKV-infected suckling mouse brains. Suckling mice were infected with either virus isolate MY/06/37348 or MY/08/065. Arrows indicate double immunofluorescence staining of CHIKV capsid with either cleaved caspase 3 (indicating activation of apoptosis; a-f), or GFAP (indicating astrocytes; g-l), or MAP-2 (indicating neurons; m-r). CHIKV capsid was stained with Liquid Permanent Red (red) while cleaved caspase 3, GFAP, and MAP-2 were stained with Alexa Fluor 488 (green). DAPI was used as counterstaining for nuclei (dark blue). Magnification: ×63.

Table 4.2: Summary of spread of Malaysian CHIKV strains in suckling mice, using CHIKV antigen staining.

Location	Days post-infection									
	MY/06/37348					MY/08/065				
	1	2	4	6	8	1	2	4	6	8
Olfactory bulb	✓	✓	✓	✓		✓	✓	✓		
Alveus	✓	✓	✓			✓	✓	✓	✓	
Choroid plexus	✓	✓				✓	✓			
Third ventricle (dorsal)	✓									
Third ventricle (ventral)	✓	✓	✓	✓		✓	✓	✓	✓	✓
Lateral ventricle (right)		✓	✓			✓				✓
Lateral ventricle (left)		✓	✓				✓	✓	✓	✓
Fourth ventricle		✓		✓		✓	✓	✓		
Cerebral aqueduct			✓			✓	✓	✓		
Hippocampus	✓	✓				✓				
Thalamus						✓	✓	✓	✓	
Cerebellum		✓				✓	✓			
Skeletal muscle (head)		✓	✓							
Skeletal muscle (thigh)			✓	✓	✓			✓	✓	✓

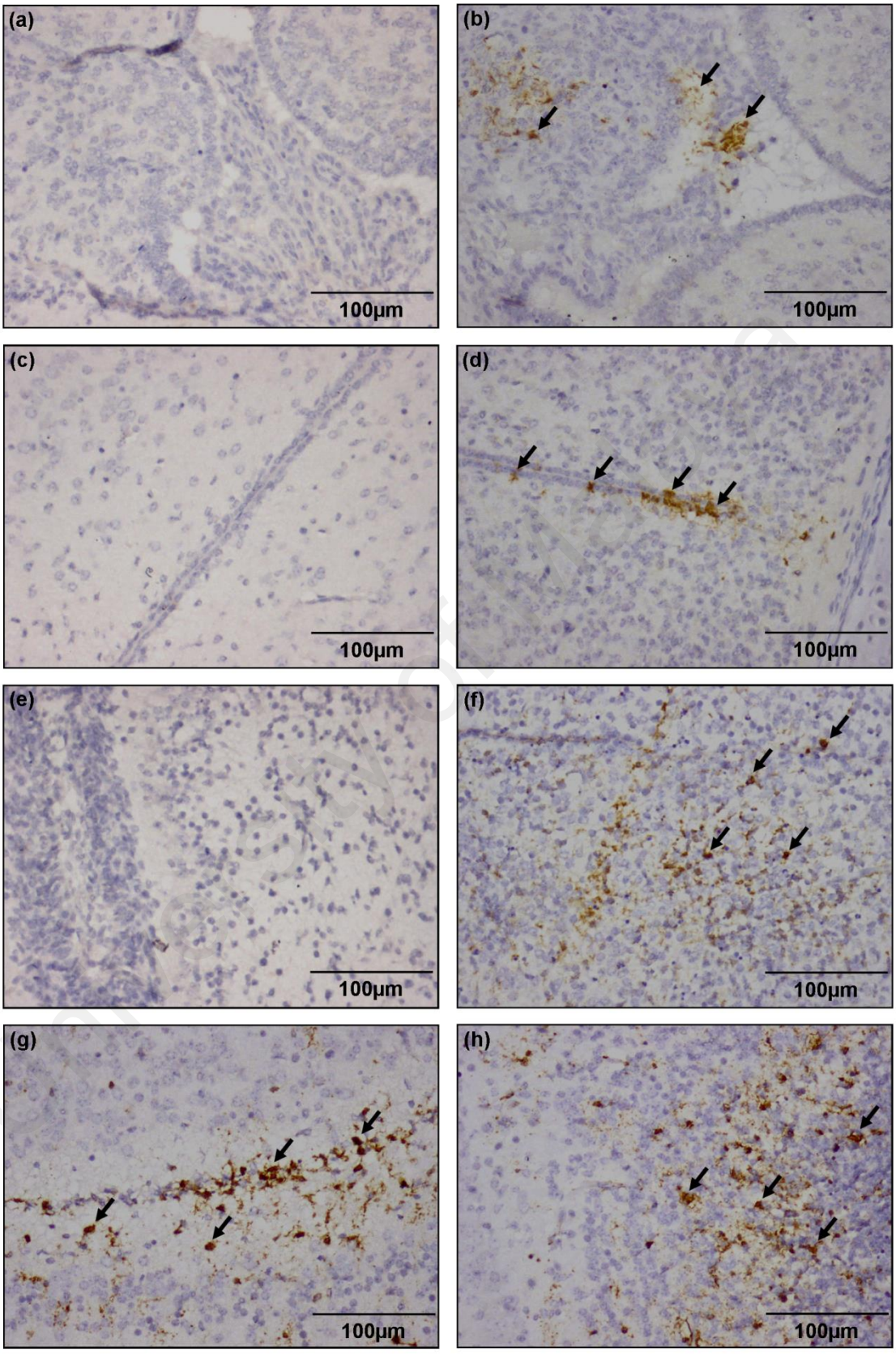
(a)
100µm
(b)
100µm
(c)
100µm
(d)
100µm
(e)
100µm
(f)
100µm
(g)
100µm
(h)
100µm

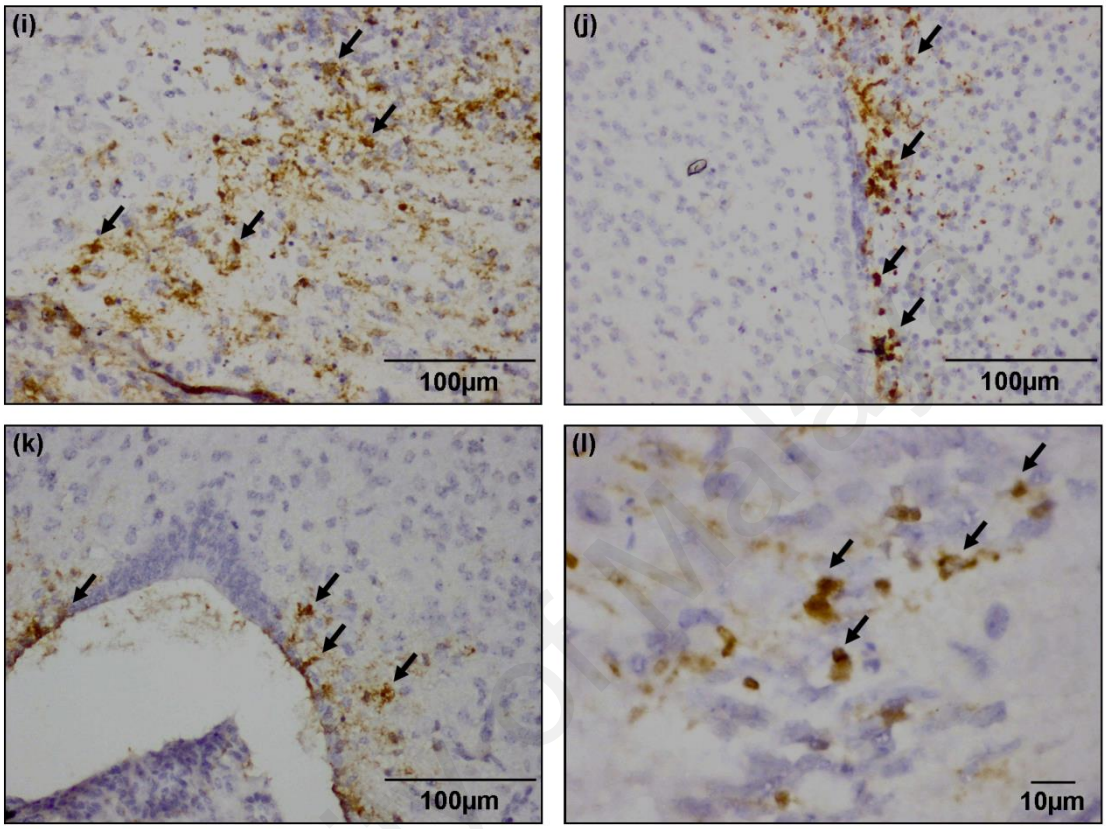

Figure 4.12, continued: Immunohistochemical staining of the brains of MY/06/37348-infected suckling mice. No CHIKV capsid antigen was detected in the choroid plexus (a), third ventricle (c), and cerebellum (e) of mock-infected mice. CHIKV capsid antigen (stained brown, arrows, ➞) was detected in the choroid plexus (b), third ventricle (d), cerebellum (f), alveus (g), olfactory bulb (h), hippocampus (i), lateral ventricle (j), fourth ventricle (k), and cerebral aqueduct (l). Immunohistochemical staining was performed with HRP, polyclonal rabbit anti-CHIKV capsid antibody, and haematoxylin counterstain. Magnification: ×20 (a-k); ×60 (l).

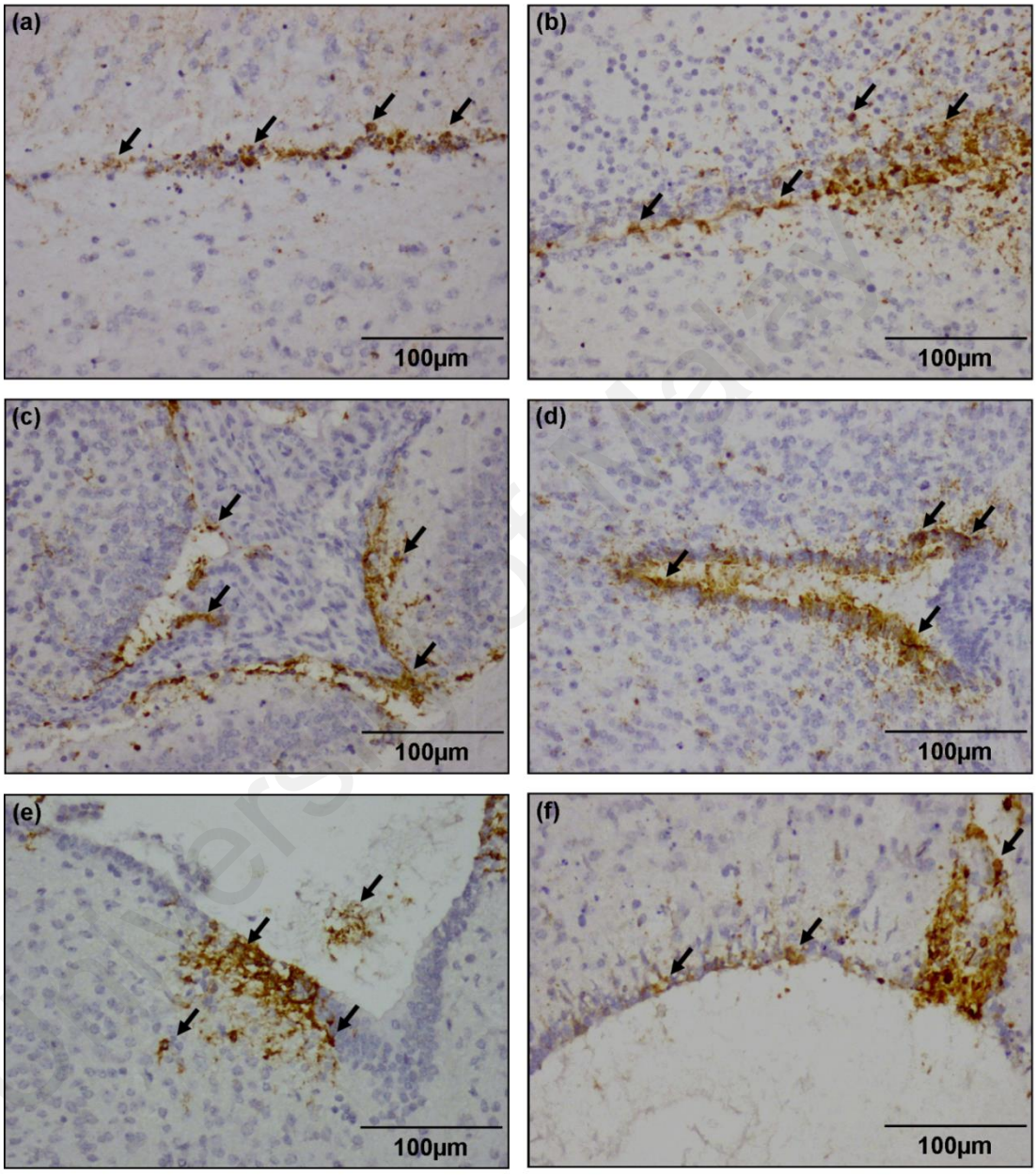
(a)
100µm
(b)
100µm
(c)
100µm
(d)
100µm
(e)
100µm
(f)
100µm

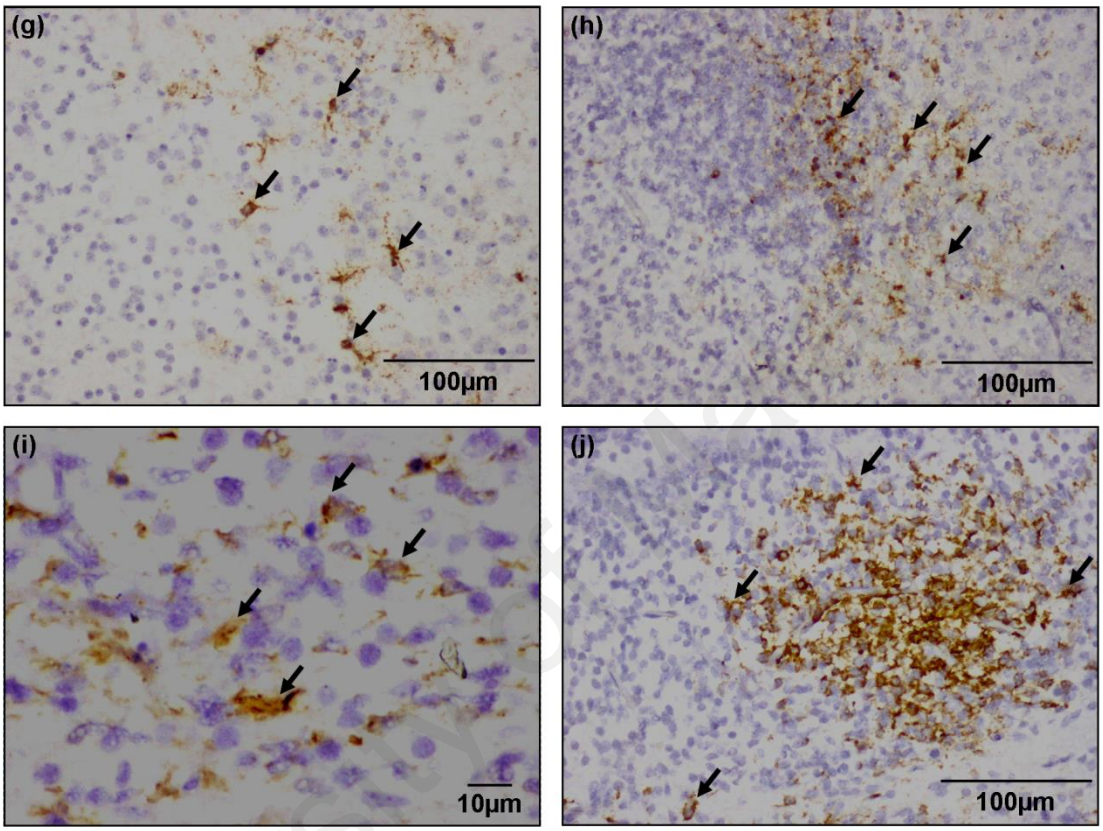

Figure 4.13, continued: Immunohistochemical staining of the brains of MY/08/065-infected suckling mice. CHIKV capsid antigen (stained brown, arrows, ➞) was detected in the alveus (a), lateral ventricle (b), choroid plexus (c), third ventricle (d), fourth ventricle (e), cerebral aqueduct (f), thalamus (g), olfactory bulb (h), cerebellum (i), and hippocampus (j). Immunohistochemical staining was performed with HRP, polyclonal rabbit anti-CHIKV capsid antibody, and haematoxylin counterstain. Magnification: ×20 (a-h, j); ×60 (i).

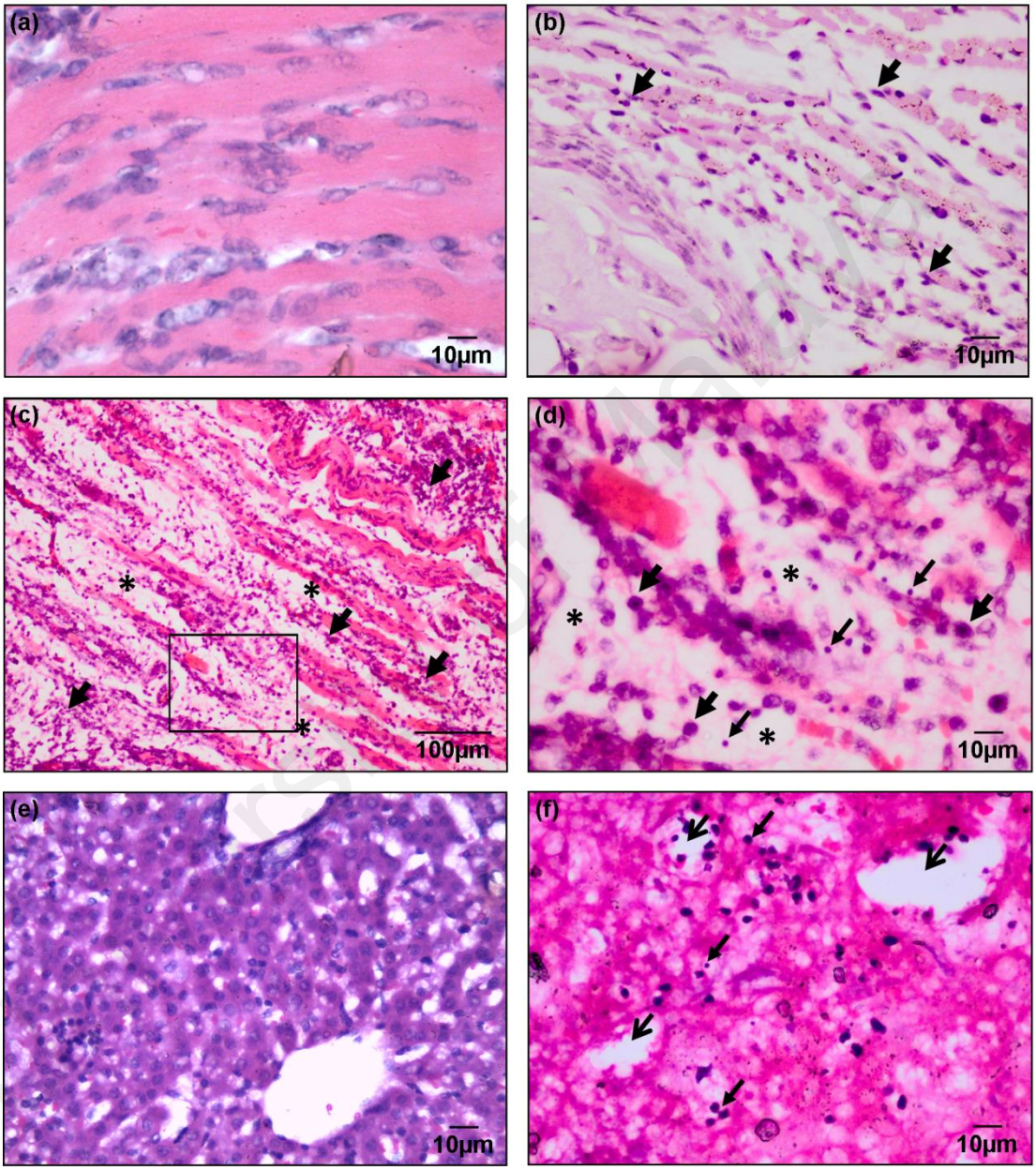
(a)
10µm
(b)
10µm
(c)
100µm
(d)
10µm
(e)
10µm
(f)
10µm

Figure 4.14, continued: Histopathological changes in liver and skeletal muscle of CHIKV-infected suckling mice. Haematoxylin and eosin sections of the thigh skeletal muscle (a) and liver (e) at 8 dpi of the mock-infected mice are also shown. Mice were intracerebrally inoculated with either virus isolate MY/06/37348 or MY/08/065. Skeletal muscle of the head (b) was harvested at 6 dpi, while thigh skeletal muscle (c, d) and liver (f) were harvested at 8 dpi. All tissue sections were stained with haematoxylin and eosin. Apoptotic bodies (thin arrows, ➞), inflammatory cells (thick arrows, ➡), vacuolization (open arrows, →), and oedema (*) can be seen. Magnification: ×10 (c); ×40 (a, b, d, e, f).

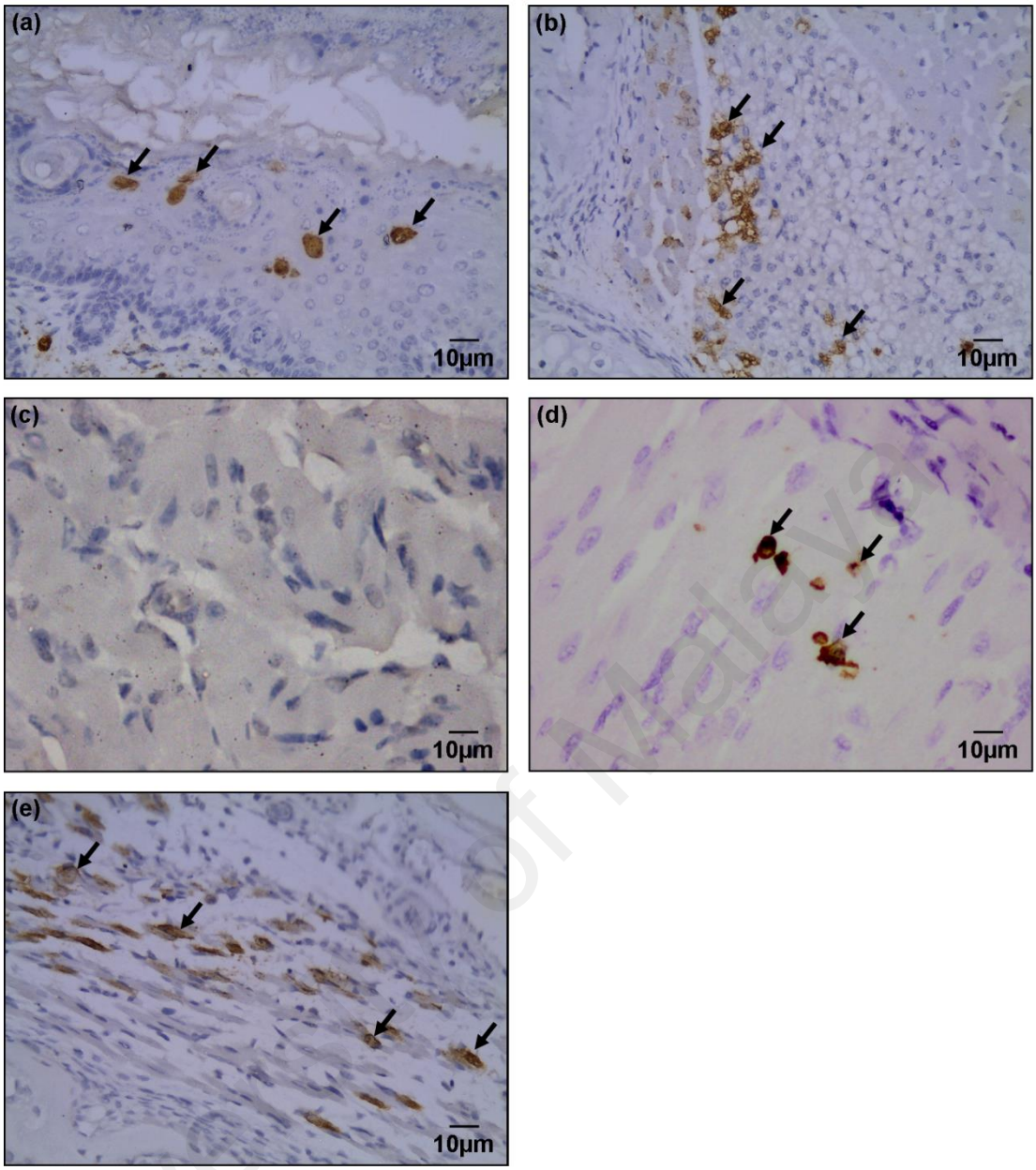

Figure 4.15: Immunohistochemical staining of the non-CNS organs of CHIKV-infected suckling mice. Immunohistochemical staining of the thigh skeletal muscle (c) of the mock-infected mice is also shown. Mice were intracerebrally inoculated with either virus isolate MY/06/37348 or MY/08/065. CHIKV capsid antigen (stained brown, arrows, ➞) was detected in the oral mucosa (a) and brown fat (b) at 2 dpi, thigh skeletal muscle at 6 dpi (d), and skeletal muscle of the head at 4 dpi (e). Immunohistochemical staining was performed with HRP, polyclonal rabbit anti-CHIKV capsid antibody, and haematoxylin counterstain. Magnification: ×40.

4.3 Transcriptomics of CHIKV-infected mouse brains

As apoptosis, necrosis, and inflammation were observed at different stages of infection with MY/06/37348 and MY/08/065, these viruses may induce differences in immune responses. Thus, the objective of this section of the study was to compare the gene expression of mouse brain cells infected with either virus isolate MY/06/37348 or MY/08/065.

4.3.1 Microarray analysis

The suckling mouse brain transcriptomic response was compared between MY/06/37348- and MY/08/065-infected suckling mice at 1 dpi (early infection) and 6 dpi (late infection), using mock-infected suckling mouse brains at the same timepoints as controls. In total, 19,945 probe sets on the microarray passed the Genespring filtration criteria (see section 3.5.3.4). Genes in CHIKV-infected suckling mice were considered to be differentially regulated if expressed at $\geq$ 2.0 or $\leq$ -2.0 fold levels compared to mock-infected suckling mice. Initial analysis found that 321 and 773 genes were significantly differentially regulated at 1 and 6 dpi, respectively.

Two biological replicates were performed for each experiment. The data were further filtered with Microsoft Excel (Microsoft, USA) to only select genes which were differentially regulated in the same direction in both biological replicates. There were 239 at 1 dpi, of which 178 (74.5%) genes were upregulated and 61 (25.5%) were downregulated; and 561 at 6 dpi, of which 454 (80.9%) genes were upregulated and 107 (19.1%) were downregulated (Figure 4.16).

To focus on the genes involved in the host immune response, the genes selected following filtration were uploaded to DAVID Bioinformatics Resources 6.7

(https://david.ncifcrf.gov/tools.jsp) for functional annotation. At 1 dpi, 7 immune-related genes involved in 25 biological processes were upregulated in MY/06/37348-infected suckling mice only (Figure 4.17), while 50 immune-related genes involved in 17 biological processes were upregulated in both MY/06/37348- and MY/08/065-infected suckling mice (Figure 4.18). No immune-related genes were significantly differentially regulated in MY/08/065 alone at 1 dpi, or in MY/06/37348 alone at 6 dpi. At 6 dpi, 2 immune-related genes involved in 3 biological processes were upregulated in MY/08/065 only (Figure 4.19), while 177 immune-related genes involved in 27 biological processes were upregulated in both MY/06/37348- and MY/08/065-infected suckling mice (Figure 4.20). In summary, a total of 189 immune-related genes in 52 immune-related biological processes were found to be differentially upregulated (summarised in Appendix 2). No genes were downregulated. Six major biological processes containing 138 genes were chosen for further study. These were antigen processing and presentation, apoptosis, defense response, immune response, inflammatory response, and response to virus, and are summarized in Figure 4.21.

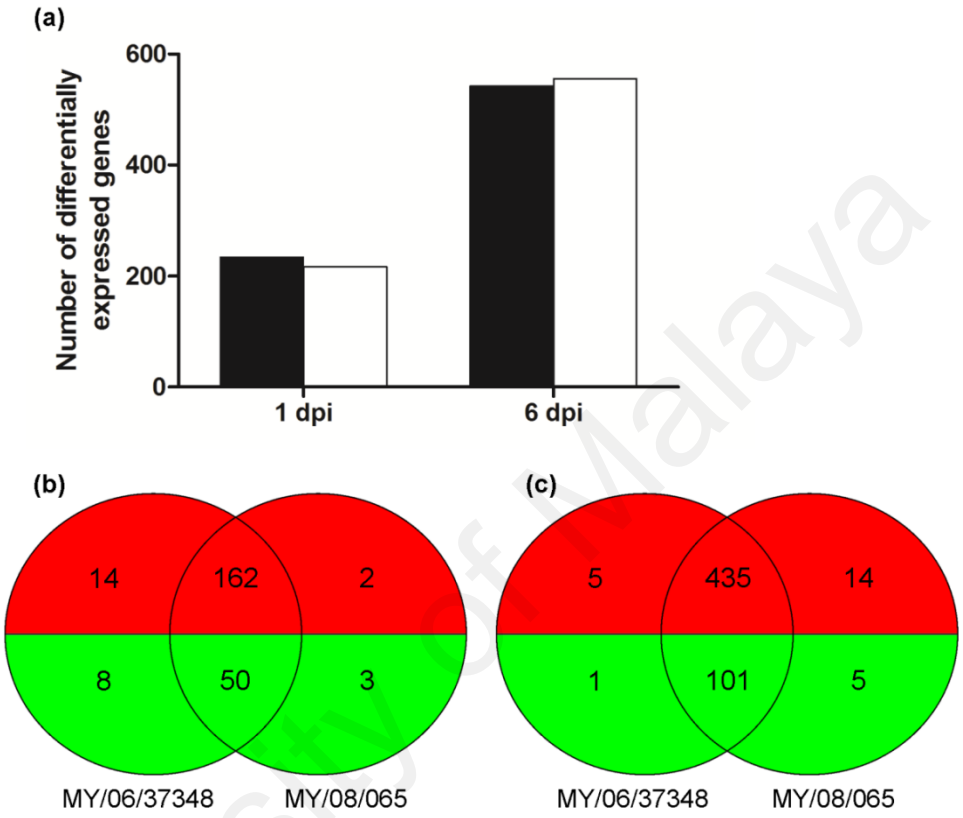

Figure 4.16: Expression profiles of infected mouse brains after filtering. Numbers of differentially expressed genes following infection with either virus isolate MY/06/37348 (black bar) or MY/08/065 (white bar) (a). Venn diagrams showing differentially expressed genes (downregulated: ≤ -2.0 fold change; upregulated: ≥ 2.0 fold change, $P < 0.05$) unique or common to MY/06/37348- and MY/08/065-infected suckling mice at 1 dpi (b) and 6 dpi (c). Down- and upregulated genes are indicated as green and red, respectively.

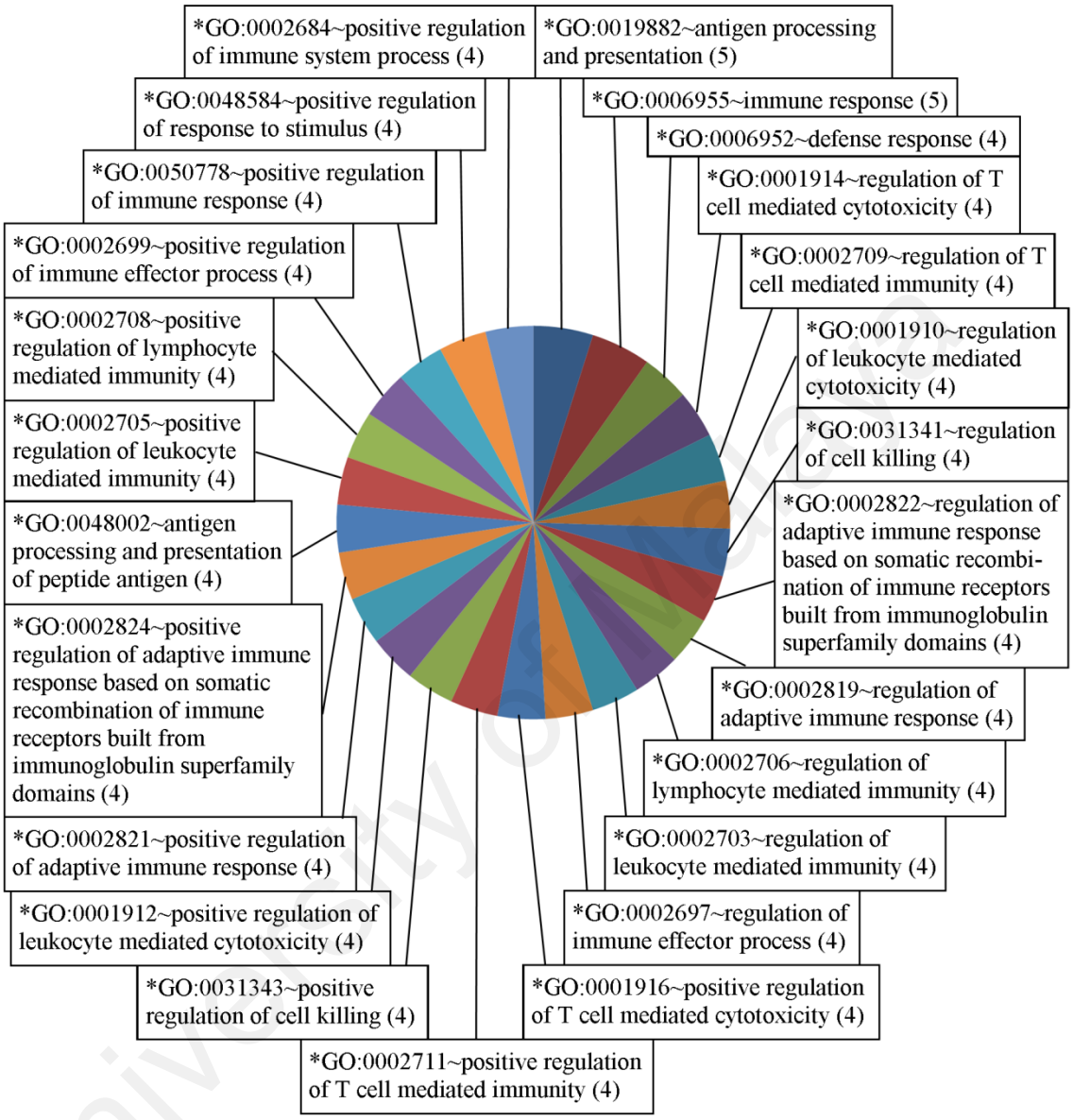

Figure 4.17: Gene ontology terms in the biological process category of upregulated genes of MY/06/37348-infected suckling mouse brains at 1 dpi. Pie chart showing differentially expressed genes (upregulated: ≥ 2.0 fold change, $P < 0.05$). Each coloured section represents a different biological process and the number of genes involved in each process is shown in brackets. * indicates biological processes involved in immune-related responses.

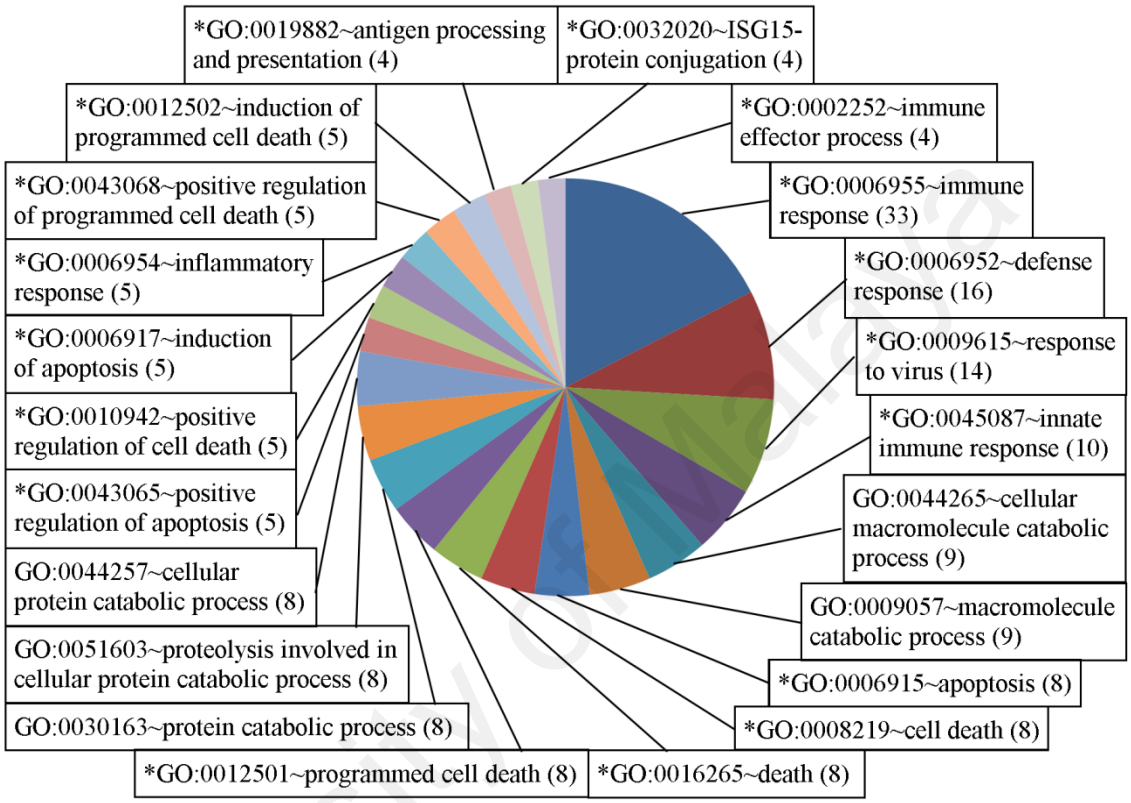

Figure 4.18: Gene ontology terms in the biological process category of upregulated genes of both MY/06/37348- and MY/08/065-infected suckling mouse brains at 1 dpi. Pie chart showing differentially expressed genes (upregulated: ≥ 2.0 fold change, $P < 0.05$). Each coloured section represents a different biological process and the number of genes involved in each process is shown in brackets. * indicates biological processes involved in immune-related responses.

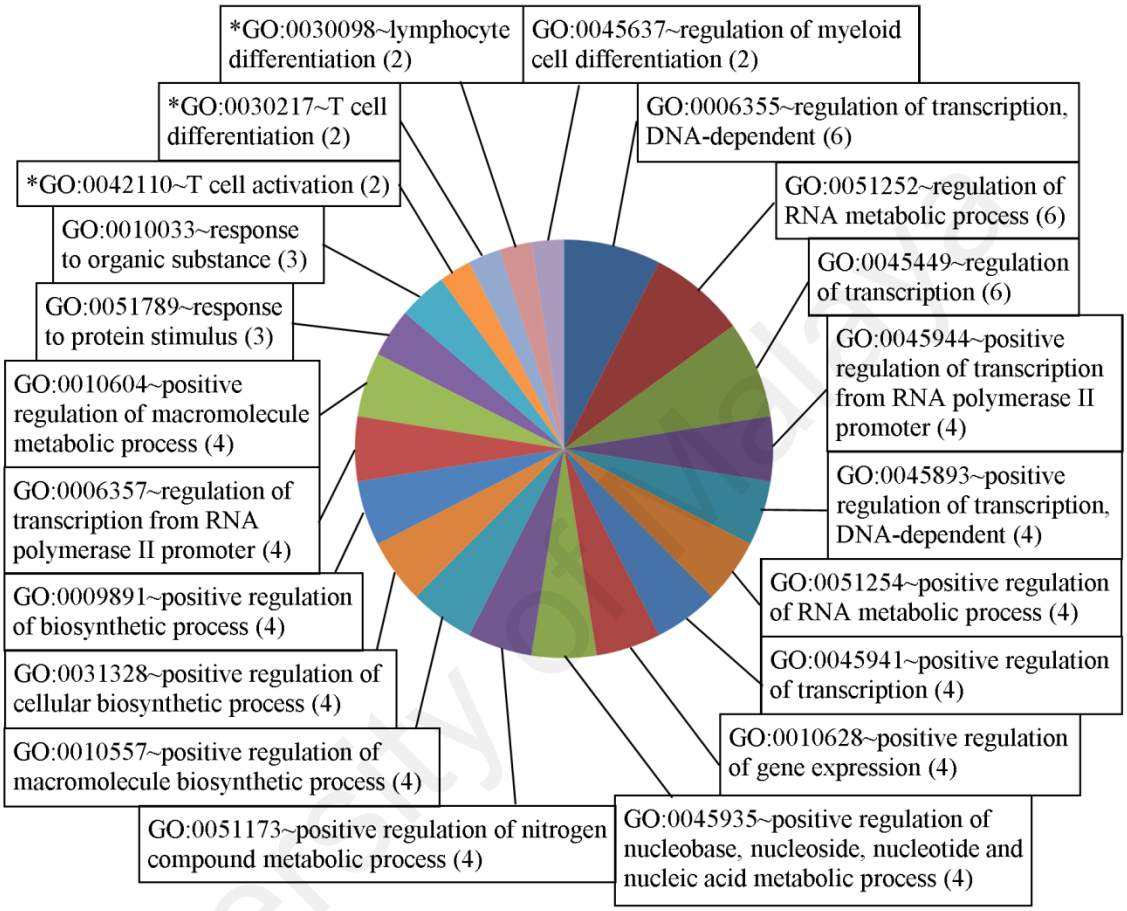

Figure 4.19: Gene ontology terms in the biological process category of upregulated genes of MY/08/065-infected suckling mouse brains at 6 dpi. Pie chart showing differentially expressed genes (upregulated: ≥ 2.0 fold change, $P < 0.05$). Each coloured section represents a different biological process and the number of genes involved in each process is shown in brackets. * indicates biological processes involved in immune-related responses.

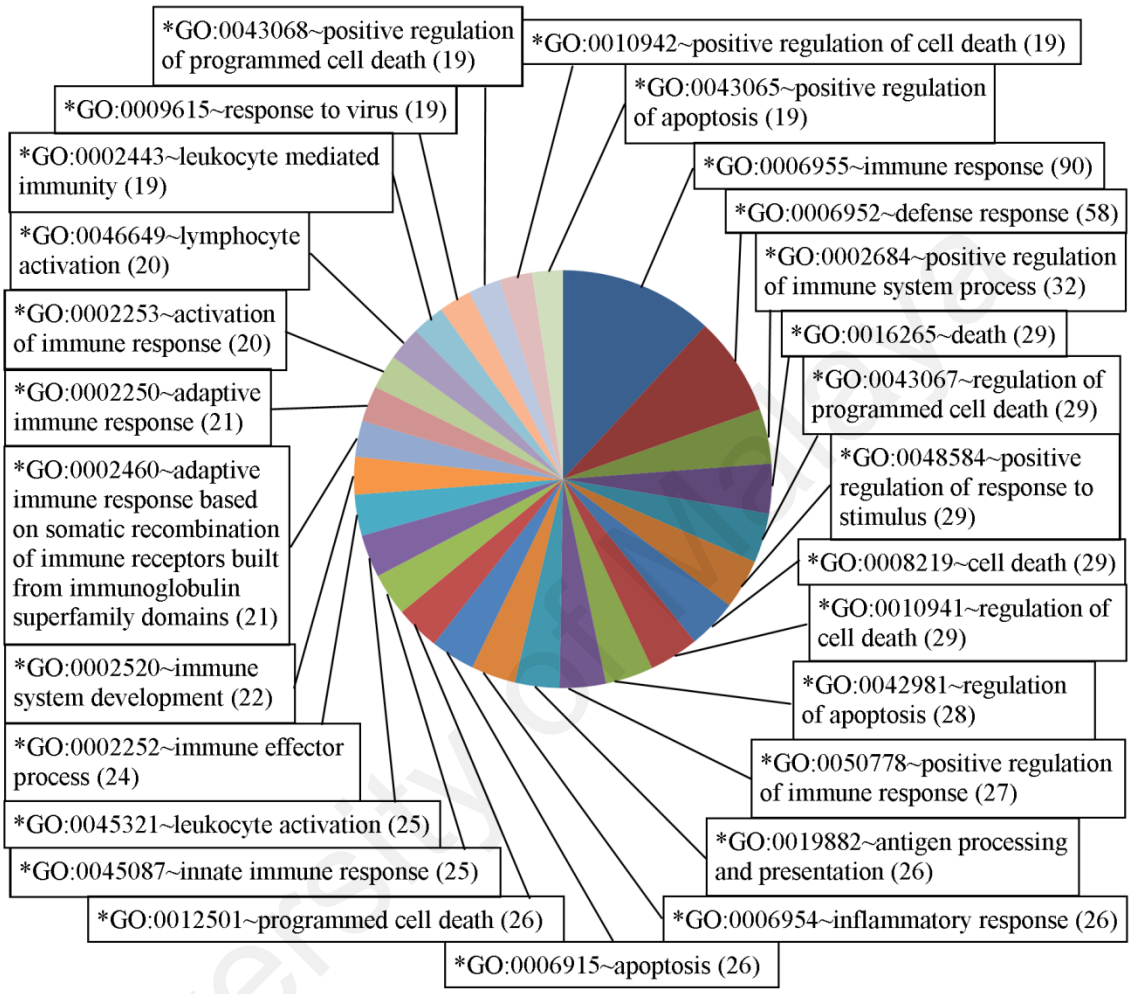

Figure 4.20: Gene ontology terms in the biological process category of upregulated genes of both MY/06/37348- and MY/08/065-infected suckling mouse brains at 6 dpi. Pie chart showing differentially expressed genes (upregulated: ≥ 2.0 fold change, $P < 0.05$). Each coloured section represents a different biological process and the number of genes involved in each process is shown in brackets. * indicates biological processes involved in immune-related responses.

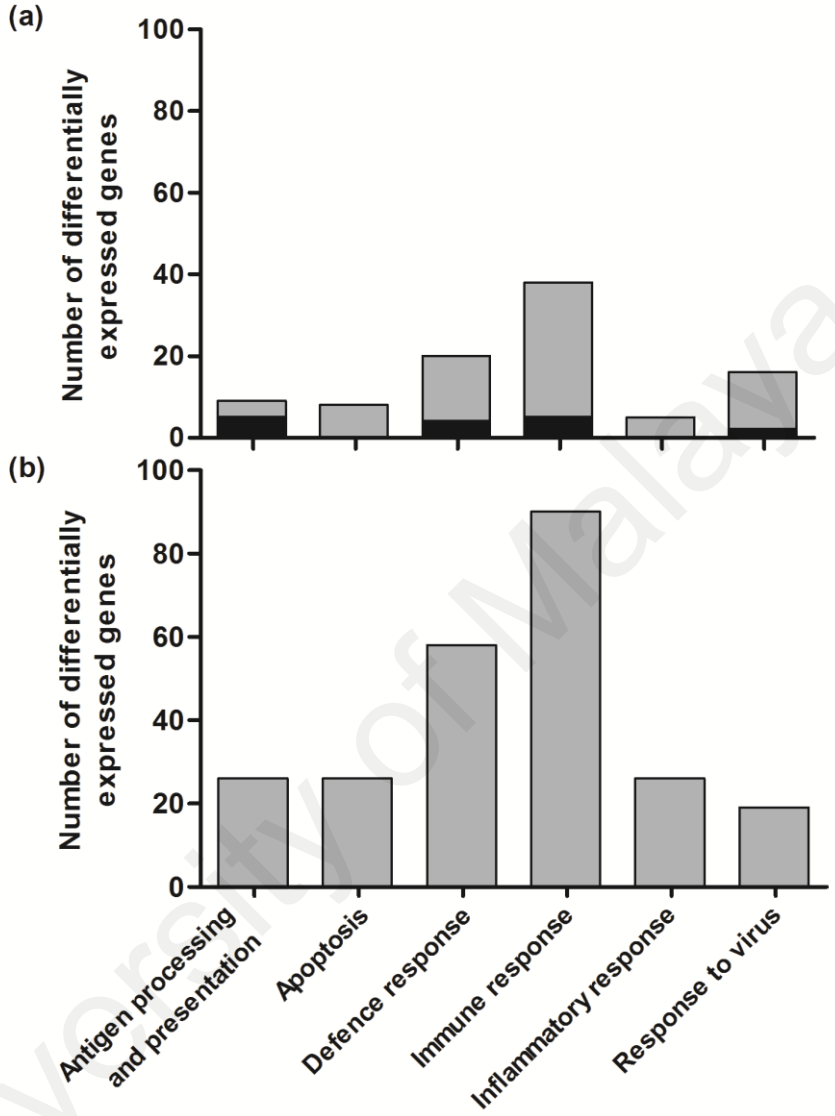

Figure 4.21: Gene expression analysis by biological processes of CHIKV-infected suckling mouse brains. Genes are categorised into biological processes after functional annotation using Database for Annotation, Visualization and Integrated Discovery Bioinformatics Resources. Genes differentially expressed following infection with only MY/06/37348 (black bar) or both MY/06/37348 and MY/08/065 (grey bar) at 1 dpi (a) and 6 dpi (b). No genes were differentially expressed in only MY/08/065-infected mice.

4.3.2 Confirmation of genes with qRT-PCR analysis

The STRING interaction maps showed the confidence view of the 45 selected immune-related genes (Figure 4.22). STAT1 has 32 associations with other genes, followed by IRF1 and TNF with 24 associations each. This suggests that these genes play major roles in the immune-related host response.

The selected immune-related genes were quantified using the TaqMan array microfluidic card assay to confirm the changes observed in the microarray data. Relative quantification analysis of the differential gene expression pattern of either MY/06/37348- and MY/08/065-infected suckling mice were compared to mock-infected suckling mice (Table 4.3). No genes were downregulated.

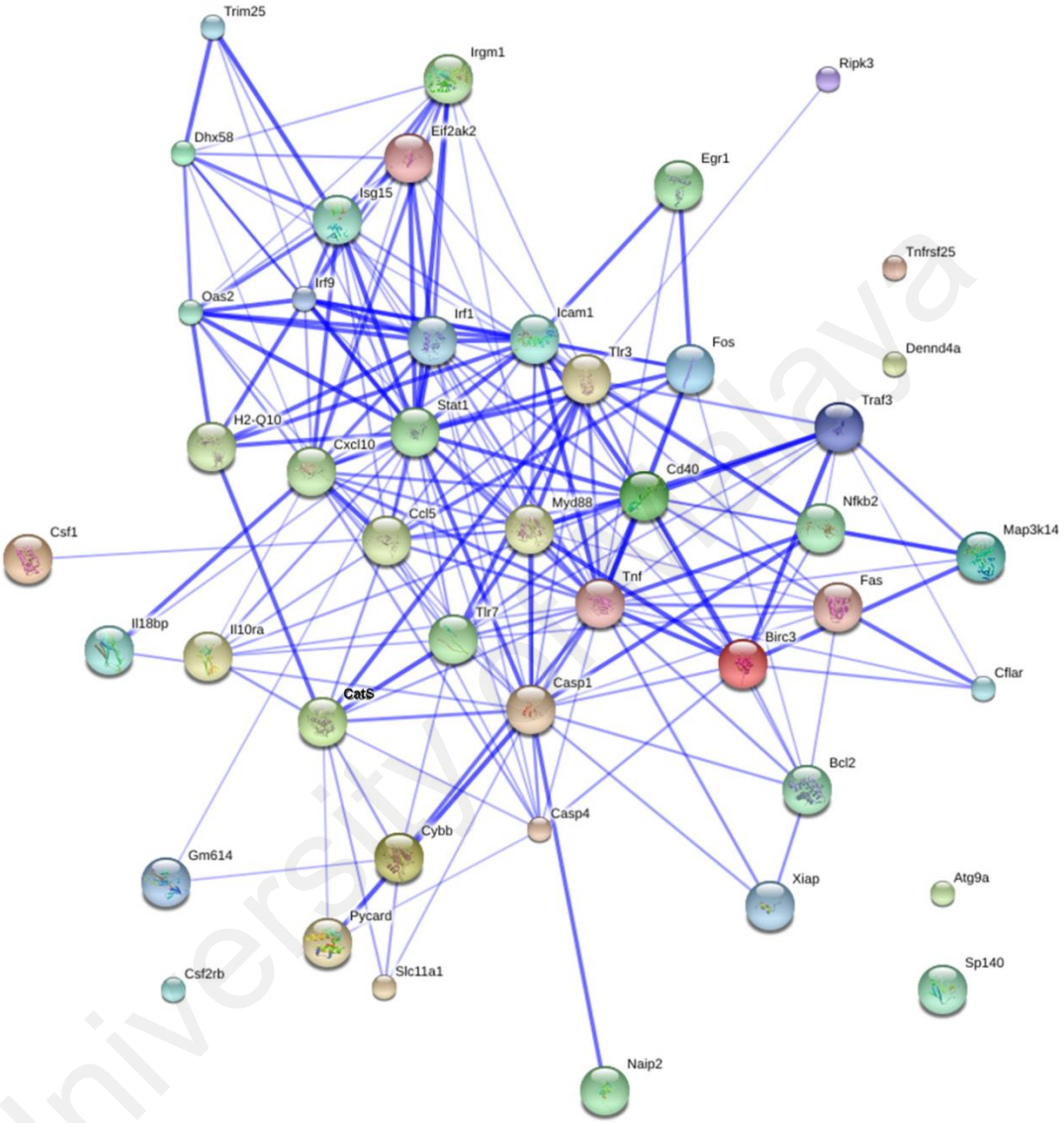

Figure 4.22: STRING interaction network showing confidence of the associations between 45 selected immune-related genes. The interaction map was generated using default settings (medium confidence of 0.4) to show the number of gene associations and association strength between genes.

Table 4.3: Relative quantification by qRT-PCR of upregulated genes in CHIKV-infected suckling mouse brains compared to mock-infected brains at 1 and 6 dpi.

GenBank accession no.	Gene symbol	Description	1 dpi		6 dpi	
			MY/06/ 37348	MY/08/ 065	MY/06/ 37348	MY/08/ 065
NM_001003917	ATG9A	Autophagy-related 9A	0.986	0.900	1.102	0.988
NM_007535	BCL2	B-cell lymphoma 2	0.879	0.904	1.041	0.991
NM_007464	**BIRC3**	**Baculoviral IAP repeat-containing 3**	1.350	1.171	3.002	**4.438***
NM_009807	Casp1	Caspase 1	1.271	0.949	3.884	5.287
NM_007609	Casp4	Caspase 4	7.756	5.269	20.515	23.275
NM_021281	**CatS**	**Cathepsin S**	1.462	1.054	5.264	**7.076***
NM_013653	CCL5	Chemokine (C-C motif) ligand 5	2.399	1.365	186.324	341.112
NM_011611	**CD40**	**CD40 antigen**	2.397	2.217	1.597	**3.612***
NM_009805	CFLAR	Casp8 and FADD-like apoptosis regulator	1.082	1.091	1.036	1.384
NM_001113530	**CSF1**	**Colony stimulating factor 1 (macrophage)**	**1.866***	1.444	1.581	1.848
NM_007780	CSF2RB	Colony stimulating factor 2 receptor, beta, low-affinity (granulocyte-macrophage)	1.741	1.349	7.790	11.772
NM_021274	CXCL10	Chemokine (C-X-C motif) ligand 10	98.283	57.090	391.772	555.653
NM_007807	CYBB	Cytochrome b-245, beta polypeptide	2.796	1.638	21.592	26.050
AK158279	DENND4A	DENN/MADD domain containing 4A	0.754	0.616	0.714	0.815
NM_030150	DHX58	DEXH (Asp-Glu-X-His) box polypeptide 58	5.931	4.751	18.461	24.328
NM_007913	EGR1	Early growth response 1	2.455	1.819	1.692	2.053
NM_011163	**eIF2αK2**	**Eukaryotic translation initiation factor 2-alpha kinase 2**	**10.426***	6.603	7.218	7.634
NM_007987	FAS	TNF receptor superfamily member 6	1.721	1.193	10.783	5.739
NM_010234	**FOS**	**FBJ osteosarcoma oncogene**	**2.242***	1.524	2.305	5.648
NM_010391	H2-Q10	Histocompatibility 2, Q region locus 10	1.382	1.490	2.757	2.613
NM_010493	ICAM1	Intercellular adhesion molecule 1	3.847	2.482	3.739	7.754
NM_008348	**IL-10RA**	**Interleukin 10 receptor, alpha**	1.114	1.234	3.211	**5.292***
NM_010531	**IL-18BP**	**Interleukin 18 binding protein**	**1.567***	1.093	5.591	4.737
NM_013563	IL-2RG	Interleukin 2 receptor, gamma chain	1.221	0.982	3.970	4.530
NM_008390	IRF1	Interferon regulatory factor 1	3.779	3.361	6.249	11.505
NM_001159417	IRF9	Interferon regulatory factor 9	6.043	5.313	7.321	7.563
NM_008326	IRGM1	Immunity-related GTPase family M member 1	17.367	12.485	46.407	56.913
NM_015783	ISG15	Interferon-stimulated gene 15	27.326	15.769	177.069	146.305
NM_016896	MAP3K14	Mitogen-activated protein kinase 14	0.761	0.732	0.813	1.195
NM_010851	**MyD88**	**Myeloid differentiation primary response gene 88**	2.312	1.556	3.398	**4.373***
NM_010872	NAIP2	NLR family, apoptosis inhibitory protein 2	1.279	1.095	7.017	8.517
NM_019408	NF-κB2	Nuclear factor of kappa light polypeptide gene enhancer in B-cells 2	1.487	1.047	2.062	2.398
NM_145227	**OAS2**	**2'-5' oligoadenylate synthetase 2**	14.767	8.141	**272.541***	163.645
NM_023258	**PYCARD**	**PYD and CARD domain containing**	1.670	1.484	2.654	**3.210***
NM_019955	RIPK3	Receptor-interacting serine-threonine kinase 3	0.922	0.698	5.419	4.142
NM_013612	SLC11A1	Solute carrier family 11 (proton-coupled divalent metal ion transporters), member 1	0.665	0.461	8.056	9.195
NM_001013817	SP140	Sp140 nuclear body protein	4.870	4.000	9.453	17.154
NM_009283	**STAT1**	**Signal transducer and activator of transcription 1**	**34.569***	20.575	34.583	30.217
NM_126166	TLR3	Toll-like receptor 3	8.688	5.311	5.733	6.003
NM_133211	TLR7	Toll-like receptor 7	1.348	1.208	3.419	3.735
NM_013693	TNF	Tumor necrosis factor	5.495	3.488	48.604	56.410
NM_033042	TNFRSF25	Tumor necrosis factor receptor superfamily, member 25	0.556	0.853	1.142	1.811

Table 4.3, continued: Relative quantification by qRT-PCR of upregulated genes in CHIKV-infected suckling mouse brains compared to mock-infected brains at 1 and 6 dpi.

GenBank accession no.	Gene symbol	Description	1 dpi		6 dpi	
			MY/06/37348	MY/08/065	MY/06/37348	MY/08/065
NM_028718	TRAF3	Tumor necrosis factor receptor-associated factor 3	1.095	1.048	1.189	0.934
NM_009546	TRIM25	Tripartite motif-containing 25	4.226	3.554	6.531	7.283
NM_001037713	XAF1	XIAP associated factor 1	13.333	7.666	53.349	40.706

Relative quantification values shown for MY/06/37348- and MY/08/065-infected mice are relative to mock-infected brains at 1 and 6 dpi. Differences in congruently-expressed genes were directly compared between MY/06/37348- and MY/08/065-infected mice if at least one group had expression of ≥ 1.5 relative quantification compared to mock-infected brains (* shows significant differences at $P < 0.01$).

4.3.3 Comparison of upregulation of immune-related genes following infection with either MY/06/37348 or MY/08/065

The relative quantification of MY/06/37348-infected and MY/08/065-infected mice were then directly compared for significant differences ($P < 0.01$). At 1 dpi, five genes were found to be upregulated significantly higher following MY/06/37348 infection than MY/08/065 infection. These were CSF1, eIF2αK2, FOS, IL-18BP, and STAT1 (Figure 4.23a).

At 6 dpi, seven genes were found to be significantly different when compared between MY/06/37348- and MY/08/065-infected suckling mice. Six genes were upregulated significantly higher following MY/08/065 infection than MY/06/37348 infection at 6 dpi (BIRC3, CatS, CD40, IL-10RA, MyD88, and PYCARD). Only OAS2 was significantly higher in MY/06/37348 infection than MY/08/065 infection at 6 dpi (Figure 4.23b).

The STRING interaction map of the genes at 1 dpi show that STAT1 has 3 associations with other genes (eIF2αK2, FOS, and IL-18BP) and 2 strongest associations with eIF2αK2 and FOS (Figure 4.24a). This suggests that STAT1 plays a major role in MY/06/37348 infection in suckling mice. Network analysis at 6 dpi showed that BIRC3, CD40, and MyD88 are associated, with BIRC3 having the strongest association with MyD88 and CD40 (Figure 4.24b).

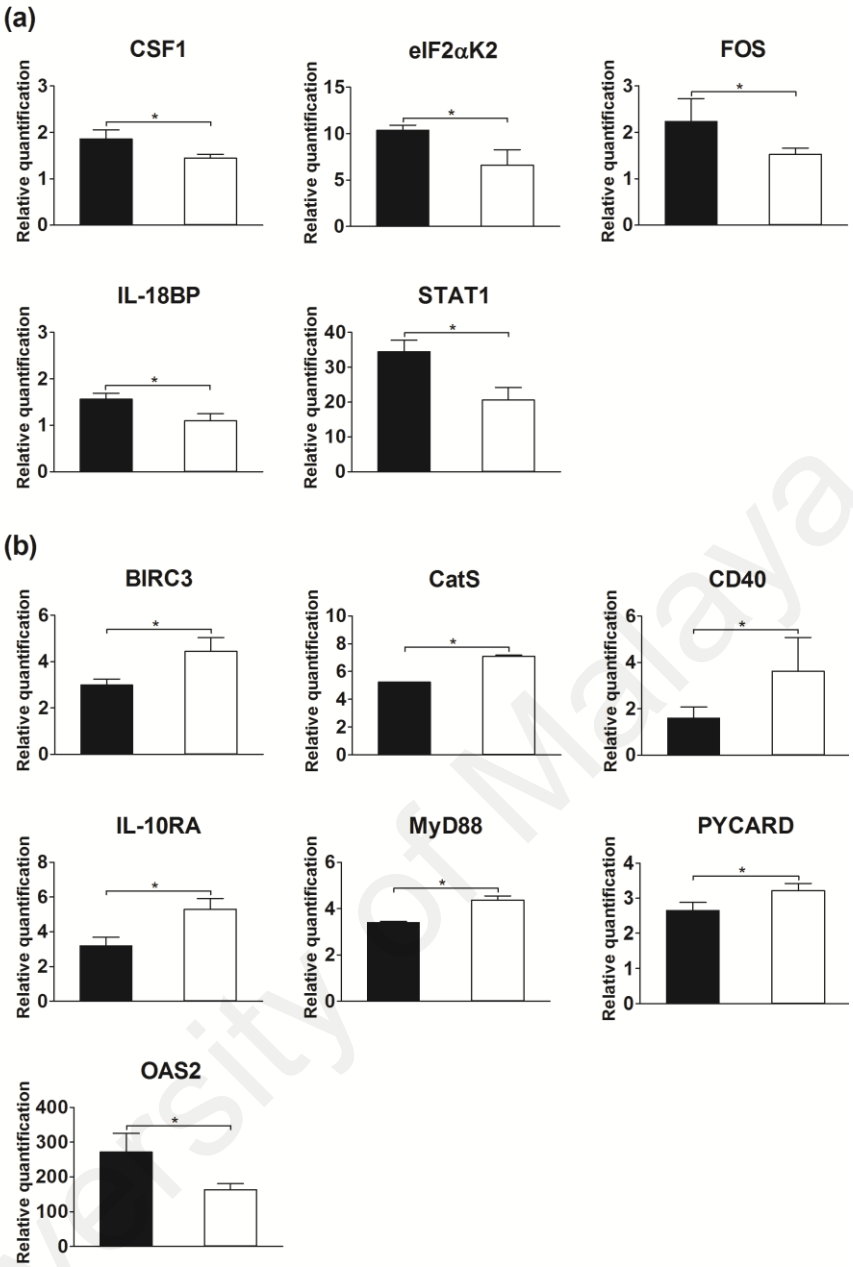

Figure 4.23: Comparison of relative quantification of upregulated immune-related genes in suckling mouse brains infected with either CHIKV isolate MY/06/37348 or MY/08/065 at 1 and 6 dpi. Relative quantification of genes expressed were measured by qRT-PCR and are shown for MY/06/37348-infected suckling mice (black bar) and MY/08/065-infected suckling mice (white bar) at 1 dpi (a) and 6 dpi (b). Relative quantification refers to gene expression of infected mice brains relative to mock-infected mice brains, and is plotted as mean ± range of 3 independent experiments. * shows significant differences in expression between MY/06/37348- and MY/08/065-infected mice ($P < 0.01$).

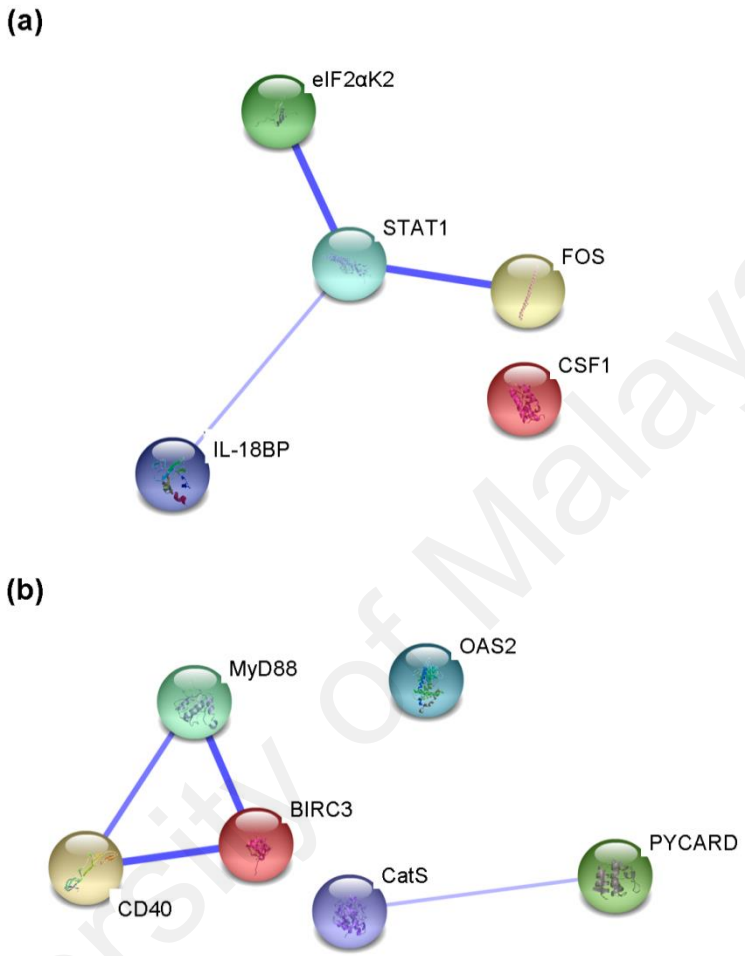

Figure 4.24: STRING interaction network showing confidence of the associations between significantly differentially expressed genes at 1 and 6 dpi. Selected genes were confirmed by qRT-PCR to be more highly expressed by either MY/06/37348-infected or MY/08/065-infected suckling mice at 1 dpi (a) and 6 dpi (b). The interaction map was generated using default settings (medium confidence of 0.4) to show the number of gene associations and association strength between genes.

CHAPTER 5

DISCUSSION

In this study, mice infected intracerebrally with CHIKV of either Asian (MY/06/37348) or ECSA genotype (MY/08/065) were compared. Although the viral titres and RNA copies of each virus within the mouse brains were similar, infection with the MY/06/37348 caused lower weight gain, higher mortality, and shorter mean time to death in suckling mice compared to the MY/08/065. There were differences in pathological changes and differential expression of immune-related genes between MY/06/37348- and MY/08/065-infected suckling mice, which may explain the observed differences in disease severity. However, no significant differences in illness, mortality, weight gain, viral replication, viral spread, and pathological changes were seen in MY/06/37348- and MY/08/065-infected adult mice.

5.1 CHIKV infection in mouse is age-dependent

CHIKV caused severe morbidity and mortality in suckling mice, but not in six-week-old adult mice. This was consistent with previous studies in which severe infection and mortality due to CHIKV (Couderc *et al.*, 2008; Ziegler *et al.*, 2008) and other alphaviruses such as SINV (Labrada *et al.*, 2002; Ryman *et al.*, 2007b) and SFV (Fleming, 1977) were observed in neonatal and suckling mice while adult mice were resistant to alphavirus infection.

Age-dependent disease manifestations of CHIKV are also seen in humans, as infection in children less frequently causes joint pain (Jadhav *et al.*, 1965; Sebastian *et al.*, 2009; Valamparampil *et al.*, 2009), while severe neurological involvement is seen particularly in neonates (Renault *et al.*, 2007; Gérardin *et al.*, 2008; Robin *et al.*, 2008; Arpino *et al.*,

2009; Couderc and Lecuit, 2009; Lewthwaite *et al.*, 2009; Sebastian *et al.*, 2009; Gérardin *et al.*, 2014).

In the brains of both suckling and adult mice, inoculated CHIKV reached peak titres at 1 to 2 dpi before declining. However, in suckling mice, titres were still detectable at 8 dpi, while in adult mice, titres were not detectable beyond 4 dpi, despite the continued presence of CHIKV RNA. A similar pattern of higher mortality in neonatal mice compared to older mice has been reported in previous studies. Ziegler *et al.* (2008) found that CHIKV replicated for up to 10 days in 2 to 3 day-old suckling mice, but for only 1 to 2 days in 14-day-old mice before clearance. Couderc *et al.* (2008) also showed that all infected six-day-old mice died, while nine-day-old mice experienced less than 50% mortality. Both age groups of mice suffered from flaccid paralysis while 12-day-old mice did not suffer any morbidity or mortality. These findings suggest that maturity of neurons and the immune system in adult mice play a role in faster viral clearance compared to suckling mice.

5.1.1 Neuron maturity contributes to age-dependent neurovirulence

Mortality due to differences of neuron maturity has been reported in mice infected with SINV and SFV. The rate and extent of SFV spread in the CNS (including the olfactory system) of mice decreased as the mice aged, and this was due to maturity of the CNS, and not the immune response or blood brain barrier (Oliver *et al.*, 1997; Oliver and Fazakerley, 1997). Brain infection with SINV induced apoptosis and resulted in death in immature mice. Meanwhile in mature mice, viral clearance from the brain was mediated by specific antibody, and mature neurons became resistant to apoptosis induced by the virus, thus delaying or preventing death (Levine and Griffin, 1992; Griffin *et al.*, 1994). Small amounts of SINV RNA remained and continued to persist, and persistent SINV

infection could be established when apoptosis was inhibited by the anti-apoptosis regulator BCL-2 (Levine *et al.*, 1993).

Differences in neuron maturity between suckling and adult mice likely contributed to the age-dependent observation of disease in this study, in which adult mice survived CHIKV infection without signs of illness, whereas suckling mice died after CHIKV infection.

5.1.2 Immune responses contribute to age-dependent neurovirulence

The age-dependent development of resistance to SFV in the brains of young mice (12 and 26 days old) compared to adult mice (35 days old) was suggested to be due to slower infection allowing antibodies to intervene before the virus causes damage and death (Fleming, 1977). This is similar to findings that specific immune responses did not reduce susceptibility of CNS to SFV infection (Oliver *et al.*, 1997).

Ryman *et al.* (2007b) observed that five-day-old mice inoculated with SINV had higher viral replication, higher mortality, and hyperinflammatory cytokine induction. Meanwhile, 11-day-old mice had limited viral replication and tissue damage with mild, immune-mediated pathology, suggesting a relationship between hyperinflammatory cytokine induction and fatal outcome. Labrada *et al.* (2002) reported that one-day-old mice infected with SINV suffered from rapid death with high viral titres and extensive apoptosis in the CNS, and this was accompanied by significant upregulation of genes involved in apoptosis and inflammation. In contrast, four-week-old mice had asymptomatic infection with low viral titres and no apoptosis in CNS which may be due to significant upregulation of an interferon-inducible neuroprotective gene.

In this study, the adult mice that survived CHIKV infection had lower and shorter viral replication rates compared to suckling mice. The role played by developmentally-regulated genes and immune responses would be an interesting topic for future study.

5.2 Amino acid differences between Malaysian CHIKV isolates may influence neurovirulence

Inter-strain variation of virulence with different mortality in mice has been observed previously in other alphaviruses such as SFV (Fleming, 1977; Balluz *et al.*, 1993; Fazakerley, 2004), SINV (Tucker *et al.*, 1993; Ubol *et al.*, 1994), VEEV (Calisher and Maness, 1974), and WEEV (Nagata *et al.*, 2006; Logue *et al*., 2009).

SFV4, a virulent strain of SFV, has higher replication ability and caused greater neuronal necrosis in mice than a less virulent strain, A7 (Fleming, 1977; Balluz *et al.*, 1993). The pathogenicity differences may be due to differences in amino acid sequences. The A7 strain has 47 amino acid changes, 2 nucleotide changes at the 5'non-coding region, and a longer and more divergent 3' non-coding region when compared to the SFV4 strain (Tarbatt *et al.*, 1997). Another engineered SFV strain, rA774, was also highly neurovirulent and lethal in adult BALB/c mice. It carried an opal termination codon at the 5' end of the nsP3 gene, and the nSP3 of the virulent SFV4 (Tuittila *et al.*, 2000; Tuittila and Hinkkanen, 2003).

Suthar *et al.* (2005) also reported that mutations of nsP1 at position 538, nsP3 at position 537, and E2 at position 243 were important in increasing SINV AR86 neurovirulence in adult mice. Amino acids at positions 10 and 24 in the macro domain of nsP3 were found to be essential for replication and RNA synthesis of SINV strain NSV in neurons, leading to encephalomyelitis in adult mice (Park and Griffin, 2009). A review by Voss *et al.* (2010) showed that in SINV, mutations of E2 at positions 55, 70, 172, 190, and 243 increased neuron binding and neurovirulence in weanling and suckling mice.

California, Fleming, and McMillan WEEV strains showed higher virulence and viral titres in mice than Imperial 181, CBA87, Mn548, B11, Mn520, and 71V-1658 strains (Nagata *et al.*, 2006; Logue *et al*., 2009). Comparison between highly virulent McMillan and the low virulent Imperial 181 strains of WEEV showed that the majority of amino acid differences occurred in E2, nsP2, and nsP4.

The TC-83 strain of VEEV also showed higher virulence and viral titres in suckling mice, guinea pigs, and duck embryo cell cultures when compared to other subtypes (Calisher and Maness, 1974). The increase of virulence may be due to E2 substitutions at position 213 from threonine to lysine or arginine, leading to increased charge (Brault *et al.*, 2002).

Virus isolates MY/06/37348 and MY/08/065 had 93.7% nucleotide and 96.8% amino acid similarities. The majority of the amino acid differences between MY/06/37348 and MY/08/065 occurred in nsP3 (6.6%), 6K (6.5%), E3 (6.3%), and E2 (4.3%) (Sam *et al.*, 2012). The positions of the differences in E1 and E2 glycoproteins between Malaysian isolates were compared with corresponding residues in other alphaviruses that have been reported to affect neurovirulence and host tropism (reviewed by Voss *et al.* (2010)). The two Malaysian isolates showed lysine at E2 position 3; in VEEV, this amino acid residue mediates attachment to heparan sulfate. Although the mutation did not cause morbidity or mortality in VEEV-infected adult mice (Bernard *et al.*, 2000), efficient heparan sulfate binding has been implicated in increased neurovirulence in SINV-infected mice (Ryman *et al.*, 2007a). Conversely, CHIKV E2 mutants with increased binding to heparan sulfate are attenuated in a mouse model of arthritis (Gardner *et al*., 2014), but the mutants did not include position 3. A notable difference between the two Malaysian viruses was the deletion of 21 nucleotides or 7 amino acids

at positions 376 to 382 of nsP3 of MY/06/37348 (Sam *et al.*, 2012). In SINV strain AR86, an 18 amino acid deletion at positions 386 to 403 of nsP3 was found to be a neurovirulence determinant (Suthar *et al.*, 2005), but a 21 nucleotide in-frame deletion from positions 5253 to 5273 of nsP3 did not alter SFV virulence phenotype (Tuittila *et al.*, 2000). All these deletions were found in the non-conserved gene region of the carboxy terminus of nsP3.

In some studies, comparison of CHIKV strains reveals virulence differences. An early study found no replication differences between CHIKV of African and Asian genotypes in baby hamster kidney (BHK-21) cells (Nakao, 1972). A more recent study showed that different ECSA strains replicated similarly in several mammalian cell lines, although the older Ross strain induced greater apoptosis in HeLa cells than a recent Thailand strain (Wikan *et al.*, 2012). CHIKV strains which caused clinical myalgia were compared to those that did not, and were found to replicate to a higher titre, cause more cytopathic effect and induce more cytokines in primary myoblast cells (Lohachanakul *et al.*, 2015). *In vivo* studies have been effective in demonstrating inter-strain differences. An enzootic West African strain caused higher viraemia and more pronounced symptoms in *M. mulatta* compared to an epidemic ECSA strain (Chen *et al.*, 2010). In an arthritis model in adult mice, an epidemic ECSA strain induced more inflammation and foot swelling than an Asian strain (Gardner *et al.*, 2010). More recently, a Caribbean strain (Asian) showed reduced mouse joint pathology compared to a La Réunion strain (ECSA), which was associated with reduced pro-inflammatory T_H1 and natural killer cell responses (Teo *et al.*, 2015).

Overall, these suggest that genetic differences found between CHIKV strains are likely to be associated with different virulence effects, including the neurovirulence seen in

the current study. These determinants are not yet understood in CHIKV, but may affect, for example, host cell binding and entry, replication efficiency, or host cellular responses.

5.3 Viral spread and pathological changes influence CHIKV neurovirulence

Following intracerebral inoculation in the left parietal region of suckling mice, CHIKV spread ipsilaterally and contralaterally from the injection site to the cerebral cortex, olfactory bulb, hippocampus, thalamus, and cerebellum as well as ependymal cells lining the choroid plexus, alveus, and ventricles. Double immunofluorescence staining showed that CHIKV infected astrocytes and neurons, and localized with apoptotic bodies. The pathological changes in mouse brains included apoptotic bodies, necrosis, inflammatory cells, and perivascular cuffing. No viral spread and pathological changes were observed in the brains of CHIKV-infected adult mice.

White (1969) reported CHIKV infection in the cerebral cortex and spinal cords of suckling mice with necrosis in the endoplasmic reticulum of neurons. Following intradermal inoculation in IFN-α/β; R-deficient 129s/v mice, CHIKV spread to the CNS, not through the blood-brain barrier (BBB) which remained intact, but through the choroid plexus route, and was found in ependymal and leptomeningeal cells (Couderc *et al*., 2008). As CHIKV antigen was also found widely in ependymal cells in the current study, these cells and possibly cerebrospinal fluid, may play an important role in local spread within the brain. However, a study by Das *et al.* (2015) found that CHIKV did not infect the choroid plexus after intracerebroventricular injection in OF1 newborn mice.

Couderc *et al*. (2008) did not find the virus in brain microvessels, parenchyma, microglial, and astrocytes of 129s/v mice. In contrast, other studies reported that CHIKV infects primary glial cells such as astrocytes and oligodendrocytes, but not microglial cells (Chatterjee and Sarkar, 1965; Das *et al.*, 2010). Contrasting findings were reported by Ziegler *et al.* (2008), who did not observe CHIKV antigen in ICR and

CD-1 strains suckling mice brains although the virus entered the CNS and replicated initially. These reported differences in susceptibility to infection, CHIKV neurovirulence and cell tropism within the CNS may depend on specific virus strains; species, strains and age of the infected mice; and dose and route used for virus inoculation (Steele and Twenhafel, 2010).

Other alphaviruses such as SFV showed neurotropism for brain endothelium and neurons (Fazakerley, 2002). Labrada *et al.* (2002) observed high CNS viral titre and extensive CNS apoptosis in one-day-old mice infected with SINV, while four-week-old mice showed asymptomatic infection with low viral titres and absence of apoptosis. Griffin (2005) reported that SINV infection in mice caused vascular lesions with cerebral capillaries congestion, pericapillary haemorrhages at the lateral ventricles, glial reaction, and neuronal lesions in the hippocampus, cortex and midbrain nuclei.

In this study, after intracerebral inoculation, CHIKV also spread to extracerebral tissue in the head, such as brown fat cells, oral mucosa, and skeletal muscle, as well as distant sites such as thigh skeletal muscle. Pathologic changes were observed in skeletal muscle of the head and thigh, as well as the liver. These included apoptotic bodies, necrosis, inflammatory cells, vacuolization, and oedema.

Intracerebral inoculation of a CHIKV strain from Thailand into mice also led to extensive haemorrhage, blood vessel dilation and congestion, and vacuolar degeneration in gut mucosal cells (Halstead and Buescher, 1961). Consistent with the results here, spread to distant organs is also seen following intradermal or subcutaneous inoculation of CHIKV in ICR, CD-1, OF1, C57BL/6, and 129s/v mice (Ziegler *et al.*, 2008; Couderc *et al.*, 2008). Reported changes in muscle include pronounced CHIKV tropism

for fibroblasts, focal individual muscle fibre wavy changes, necrotic myositis, muscle atrophy, and multifocal inflammation with lymphocyte and macrophage infiltration. In skin tissue, viral antigen staining is seen with infiltration of inflammatory cells, muscle necrosis, and calcification. In *M. fascicularis*, CHIKV mainly infected macrophages, dendritic cells, and endothelial cells found in lymphoid tissues, liver, cerebrospinal fluid, joints, and muscle; in later stages, persistent histiocytosis in the spleen was seen (Labadie *et al.*, 2010).

Dissemination of CHIKV to sites outside the brain following intracranial inoculation may occur through several routes. The virus may have spread systemically following direct invasion of blood vessels in the brain. It is also possible that following infection of ependymal cells and intracranial spread via cerebrospinal fluid, the virus could have entered the bloodstream after penetrating the blood-cerebrospinal fluid barrier. Spread of CHIKV to the CNS following systemic infection is well-known to occur in humans, and CHIKV antigen and RNA has been detected in cerebrospinal fluid (Robin *et al.*, 2008; Lemant *et al.*, 2008; Das *et al.*, 2010; Kashyap *et al.*, 2010; Gauri *et al.*, 2012). In mice infected intradermally with CHIKV, the BBB remained intact (Couderc *et al*., 2008), but other alphaviruses like SFV and VEEV have been reported to cross the BBB to multiply in CNS before causing lethal encephalomyelitis (Atkins, 2013). Viral spread into the CNS via the olfactory nerve is also well described in several viruses, including CHIKV, showing that viruses have tropism for olfactory tissue (Powers and Logue, 2007; van Riel *et al.*, 2015). In this study, CHIKV antigen was detected in the olfactory bulbs of the suckling mice, and this may represent a possible route by which CHIKV in the brain may have spread to extracranial tissue, followed by spread via blood or the lymphatic circulation throughout the body.

In humans, recent reports suggest that the ECSA strain was associated with higher death rates and neurological complications compared to historical reports of Asian strain outbreaks. These include encephalitis, acute encephalopathy, meningeal syndrome, acute flaccid paralysis, myoclonus, cerebral ataxia, and seizures (Rampal *et al.*, 2007; Casolari *et al.*, 2008; Robin *et al.*, 2008; Economopoulou *et al.*, 2009; Chusri *et al.*, 2011; Gauri *et al.*, 2012; Kalita *et al.*, 2013; Nelson *et al.*, 2014). The occurrence of seizures may be due to innate immune responses to viral infection (Kirkman *et al.*, 2010). Magnetic resonance imaging scanning of CHIKV-infected neonates and adults showed brain swelling, demyelination, and scattered white matter lesions in the corpus callosum, and frontal, parietal, and temporal lobes (Ganesan *et al.*, 2008; Musthafa *et al.*, 2008; Gérardin *et al.*, 2008; Chandak *et al.*, 2009; Gauri *et al.*, 2012). Autopsy findings of CHIKV patients are rare, but have revealed oedema, ischemic changes, and focal haemorrhages at the cerebral cortex and internal capsule. Microscopic observation showed small foci of demyelination in the subcortical white matter (consistent with magnetic resonance imaging findings), sparse microglial response without glial nodules or neuronophagia in the cortical gray matter and diencephalic area, and perivascular lymphocytic infiltration and gitter cells in the basal ganglia (Ganesan *et al.*, 2008). These radiological and autopsy findings of white matter involvement suggest that CHIKV may not be neurotropic in humans.

In this study, the MY/06/37348 isolate caused greater neurovirulence and mortality, and more extensive viral spread and pathologic changes in skeletal muscle, compared to MY/08/065. This supports past findings of inter-strain virulence of other alphaviruses. It is not yet clear if such clinical differences in neurovirulence are seen in humans; the high numbers of neurological complications observed after the worldwide outbreaks in 2005-2010 of the ECSA genotype of CHIKV led to suggestions that this epidemic strain

may be more neurovirulent compared to historical reports of Asian CHIKV. As the recent large outbreak of Asian CHIKV in the Americas unfolds, reports of neurological complications may shed light on possible differences in clinical disease between the genotypes in humans.

5.4 Higher neurovirulence observed in MY/06/37348-infected suckling mice may be due to early induction of apoptosis

Apoptosis is a process of energy-dependent programmed cell death. Apoptosis involves cell shrinkage, membrane blebbing, chromatin condensation, intranucleosomal DNA cleavage, and segmentation of the cell into membrane-bound apoptotic bodies which is important to eliminate unnecessary or harmful cells (Nargi-Aizenman and Griffin, 2001; Gump and Thorburn, 2011). In this study, apoptotic bodies were observed in haematoxylin and eosin staining of CHIKV-infected mouse brains and confirmed with immunofluorescence staining. This was consistent with a previous study in which apoptotic machinery was activated in HeLa cells, human fibroblasts, astrocytes, and neurons of primary mouse brain cells following CHIKV infection (Krejbich-Trotot *et al.*, 2011a; Das *et al.*, 2015). However, Kumar *et al.* (2012b) did not show apoptosis in RAW264.7 mouse macrophage cells, while Joubert *et al.* (2012) showed that apoptosis in mouse embryonic fibroblasts was delayed due to activation of autophagy. Autophagy is another type of cell process that maintains cellular homeostasis by degrading, and recycling long-lived proteins and organelles (Walsh and Edinger, 2010; Krejbich-Trotot *et al.*, 2011b; Gump and Thorburn, 2011). Studies showed that autophagy promotes CHIKV viral replication in HeLa and HEK293 cells (Krejbich-Trotot *et al.*, 2011b; Judith *et al.*, 2013). Apoptosis was also observed *in vitro* (BHK-21, CHO (Chinese hamster ovary), AT-3 (rat prostate carcinoma), and primary cortical cells), and *in vivo* infection with alphaviruses such as SINV (Ubol *et al.*, 1994; Lewis *et al.*, 1996; Griffin and Hardwick, 1998; Jan and Griffin, 1999; Havert *et al.*, 2000; Nargi-Aizenman and Griffin, 2001; Labrada *et al.*, 2002), SFV (Glasgow *et al.*, 1997; Scallan *et al.*, 1997), and VEEV (Jackson and Rossiter, 1997).

In this study, apoptosis was observed as early as 4 dpi in MY/06/37348-infected suckling mice, and later at 4 to 6 dpi in MY/08/065-infected suckling mice. Apoptosis was not observed in CHIKV-infected adult mice, none of which died. As apoptosis has been found to correlate positively with neurovirulence (Lewis *et al.*, 1996; Jackson and Rossiter, 1997; Griffin and Hardwick, 1998; Havert *et al.*, 2000; Nargi-Aizenman and Griffin, 2001; Labrada *et al.*, 2002), this may help explain the survival of adult mice. Differences in timing of apoptosis may have contributed to the differences in mortality seen in the suckling mice.

5.5 Differential expression of immune-related genes influences CHIKV neurovirulence

As there were minimal differences between viral titres of MY/06/37348 and MY/08/065 in the mouse brains, the higher mortality caused by MY/06/37348 could not be due to increased viral replication. Strain variation may influence host expression of genes involved in inflammation and CNS protection, ultimately affecting mortality. The gene expression in adult mice was not studied as none of them died.

Five genes were found to be upregulated significantly higher following MY/06/37348 infection than MY/08/065 infection when gene expression was directly compared between the suckling mice infected with different CHIKV isolates at 1 dpi. These were CSF1, eIF2αK2, FOS, IL-18BP, and STAT1. At 6 dpi, six genes were expressed at significantly higher levels in MY/08/065-infected suckling mice than MY/06/37348-infected suckling mice. These genes were BIRC3, CatS, CD40, IL-10RA, MyD88, and PYCARD. OAS2 was found to have significantly higher upregulation after MY/06/37348 infection compared to MY/08/065 infection at 6 dpi. All the genes were linked together to form a network of signalling pathways such as TLR, NF-κB, Jak-STAT, NOD-like receptor, T cell receptor, RIG-I-like receptor and TNF signalling pathways (summarised in Figure 5.1).

Further discussion will focus on the immune-related genes of interest which were differentially expressed when comparing MY/08/065- with MY/06/37348-infected suckling mice, and the roles they play in response to CHIKV infection.

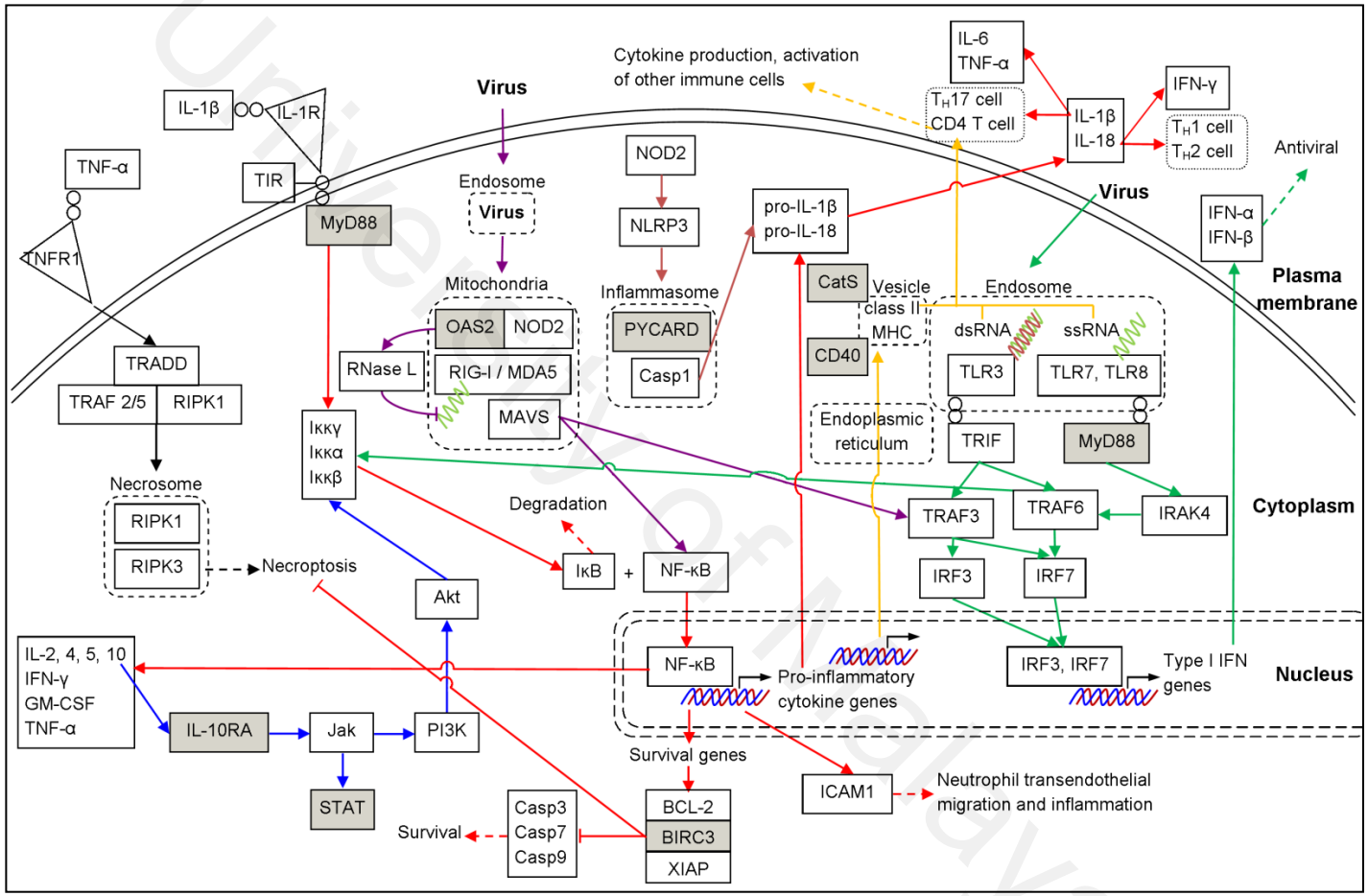

Figure 5.1: Signalling pathways activated following CHIKV infection in mice. TLR (→), NF-κB (→), Jak-STAT (→), NOD-like receptor (→), T cell receptor (→), RIG-I-like receptor (→), and TNF (→) signalling pathways. Genes that were significantly upregulated in this study are indicated in black shaded box.

5.5.1 Immune-related genes upregulated in the brains of MY/06/37348-infected suckling mice at 1 dpi

Five genes (CSF1, eIF2αK2, FOS, IL-18BP, and STAT1) were upregulated to a greater extent in MY/06/37348-infected suckling mice compared to MY/08/065-infected suckling mice at 1 dpi.

CSF1, also known as macrophage colony-stimulating factor, is essential for regulation of production, differentiation, and function of macrophages and osteoclasts (Maysinger *et al.*, 1996; Sweet and Hume, 2003). CSF1 is also a proinflammatory mediator in innate immunity and inflammation involved in TNF and PI3K-Akt signalling pathways. It has been associated with persistent arthralgia in CHIKV-infected patients, similar with rheumatoid arthritis (Chow *et al.*, 2011; Dupuis-Maguiraga *et al.*, 2012; Chirathaworn *et al.*, 2013). However, binding to CSF1 receptor was found to reduce apoptosis, thus protecting CNS from cell death (Wang *et al.*, 1999; Nandi *et al.*, 2012).

In cell death, eIF2αK2 was found to be implicated with apoptosis and autophagy. eIF2αK2 encodes interferon-induced, double-stranded RNA-activated PKR which plays a role in NF-κB and Jak-STAT signalling pathways as well as mediating genes encoding proinflammatory cytokines and IFNs (Wong *et al.*, 1997; Barry *et al.*, 2009). Activation of eIF2αK2 phosphorylates eIF2α which renders eIF2α inactive, blocking initiation of translation, which in turn inhibits protein synthesis as well as enhancing apoptosis, autophagy, and neuronal degeneration (Chang *et al.*, 2002; Jiang and Wek, 2005; Tallóczy *et al.*, 2005; Samuel *et al.*, 2006). Phosphorylation of eIF2α was observed during WNV infection in neurons (Samuel *et al.*, 2006) as well as alphaviruses SINV, SFV, and CHIKV infection in mouse embryonic fibroblasts cells (Barry *et al.*, 2009), primary mouse bone marrow-derived dendritic cells (Ryman *et al.*, 2005), human

myoblast cells (Gad *et al.*, 2012), HEK293 human embryonic kidney cells (Rathore *et al.*, 2013), primary human foreskin fibroblasts (White *et al.*, 2011), and mice (Barry *et al.*, 2009).

FOS is a transcriptional factor that is part of the AP-1 complex, which is involved in the MAPK, NF-κB, TLR, and TNF signalling pathways. The AP-1 complex binds to DNA to regulate cell proliferation, differentiation, and transformation (Maulik *et al.*, 2006; Saijo *et al.*, 2013). FOS was observed during VEEV infection in mouse brains (Sharma and Maheshwari, 2009) but was not observed during SINV infection in mouse N18 neuroblastoma cells (Lin *et al.*, 1995). Hence, this factor may be upregulated in selected and not all alphaviruses.

IL-18BP encodes proteins to inhibit synthesis of the proinflammatory cytokine IL-18, thus inhibiting IFN-γ production and early T_H1 cytokine responses. The high levels of IL-18BP during acute CHIKV infection was likely due to the need to regulate the IL-18 induced (Chirathaworn *et al.*, 2010).

STAT1 is a transcription factor activated by Jak as part of the Jak-STAT pathway. The association of STAT1 with IRF9 and binding to IFN-stimulated response elements of the ISG leads to inhibition of viral replication (Gasque, 2013). STAT1 was found during SINV infection in CD-1 mice (Johnston *et al.*, 2001). However, CHIKV infection can inhibit STAT1 phosphorylation through inhibition of IFN gene expression (Fros *et al.*, 2010) and prevent nuclear translocation of STAT1 in human fibroblast cells (Thon-Hon *et al.*, 2012).

In summary, the apoptotic bodies (confirmed with Casp3 immunofluorescence staining) and inflammation observed during early infection in brains of MY/06/37348-infected suckling mice was associated with significant upregulation of pro-apoptotic eIF2αK2 at 1 dpi, when compared to MY/08/065-infected suckling mice. The upregulation of eIF2αK2 and STAT1 may have inhibited CHIKV replication during early CHIKV infection. However, upregulation of IL-18BP (which inhibits proinflammatory cytokine IL-18, IFN-γ production, and early T_H1 cytokine responses) may have promoted CHIKV replication in MY/06/37348-infected suckling mice. Increased apoptosis during earlier infection may help explain the greater neurovirulence seen in MY/06/37348-infected suckling mice.

5.5.2 Immune-related genes upregulated in the brains of MY/08/065-infected suckling mice at 6 dpi

In this group, six genes (BIRC3, CatS, CD40, IL-10RA, MyD88, and PYCARD) were upregulated to a greater extent in MY/08/065-infected suckling mice compared to MY/06/37348-infected suckling mice at 6 dpi.

BIRC3, also known as c-IAP2, is a member of the IAP family of proteins that regulates apoptosis and inflammatory signalling. BIRC3 does not inhibit caspase, but has an anti-apoptotic function through polyubiquitination of RIPK1 and RIPK2 through E3 ubiquitin ligases (Eckelman and Salvesan, 2006). As an important regulator of innate immune responses, BIRC3 also facilitates NOD-like signalling which activates NF-κB to promote cell survival (Bertrand *et al.*, 2008; Bertrand *et al.*, 2009). Vince *et al.* (2012) also demonstrated that BIRC3 inhibits formation of ripoptosomes and RIPK3-mediated IL-1 signalling through Casp1 and Casp8 activation. This will lead to

inhibition of inflammation-mediated anti-apoptosis responses and necroptosis (Wallach *et al.*, 2011; Wang *et al.*, 2012; Newton *et al.*, 2014; Vitner *et al.*, 2014).

CatS is a member of the peptidase C1 family, a lysosomal cysteine proteinase that is expressed in cells of mononuclear phagocytic origin such as microglia to degrade proteins (Nakagawa *et al.*, 1999; Wendt *et al.*, 2008; Clark *et al.*, 2010). CatS also plays a role in class II MHC-mediated antigen presentation for $CD4^+$ T cells to produce cytokines and activate immune cells (Nakagawa *et al.*, 1999; Wendt *et al.*, 2008). Although activated microglia initiate inflammatory and cytokine responses, some cathepsin members also induce neuronal death by degrading extracellular matrix proteins (Nakanishi, 2003). Cathepsins have been proposed to play an essential role upstream of NLRP3 activation (Latz, 2010). CatS is activated by infection with SINV (Johnston *et al.*, 2001; Labrada *et al.*, 2002) and WNV (Venter *et al.*, 2005).

CD40, of the TNF-receptor superfamily 5, is a receptor. CD40 expression was reported previously during VEEV (Taylor *et al.*, 2012) and CHIKV infection (Das *et al.*, 2015). CD40 is a costimulatory molecule found on antigen presenting cells including microglia (O'Keefe *et al.*, 2002), which is involved in a wide range of T-cell and B-cell immune responses, including those in response to VEEV (Taylor *et al.*, 2012) and CHIKV infection (Das *et al.*, 2015).

IL-10RA, a receptor for anti-inflammatory IL-10, mediates high affinity ligand binding and signal transduction (Riley *et al.*, 1999) in the Jak-STAT, NF-κB, and PI3K-Akt pathways (Riley *et al.*, 1999; Zhou *et al.*, 2009; Sharma *et al.*, 2011). These pathways lead to activation of I kappa B kinase complex and IκB. Degradation of activated IκB leads to activation and release of NF-κB which promotes survival. IL-10 promotes

neuroprotection following trauma, possibly by its anti-apoptotic effects (Bachis *et al.*, 2001; Xin *et al.*, 2011). IL-10 is secreted by T_H2 cells, B lymphocytes, monocyte-macrophages, mast cells, and keratinocytes, and promotes proliferation and differentiation of B lymphocytes (Samoilova *et al.*, 1998; Moore *et al.*, 2001). IL-10 also augments IL-2 to induce proliferation and cytotoxic activity of natural killer cells against infection (Carson *et al.*, 1995; Taylor *et al.*, 2012). In the CNS, IL-10 is produced in microglia, astrocytes, and oligodendrocytes (Zhou *et al.*, 2009). This cytokine inhibits synthesis of pro-inflammatory cytokines such as TNF-α, IL-1β, IL-6, IL-8, and IL-12 (Jenkins *et al.*, 1994; Riley *et al.*, 1999; Bachis *et al.*, 2001). IL-10 also regulates expression of class II MHC and co-stimulatory molecules on antigen-presenting cells (Howard *et al.*, 1992; Moore *et al.*, 2001), and prevents glutamate-induced apoptosis by blocking the activation of NF-κB p52 and p65 (Zhou *et al.*, 2009). IL-10 production against neuroinflammatory responses has been shown in SFV infection (Morris *et al.*, 1997).

The significantly higher upregulation of MyD88 in MY/08/065-infected suckling mice than MY/06/37348-infected suckling mice shows the importance of TLR, NF-κB, and RIG-I-like receptor signalling pathways in CHIKV infection. Kam *et al.* (2009) had previously shown that MyD88 is involved in the TLR7-MyD88 pathway to induce production of type I IFN and pro-inflammatory cytokines to clear CHIKV. MyD88 stimulates innate immunity by controlling the efficiency of cross-presentation of viral antigens from infected antigen-presenting cells (Chen *et al.*, 2005). MyD88, a Toll-IL-1 receptor domain-containing protein used by all TLRs except TLR3, recruits IL-1 receptor-associated kinase and TRAF6 to the TLRs. These signalling pathways phosphorylate the transcription factors IRF3, IRF7, and NF-κB. IRF3 and IRF7 activation leads to type I IFN production essential for antiviral responses (Hemmi *et al.*,

2002; Takeda *et al.*, 2003; Loiarro *et al.*, 2009; Rudd *et al.*, 2012; Schwartz and Albert, 2010; Wang *et al.*, 2014). MyD88 and TRAF6 also activate I kappa B kinase complex in non-infected cells, followed by activation of IκB. Degradation of IκB activates and releases NF-κB to the nucleus for production of pro-inflammatory cytokines such as IL-1β, IL-6, and TNF-α (He *et al.*, 2006; Schwartz and Albert, 2010; Wang *et al.*, 2014). NF-κB also regulates expression of class II MHC during adaptive immune responses (Zhang *et al.* 2001) and induces expression of NLR family pyrin domain-containing protein 3 (NRLP3) that are essential for maturation of pro-inflammatory cytokines IL-1β and IL-18 (Franchi *et al.*, 2012).

MyD88 was found to restrict replication and protect the CNS from viruses such as VEEV (Sharma and Maheshwari, 2009), WNV (Szretter *et al.*, 2010), and vesicular stomatitis virus (Lang *et al.*, 2007). MyD88 also protects joints from RRV (Assunção-Miranda *et al.*, 2013). However, necrotic neurons are also known to activate microglia through the MyD88-dependent pathway to release factors that are toxic to neurons (Pais *et al.*, 2008; Dean *et al.*, 2010). The significant upregulation of MyD88 in this study may have contributed to protecting the CNS of MY/08/065-infected suckling mice, thus improving survival compared to MY/06/37348-infected suckling mice.

PYCARD is an adaptor protein with two domains, N-terminal pyrin domain (PYD) and C-terminal caspase-recruitment domain (CARD), which is involved in the NLR signalling pathways. PYCARD is expressed during VEEV infection (Sharma *et al.*, 2008). PYCARD is involved in innate immunity as part of the inflammasome, a cytosolic multi-protein complex which mediates apoptosis and inflammation (Osawa *et al.*, 2011), and which is activated by a variety of molecules. The inflammasome family includes NLR family pyrin domain-containing protein 3 (NLRP3), which is activated by

ligands, DNA, and RNA (van de Veerdonk *et al.*, 2011). TLRs, RNA helicases such as RIG-I, and MDA5 detect virus-associated PAMPs and danger-associated molecular patterns (Poeck *et al.*, 2010; Latz, 2010; Osawa *et al.*, 2011; Pothlichet *et al.*, 2013). This leads to activation of IRF3, IRF7, NF-κB, and NLRP3. NF-κB also induced expression of NRLP3 (Franchi *et al.*, 2012). The NLRP3 inflammasome produces activated Casp1 that cleaves pro-IL-1β and pro-IL-18 from the NF-κB signalling pathway to produce IL-1β and IL-18, which contribute to suppression of viral replication, while IRF3 and IRF 7 stimulates production of type I IFN antivirals (Barker *et al.*, 2011; Burdette *et al.*, 2012; Franchi *et al.*, 2012). IL-18 later induces T_H1, which in turn produces IFN-γ to activate neutrophils and macrophages (Schwartz and Albert, 2010; Wang *et al.*, 2014). Viruses previously reported to activate the NLRP3 inflammasome include adenovirus (Doronin *et al.*, 2012), influenza virus (Allen *et al.*, 2009), and hepatitis C (Burdette *et al.*, 2012). It is possible that the CHIKV-infected mouse host response engages the NLRP3 inflammasome due to the single- and double-stranded viral RNA generated during replication.

To summarise, six genes were upregulated at higher levels in MY/08/065-infected suckling mice compared to MY/06/37348-infected suckling mice. The greater upregulation of MyD88 and BIRC3 in NF-κB pathway may be associated with CNS protection against other alphaviruses. This may contribute to the better survival observed in MY/08/065–infected suckling mice. IL-10RA activates the Jak-STAT, NF-κB, and PI3K-Akt pathways, which eventually further activate NF-κB. MyD88 expression also leads to production of type I IFN, which has antiviral activity. PYCARD and CatS are also upregulated in other viral infections, and likely involved in inflammation during CHIKV infection as well. The lower mortality observed in MY/08/065-infected suckling mice compared to MY/06/37348-infected suckling mice

may be due to differences in induced expression of genes involved in antiviral and CNS protection from cell death.

5.5.3 Immune-related genes upregulated in the brains of MY/06/37348-infected suckling mice at 6 dpi

In this group, only one gene, OAS2 was significantly upregulated to a greater extent in MY/06/37348-infected suckling mice compared to MY/08/065-infected suckling mice at 6 dpi. Activation of OAS2, an interferon-induced antiviral protein important in the RIG-I-like receptor and NF-κB signalling pathway, has been observed in CHIKV infection (Bréhin *et al.*, 2009; Fros *et al.*, 2010; Dhanwani *et al.*, 2011). OAS2 is an isoform of the OAS family involved in innate immunity that responds to PAMPs and IFN. OAS2 activates endogenous ribonuclease (RNase L), which degrades viral and cellular single-stranded RNA leading to inhibition of viral protein synthesis (Saha and Rangarajan, 2003; Silverman, 2007). Another type of OAS, OAS3 has been reported to have antiviral activity against CHIKV in HeLa cells (Bréhin *et al.*, 2009). OAS2 is also involved in activation of NF-κB through mitochondrial antiviral signalling protein (Ting *et al.*, 2010) which leads to production of pro-inflammatory cytokines and type I IFN which also cause antiviral responses (Hemmi *et al.*, 2002; Takeda *et al.*, 2003; Loiarro *et al.*, 2009; Rudd *et al.*, 2012; Schwartz and Albert, 2010; Wang *et al.*, 2014). OAS family members are activated by many other alphaviruses such as VEEV (Koterski *et al.*, 2007), SFV, and SINV (Schoggins and Rice, 2011).

In summary, although OAS2 appears to be important for antiviral immune responses, the higher level of upregulation seen in MY/06/37348-infected suckling mice, which had higher mortality, suggests it may be less critical than other antiviral genes seen at higher levels in MY/08/065-infected suckling mice at 6 dpi.

5.6 Limitations of the current study

Virus isolates MY/06/37348 and MY/08/065 were used to represent Asian and ECSA genotypes of CHIKV, respectively, as they are well characterised clinical strains with available complete genomes. Further studies can be performed with more clinical strains to more fully represent the genotypes.

Microarray analysis was performed with duplicates samples only. Nonetheless, all the selected immune-related genes were consistently upregulated in both biological samples and were further confirmed with qRT-PCR with three biological replicates. Further studies of other host factors can be performed with more biological replicates or other newer techniques such as next-generation sequencing.

CHAPTER 6

CONCLUSION

This study showed that CHIKV Asian MY/06/37348 and ECSA MY/08/065 replicated and caused cell death and inflammation following intracranial inoculation into suckling mice, but not adult mice. Differences in neuron maturity and immune responses between suckling and adult mice may have caused age-dependent CHIKV infection as observed in this study, consistent with previous studies on CHIKV and other alphaviruses. Both viruses caused similar histopathologic findings of apoptosis, necrosis, and inflammation, with viral antigen detectable in widespread areas of the brain, possibly via spread through ependymal cells and cerebrospinal fluid of the ventricular system. CHIKV was localised to astrocytes and neurons. MY/06/37348 caused greater mortality in suckling mice, but this was not due to higher viral replication, as titres of both virus isolates were similar. MY/06/37348-infected suckling mice also showed greater spread of virus beyond the CNS, to skeletal muscle. This inter-strain variation in neurovirulence may have been due to differentially-expressed genes involved in the immune response. In MY/06/37348-infected suckling mice, there was greater upregulation of pro-apoptotic gene eIF2αK2 compared to MY/08/065-infected suckling mice at 1 dpi, which was supported by histopathologic evidence of apoptosis during early stages of infection. In MY/08/065-infected suckling mice, there was greater upregulation of genes involved in antiviral responses and CNS protection from cell death compared to MY/06/37348-infected suckling mice at 6 dpi, such as BIRC3, IL-10RA, MyD88, and PYCARD. At 6 dpi, MY/06/37348-infected suckling mice showed greater upregulation of OAS2 compared to MY/08/065-infected suckling mice, which is involved in antiviral immune response. These differences in immune responses induced by the different virus isolates are likely due to differences in viral

sequences encoding neurovirulence determinants, which would be of interest for future study.

This study has provided novel information on important host responses against intracerebral CHIKV infection in a mouse model, which may be potentially used to develop therapeutic and prophylactic strategies against CHIKV infection, and identify biomarkers for severity of neurological infections.

REFERENCES

Abere B, Wikan N, Ubol S, Auewarakul P, Paemanee A, Kittisenachai S, Roytrakul S, Smith DR. Proteomic analysis of chikungunya virus infected microglial cells. PLoS ONE. 2012;7:e34800.

AbuBakar S, Sam IC, Wong PF, MatRahim N, Hooi PS, Roslan N. Reemergence of endemic chikungunya, Malaysia. Emerging Infectious Diseases. 2007;13:147-149.

Aguilar PV, Weaver SC, Basler CF. Capsid protein of eastern equine encephalitis virus inhibits host cell gene expression. Journal of Virology. 2007;81:3866-3876.

Akahata W, Yang Z-Y, Andersen H, Sun S, Holdaway HA, Kong W-P, Lewis MG, Higgs S, Rossmann MG, Rao S, Nabel GJ. A virus-like particle vaccine for epidemic chikungunya virus protects nonhuman primates against infection. Nature Medicine. 2010;16:334-339.

Allen IC, Scull MA, Moore CB, Holl EK, McElvania-TeKippe E, Taxman DJ, Guthrie EH, Pickles RJ, Ting JP-Y. The NLRP3 inflammasome mediates *in vivo* innate immunity to influenza A virus through recognition of viral RNA. Immunity. 2009;30:556-565.

Apandi Y, Nazni WA, Noor Azleen ZA, Vythilingam I, Noorazian MY, Azahari AH, Zainah S, Lee HL. The first isolation of chikungunya virus from nonhuman primates in Malaysia. Journal of General and Molecular Virology. 2009;1:35-39.

Arpino C, Curatolo P, Rezza G. Chikungunya and the nervous system: what we do and do not know. Reviews in Medical Virology. 2009;19:121-129.

Assunção-Miranda I, Cruz-Oliveira C, Da Poian AT. Molecular mechanisms involved in the pathogenesis of alphavirus-induced arthritis. BioMed Research International. 2013;2013:973516.

Atkins GJ. The pathogenesis of alphaviruses. ISRN Virology. 2013;2013:861912.

Bachis A, Colangelo AM, Vicini S, Doe PP, De Bernardi MA, Brooker G, Mocchetti I. Interleukin-10 prevents glutamate-mediated cerebellar granule cell death by blocking caspase-3-like activity. Journal of Neuroscience. 2001;21:3104-3112.

Balluz IM, Glasgow GM, Killen HM, Mabruk MJMEF, Sheahan BJ, Atkins GJ. Virulent and avirulent strains of Semliki Forest virus show similar tropism for the murine central nervous system but differ in the severity and rate of induction of cytolytic damage. Neuropathology and Applied Neurobiology. 1993;19:233-239.

Barker BR, Taxman DJ, Ting JP-Y. Cross-regulation between the IL-1β/IL-18 processing inflammasome and other inflammatory cytokines. Current Opinion in Immunology. 2011;23:591-597.

Barry G, Breakwell L, Fragkoudis R, Attarzadeh-Yazdi G, Rodriguez-Andres J, Kohl A, Fazakerley JK. PKR acts early in infection to suppress Semliki Forest virus production and strongly enhances the type I interferon response. Journal of General Virology. 2009;90:1382-1391.

Bernard KA, Klimstra WB, Johnston RE. Mutations in the E2 glycoprotein of Venezuelan equine encephalitis virus confer heparan sulfate interaction, low morbidity, and rapid clearance from blood of mice. Virology. 2000;276:93-103.

Bertrand MJM, Doiron K, Labbé K, Korneluk RG, Barker PA, Sale M. Cellular inhibitors of apoptosis cIAP1 and cIAP2 are required for innate immunity signaling by the pattern recognition receptors NOD1 and NOD2. Immunity. 2009;30:789-801.

Bertrand MJM, Milutinovic S, Dickson KM, Ho WC, Boudreault A, Durkin J, Gillard JW, Jaquith JB, Morris SJ, Barker PA. cIAP1 and cIAP2 facilitate cancer cell survival by functioning as E3 ligases that promote RIP1 ubiquitination. Molecular Cell. 2008;30:689-700.

Bordignon J, Probst CM, Mosimann ALP, Pavoni DP, Stella V, Buck GA, Satproedprai N, Fawcett P, Zanata SM, de Noronha L, Krieger MA, dos Santos CND. Expression profile of interferon stimulated genes in central nervous system of mice infected with dengue virus type-1. Virology. 2008;377:319-329.

Bouquillard E, Combe B. A report of 21 cases of rheumatoid arthritis following chikungunya fever. A mean follow-up of two years. Joint Bone Spine. 2009;76:654-657.

Brault AC, Powers AM, Holmes EC, Woelk CH, Weaver SC. Positively charged amino acid substitutions in the E2 envelope glycoprotein are associated with the emergence of Venezuelan equine encephalitis virus. Journal of Virology. 2002;76:1718-1730.

Bréhin AC, Casadémont I, Frenkiel MP, Julier C, Sakuntabhai A, Desprès P. The large form of human 2′,5′-oligoadenylate synthetase (OAS3) exerts antiviral effect against chikungunya virus. Virology. 2009;384:216-222.

Burdette D, Haskett A, Presser L, McRae S, Iqbal J, Waris G. Hepatitis C virus activates interleukin-1β via caspase-1-inflammasome complex. Journal of General Virology. 2012;93:235-246.

Calisher CH, Maness KSC. Virulence of Venezuelan equine encephalomyelitis virus subtypes for various laboratory hosts. Applied Microbiology. 1974;28:881-884.

Carson WE, Lindemann MJ, Baiocchi R, Linett M, Tan JC, Chou CC, Narula S, Caligiuri MA. The functional characterization of interleukin-10 receptor expression on human natural killer cells. Blood. 1995;85:3577-3585.

Casolari S, Briganti E, Zanotti M, Zauli T, Nicoletti L, Magurano F, Fortuna C, Fiorentini C, Ciufolini MG, Rezza G. A fatal case of encephalitis associated with chikungunya virus infection. Scandinavian Journal of Infectious Diseases. 2008;40:995-996.

Chaaithanya IK, Muruganandam N, Raghuraj U, Sugunan AP, Rajesh R, Anwesh M, Rai SK, Vijayachari P. Chronic inflammatory arthritis with persisting bony erosions in patients following chikungunya infection. Indian Journal of Medical Research. 2014;140:142-145.

Chaaithanya IK, Muruganandam N, Sundaram SG, Kawalekar O, Sugunan AP, Manimunda SP, Ghosal SR, Muthumani K, Vijayachari P. Role of proinflammatory cytokines and chemokines in chronic arthropathy in CHIKV infection. Viral Immunology. 2011;24:265-271.

Chandak NH, Kashyap RS, Kabra D, Karandikar P, Saha SS, Morey SH, Purohit HJ, Taori GM, Daginawala HF. Neurological complications of chikungunya virus infection. Neurology India. 2009;57:177-180.

Chang L-J, Dowd KA, Mendoza FH, Saunders JG, Sitar S, Plummer SH, Yamshchikov G, Sarwar UN, Hu Z, Enama ME, Bailer RT, Koup RA, Schwartz RM, Akahata W, Nabel GJ, Mascola JR, Pierson TC, Graham BS, Ledgerwood JE, the VRC 311 Study Team. Safety and tolerability of chikungunya virus-like particle vaccine in healthy adults: a phase 1 dose-escalation trial. Lancet. 2014;384:2046-2052.

Chang RCC, Wong AKY, Ng H-K, Hugon J. Phosphorylation of eukaryotic initiation factor-2α (eIF2α) is associated with neuronal degeneration in Alzheimer's disease. Clinical Neuroscience and Neuropathology. 2002;13:2429-2432.

Chatterjee SN, Sarkar JK. Electron microscopic studies of suckling mouse brain cells infected with chikungunya virus. Indian Journal of Experimental Biology. 1965;3:227-234.

Chen C-I, Clark DC, Pesavento P, Lerche NW, Luciw PA, Reisen WK, Brault AC. Comparative pathogenesis of epidemic and enzootic chikungunya viruses in a pregnant rhesus macaque model. American Journal of Tropical Medicine and Hygiene. 2010;83:1249-1258.

Chen M, Barnfield C, Näslund TI, Fleeton MN, Liljeström P. MyD88 expression is required for efficient cross-presentation of viral antigens from infected cells. Journal of Virology. 2005;79:2964-2972.

Chiam CW, Chan YF, Loong SK, Yong SSJ, Hooi PS, Sam I-C. Real-time polymerase chain reaction for diagnosis and quantitation of negative strand of chikungunya virus. Diagnostic Microbiology and Infectious Disease. 2013;77:133-137.

Chirathaworn C, Poovorawan Y, Lertmaharit S, Wuttirattanakowit N. Cytokine levels in patients with chikungunya virus infection. Asian Pacific Journal of Tropical Medicine. 2013;6:631-634.

Chirathaworn C, Rianthavorn P, Wuttirattanakowit N, Poovorawan Y. Serum IL-18 and IL-18BP levels in patients with chikungunya virus infection. Viral Immunology. 2010;23:113-117.

Chow A, Her Z, Ong EKS, Chen JM, Dimatatac F, Kwek DJC, Barkham T, Yang H, Rénia L, Leo YS, Ng LFP. Persistent arthralgia induced by chikungunya virus infection is associated with interleukin-6 and granulocyte macrophage colony-stimulating factor. Journal of Infectious Diseases. 2011;203:149-157.

Chu H, Das SC, Fuchs JF, Suresh M, Weaver SC, Stinchcomb DT, Charalambos D Partidos, Jorge E Osorio. Deciphering the protective role of adaptive immunity to CHIKV/IRES a novel candidate vaccine against chikungunya in the A129 mouse model. Vaccine. 2013;31:3353-3360.

Chusri S, Siripaitoon P, Hirunpat S, Silpapojakul K. Case reports of neuro-chikungunya in Southern Thailand. American Journal of Tropical Medicine and Hygiene. 2011;85:386-389.

Clark AK, Marchand F, Auria MD, Davies M, Grist J, Malcangio M, McMahon SB. Cathepsin S inhibition attenuates neuropathic pain and microglial response associated with spinal cord injury. Open Pain Journal. 2010;3:117-122.

Clavarino G, Cláudio N, Couderc T, Dalet A, Judith D, Camosseto V, Schmidt EK, Wenger T, Lecuit M, Gatti E, Pierre P. Induction of GADD34 is necessary for dsRNA-dependent interferon-β production and participates in the control of chikungunya virus infection. PLoS Pathogens. 2012;8:e1002708.

Couderc T, Chrétien F, Schilte C, Disson O, Brigitte M, Guivel-Benhassine F, Touret Y, Barau G, Cayet N, Schuffenecker I, Desprès P, Arenzana-Seisdedos F, Michault A, Albert ML, Lecuit M. A mouse model for chikungunya: young age and inefficient Type-I interferon signaling are risk factors for severe disease. PLoS Pathogens. 2008;4:e29.

Couderc T, Khandoudi N, Grandadam M, Visse C, Gangneux N, Bagot S, Prost JF, Lecuit M. Prophylaxis and therapy for chikungunya virus infection. Journal of Infectious Diseases. 2009;200:516-523.

Couderc T, Lecuit M. Focus on chikungunya pathophysiology in human and animal models. Microbes and Infection. 2009;11:1197-1205.

Das T, Hoarau JJ, Bandjee MCJ, Maquart M, Gasque P. Multifaceted innate immune responses engaged by astrocytes, microglia and resident dendritic cells against chikungunya neuroinfection. Journal of General Virology. 2015;96:294-310.

Das T, Jaffar-Bandjee MC, Hoarau JJ, Krejbich-Trotot P, Denizot M, Lee-Pat-Yuen G, Sahoo R, Guiraud P, Ramful D, Robin S, Alessandri JL, Gauzere BA, Gasque P. Chikungunya fever: CNS infection and pathologies of a re-emerging arbovirus. Progress in Neurobiology. 2010;91:121-129.

De Kruif MD, Setiati TE, Mairuhu ATA, Koraka P, Aberson HA, Spek CA, Osterhaus ADME, Reitsma PH, Brandjes DPM, Soemantri A, van Gorp ECM. Differential gene expression changes in children with severe dengue virus infections. PLoS Neglected Tropical Diseases. 2008;2:e215.

De Lamballerie X, Leroy E, Charrel RN, Ttsetsarkin K, Higgs S, Gould EA. Chikungunya virus adapts to tiger mosquito via evolutionary convergence: a sign of things to come? Virology Journal. 2008;5:33.

De Ranitz CM, Myers RM, Varkey MJ, Isaac ZH, Carey DE. Clinical impressions of chikungunya in Vellore gained from study of adult patients. Indian Journal of Medical Research. 1965;53:756-763.

Dean JM, Wang X, Kaindl AM, Gressens P, Fleiss B, Hagberg H, Mallard C. Microglial MyD88 signaling regulates acute neuronal toxicity of LPS-stimulated microglia in vitro. Brain, Behavior, and Immunity. 2010;24:776-783.

Dhanwani R, Khan M, Alam SI, Rao PVL, Parida M. Differential proteome analysis of chikungunya virus-infected new-born mice tissues reveal implication of stress, inflammatory and apoptotic pathways in disease pathogenesis. Proteomics. 2011;11:1936-1951.

Diallo D, Sall AA, Buenemann M, Chen R, Faye O, Diagne CT, Faye O, Ba Y, Dia I, Watts D, Weaver SC, Hanley KA, Diallo M. Landscape ecology of sylvatic chikungunya virus and mosquito vectors in Southeastern Senegal. PLoS Neglected Tropical Diseases. 2012;6:e1649.

Doronin K, Flatt JW, di Paolo NC, Khare R, Kalyuzhniy O, Acchione M, Sumida JP, Ohto U, Shimizu T, Akashi-Takamura S, Miyake K, MacDonald JW, Bammler TK, Beyer RP, Farin FM, Stewart PL, Shayakhmetov DM. Coagulation factor X activates innate immunity to human species C adenovirus. Science. 2012;338:795-798.

Dupuis-Maguiraga L, Noret M, Brun S, Grand RL, Gras G, Roques P. Chikungunya disease: infection-associated markers from the acute to the chronic phase of arbovirus-induced arthralgia. PLoS Neglected Tropical Diseases. 2012;6:e1446.

Eckelman BP, Salvesen GS. The human anti-apoptotic proteins cIAP1 and cIAP2 bind but do not inhibit caspases. Journal of Biological Chemistry. 2006;281:3254-3260.

Eckels KH, Harrison VR, Hetrick FM. Chikungunya virus vaccine prepared by Tween-Ether extraction. Applied Microbiology. 1970;19:321-325.

Economopoulou A, Dominguez M, Helynck B, Sissoko D, Wichmann O, Quenel P, Germonnea P, Quatresous I. Atypical chikungunya virus infections: clinical manifestations, mortality and risk factors for severe disease during the 2005–2006 outbreak on Réunion. Epidemiology and Infection. 2009;137:534-541.

Edelman R, Tacket CO, Wasserman SS, Bodison SA, Perry JG, Mangiafico JA. Phase II safety and immunogenicity study of live chikungunya virus vaccine TSI-GSD-218. American Journal of Tropical Medicine and Hygiene. 2000;62:681-685.

Esen N, Rainey-Barger EK, Huber AK, Blakely PK, Irani DN. Type-I interferons suppress microglial production of the lymphoid chemokine, CXCL13. Glia. 2014;62:1452-1462.

Fazakerley JK. Pathogenesis of Semliki Forest virus encephalitis. Journal of Neurovirology. 2002;8:66-74.

Fazakerley JK. Semliki Forest virus infection of laboratory mice: a model to study the pathogenesis of viral encephalitis. Archives of Virology. 2004;18:179-190.

Fink J, Gu F, Ling L, Tolfvenstam T, Olfat F, Chin KC, Aw P, George J, Kuznetsov VA, Schreiber M, Vasudevan SG, Hibberd ML. Host gene expression profiling of dengue virus infection in cell lines and patients. PLoS Neglected Tropical Diseases. 2007;1:e86.

Fleming P. Age-dependent and strain-related differences of virulence of Semliki Forest virus in mice. Journal of General Virology. 1977;37:93-105.

Fragkoudis R, Ballany CM, Boyd A, Fazakerley JK. In Semliki Forest virus encephalitis, antibody rapidly clears infectious virus and is required to eliminate viral material from the brain, but is not required to generate lesions of demyelination. Journal of General Virology. 2008;89:2565-2568.

Franchi L, Muñoz-Planillo R, Núñez G. Sensing and reacting to microbes through the inflammasomes. Nature Immunology. 2012;13:325-332.

Frolova EI, Fayzulin RZ, Cook SH, Griffin DE, Rice CM, Frolov I. Roles of nonstructural protein nsP2 and alpha/beta interferons in determining the outcome of Sindbis virus infection. Journal of Virology. 2002;76:11254-11264.

Fros JJ, Liu WJ, Prow NA, Geertsema C, Ligtenberg M, Vanlandingham DL, Schnettler E, Vlak JM, Suhrbier A, Khromykh AA, Pijlman GP. Chikungunya virus nonstructural protein 2 inhibits type I/II interferon-stimulated Jak-STAT signaling. Journal of Virology. 2010;84:10877-10887.

Gad HH, Paulous S, Belarbi E, Diancourt L, Drosten C, Kümmerer BM, Aileen E Plate, Valérie Caro, Philippe Desprès. The E2-E166K substitution restores chikungunya virus growth in OAS3 expressing cells by acting on viral entry. Virology. 2012;434:27-37.

Galbraith SE, Sheahan BJ, Atkins GJ. Deletions in the hypervariable domain of the nsP3 gene attenuate Semliki Forest virus virulence. Journal of General Virology. 2006;87:893-947.

Galluzzi L, Vitale I, Abrams JM, Alnemri ES, Baehrecke EH, Blagosklonny MV, Dawson TM, Dawson VL, El-Deiry WS, Fulda S, Gottlieb E, Green DR, Hengartner MO, Kepp O, Knight RA, Kumar S, Lipton SA, Lu X, Madeo F, Malorni W, Mehlen P, Nuñez G, Peter ME, Piacentini M, Rubinsztein DC, Shi Y, Simon H-U, Vandenabeele P, White E, Yuan J, Zhivotovsky B, Melino G, Kroemer G. Molecular definitions of cell death subroutines: recommendations of the Nomenclature Committee on Cell Death 2012. Cell Death and Differentiation. 2012;19:107-120.

Ganesan K, Diwan A, Shankar SK, Desai SB, Sainani GS, Katrak SM. Chikungunya encephalomyeloradiculitis: report of 2 cases with neuroimaging and 1 case with autopsy findings. American Journal of Neuroradiology. 2008;29:1636-1637.

Gardner CL, Burke CW, Higgs ST, Klimstra WB, Ryman KD. Interferon-alpha/beta deficiency greatly exacerbates arthritogenic disease in mice infected with wild-type chikungunya virus but not with the cell culture-adapted live-attenuated 181/25 vaccine candidate. Virology. 2012;425:103-112.

Gardner CL, Hritz J, Sun C, Vanlandingham DL, Song TY, Ghedin E, Higgs S, Klimstra WB, Ryman KD. Deliberate attenuation of chikungunya virus by adaptation to heparan sulfate-dependent infectivity: a model for rational arboviral vaccine design. PLoS Neglected Tropical Diseases. 2014;8:e2719.

Gardner J, Anraku I, Le TT, Larcher T, Major L, Roques P, Schroder WA, Higgs S, Suhrbier A. Chikungunya virus arthritis in adult wild-type mice. Journal of Virology. 2010;84:8021-8032.

Garmashova N, Gorchakov R, Volkova E, Paessler S, Frolova E, Frolov I. The old world and new world alphaviruses use different virus-specific proteins for induction of transcriptional shutoff. Journal of Virology. 2007;81:2472-2484.

Gasque P, editor. Chikungunya virus infection. Basel: Springer Basel; 2013. 21 p. (Jackson AC, editor. Viral infections of the human nervous system).

Gauri L, Ranwa B, Nagar K, Vyas A, Fatima Q. Post chikungunya brain stem encephalitis. Journal of the Association of Physicians of India. 2012;16:68-69.

Gérardin P, Barau G, Michault A, Bintner M, Randrianaivo H, Choker G, Lenglet Y, Touret Y, Bouveret A, Grivard P, le Roux K, Blanc S, Schuffenecker I, Couderc T, Arenzana-Seisdedos F, Lecuit M, Robillard PY. Multidisciplinary prospective study of mother-to-child chikungunya virus infections on the Island of La Réunion. PLoS Medicine. 2008;5:e60.

Gérardin P, Sampériz S, Ramful D, Boumahni B, Bintner M, Alessandri JL, Carbonnier M, Tiran-Rajaoefera I, Beullier G, Boya I, Noormahomed T, Okoï J, Rollot O, Cotte L, Jaffar-Bandjee MC, Michault A, Favier F, Kaminski M, Fourmaintraux A, Fritel X. Neurocognitive outcome of children exposed to perinatal mother-to-child chikungunya virus infection: the CHIMERE cohort study on Reunion Island. PLoS Neglected Tropical Diseases. 2014;8:e2996.

Glasgow GM, McGee MM, Sheahan BJ, Atkins GJ. Death mechanisms in cultured cells infected by Semliki Forest virus. Journal of General Virology. 1997;78:1559-1563.

Griffin DE, Hardwick JM. Apoptosis in alphavirus encephalitis. Virology. 1998;8:481-489.

Griffin DE, Levine B, Ubol S, Hardwick JM. The effects of alphavirus infection on neurons. Annals of Neurology. 1994;35:S23-S27.

Griffin DE, editor. Chapter 31, Alphaviruses. Philadelphia: Lippincott Williams & Wilkins; 2007. 43 p. (Knipe DM, Howley PM, editors. Fields virology; vol. 6).

Griffin DE. Neuronal cell death in alphavirus encephalomyelitis. Current Topics in Microbiology and Immunology. 2005;289:57-77.

Gump JM, Thorburn A. Autophagy and apoptosis- what's the connection? Trends in Cell Biology. 2011;21:387-392.

Gupta N, Rao PVL. Transcriptomic profile of host response in Japanese encephalitis virus infection. Virology Journal. 2011;8:92.

Hallengärd D, Lum F-M, Kümmerer BM, Lulla A, Lulla V, García-Arriaza J, Fazakerley JK, Roques P, le Grand R, Merits A, Ng LFP, Esteban M, Liljeström P. Prime-boost immunization strategies against chikungunya virus. Journal of Virology. 2014;88:13333-13343.

Halstead SB, Buescher EL. Hemorrhagic disease in rodents infected with virus associated with Thai hemorrhagic fever. Science. 1961;134:475-476.

Hammon WMcD, Rundnick A, Sather GE. Viruses associated with epidemic hemorrhagic fevers of the Philippines and Thailand. Science. 1960;131:1102-1103.

Harrison VR, Binn LN, Randall R. Comparative immunogenicities of chikungunya vaccines prepared in avian and mammalian tissues. American Journal of Tropical Medicine and Hygiene. 1967;16:786-791.

Havert MB, Schofield B, Griffin DE, Irani DN. Activation of divergent neuronal cell death pathways in different target cell populations during neuroadapted Sindbis virus infection of mice. Journal of Virology. 2000;74:5352-5356.

Hawman DW, Stoermer KA, Montgomery SA, Pal P, Oko L, Diamond MS, Morrison TE. Chronic joint disease caused by persistent chikungunya virus infection is controlled by the adaptive immune response. Journal of Virology. 2013;87:13878-13888.

He JQ, Zarnegar B, Oganesyan G, Saha SK, Yamazaki S, Doyle SE, Dempsey PW, Cheng G. Rescue of TRAF3-null mice by p100 NF-κB deficiency. Journal of Experimental Medicine. 2006;203:2413.

Hemmi H, Kaisho T, Takeuchi O, Sato S, Sanjo H, Hoshino K, Horiuchi T, Tomizawa H, Takeda K, Akira S. Small anti-viral compounds activate immune cells via the TLR7 MyD88–dependent signaling pathway. Nature Immunology. 2002;3:196-200.

Her Z, Malleret B, Chan M, Ong EKS, Wong S-C, Kwek DJC, Tolou H, Lin RTP, Tambyah PA, Rénia L, Ng LFP. Active infection of human blood monocytes by chikungunya virus triggers an innate immune response. Journal of Immunology. 2010;184:5903-5913.

Hoarau JJ, Jaffar-Bandjee MC, Trotot PK, Das T, Li-Pat-Yuen G, Dassa B, Denizot M, Guichard E, Ribera A, Henni T, Tallet F, Moiton MP, Gauzère BA, Bruniquet S, Bandjee ZJ, Morbidelli P, Martigny G, Jolivet M, Gay F, Grandadam M, Tolou H, Vieillard V, Debré P, Autran B, Gasque P. Persistent chronic inflammation and infection by chikungunya arthritogenic alphavirus in spite of a robust host immune response. Journal of Immunology. 2010;184:5914-5927.

Howard M, O'Garra A, Ishida H, de Waal Malefyt R, de Vries J. Biological properties of interleukin 10. Journal of Clinical Immunology. 1992;12:239-247.

Huang J-H, Yang C-F, Su C-L, Chang S-F, Cheng C-H, Yu S-K, Lin C-C, Shu P-Y. Imported chikungunya virus strains, Taiwan 2006-2009. Emerging Infectious Diseases. 2009;15:1854-1856.

Inoue S, Morita K, Matias RR, Tuplano JV, Resuello RR, Candelario JR, Cruz DJ, Mapua CA, Hasebe F, Igarashi A, Natividad FF. Distribution of three arbovirus antibodies among monkeys (*Macaca fascicularis*) in the Philippines. Journal of Medical Primatology. 2003;32:89-94.

Jackson AC, Rossiter J. Apoptotic cell death is an important cause of neuronal injury in experimental Venezuelan equine encephalitis virus infection of mice. Acta Neuropathology. 1997;93:349-353.

Jadhav M, Namboodripad M, Carman RH, Carey DE, Myers RM. Chikungunya disease in infants and children in Vellore: a report of clinical and haematological features of virologically proved cases. Indian Journal of Medical Research. 1965;53:764-776.

Jan J-T, Griffin DE. Induction of apoptosis by Sindbis virus occurs at cell entry and does not require virus replication. Journal of Virology. 1999;73:10296-10302.

Jenkins JK, Malyak M, Arend WP. The effects of interleukin-10 on interleukin-1 receptor antagonist and interleukin-1 beta production in human monocytes and neutrophils. Lymphokine and Cytokine Research. 1994;13:47-54.

Jiang H-Y, Wek RC. Phosphorylation of the α-subunit of the eukaryotic initiation factor-2 (eIF2α) reduces protein synthesis and enhances apoptosis in response to proteasome inhibition. Journal of Biological Chemistry. 2005;280:14189-14202.

Johnston C, Jiang W, Chu T, Levine B. Identification of genes involved in the host response to neurovirulent alphavirus infection. Journal of Virology. 2001;75:10431-10445.

Jose J, Snyder JE, Kuhn RJ. A structural and functional perspective of alphavirus replication and assembly. Future Microbiology. 2009;4:837-856.

Joubert PE, Werneke SW, de la Calle C, Guivel-Benhassine F, Giodini A, Peduto L, Levine B, Schwartz O, Lenschow DJ, Albert ML. Chikungunya virus-induced autophagy delays caspase-dependent cell death. Journal of Experimental Medicine. 2012;209:1029-1047.

Judith D, Mostowy S, Bourai M, Gangneux N, Lelek M, Lucas-Hourani M, Cayet N, Jacob Y, Prévost MC, Pierre P, Tangy F, Zimmer C, Vidalain PO, Couderc T, Lecuit M. Species-specific impact of the autophagy machinery on chikungunya virus infection. EMBO reports. 2013;14:534-543.

Kalita J, Kumar P, Misra UK. Stimulus-sensitive myoclonus and cerebellar ataxia following chikungunya meningoencephalitis. Infection. 2013;41:727-729.

Kam Y-W, Ong EKS, Rénia L, Tong J-C, Ng LFP. Immuno-biology of chikungunya and implications for disease intervention. Microbes and Infection. 2009;11:1186-1196.

Kashyap RS, Morey SH, Chandak NH, Purohit HJ, Taori GM, Daginawala HF. Detection of viral antigen, IgM and IgG antibodies in cerebrospinal fluid of chikungunya patients with neurological complications. Cerebrospinal Fluid Research. 2010;7:12.

Kelvin AA, Banner D, Silvi G, Moro ML, Spataro N, Gaibani P, Cavrini F, Pierro A, Rossini G, Cameron MJ, Bermejo-Martin JF, Paquette SG, Xu L, Danesh A, Farooqui A, Borghetto I, Kelvin DJ, Sambri V, Rubino S. Inflammatory cytokine expression is associated with chikungunya virus resolution and symptom severity. PLoS Neglected Tropical Diseases. 2011;5:e1279.

Khan AH, Morita K, Parquet MdC, Hasebe F, Mathenge EGM, Igarashi A. Complete nucleotide sequence of chikungunya virus and evidence for an internal polyadenylation site. Journal of General Virology. 2002;83:3075-3084.

Khan M, Dhanwani R, Rao PVL, Parida M. Subunit vaccine formulations based on recombinant envelope proteins of chikungunya virus elicit balanced Th1/Th2 response and virus-neutralizing antibodies in mice. Virus Research. 2012;167:236-246.

Kirkman NJ, Libbey JE, Wilcox KS, White HS, Fujinami RS. Innate but not adaptive immune responses contribute to behavioral seizures following viral infection. Epilepsia. 2010;51:454-464.

Komurian-Pradel F, Perret M, Deiman B, Sodoyer M, Lotteau V, Paranhos-Baccalà G, André P. Strand specific quantitative real-time PCR to study replication of hepatitis C virus genome. Journal of Virological Methods. 2004;116:103-106.

Koterski J, Twenhafel N, Porter A, Reed DS, Martino-Catt S, Sobral B, Crasta O, Downey T, da Silva L. Gene expression profiling of nonhuman primates exposed to aerosolized Venezuelan equine encephalitis virus. FEMS Immunology and Medical Microbiology. 2007;51:462-472.

Krejbich-Trotot P, Denizot M, Hoarau JJ, Jaffar-Bandjee MC, Das T, Gasque P. Chikungunya virus mobilizes the apoptotic machinery to invade host cell defenses. The FASEB Journal. 2011a;25:314-325.

Krejbich-Trotot P, Gay B, Li-Pat-Yuen G, Hoarau JJ, Jaffar-Bandjee MC, Briant L, Gasque P, Denizot M. Chikungunya triggers an autophagic process which promotes viral replication. Virology Journal. 2011b;8:432.

Kumar M, Sudeep AB, Arankalle VA. Evaluation of recombinant E2 protein-based and whole-virus inactivated candidate vaccines against chikungunya virus. Vaccine. 2012a;30:6142-6149.

Kumar S, Jaffar-Bandjee MC, Giry C, de Kerillis LC, Merits A, Gasque P, Hoarau JJ. Mouse macrophage innate immune response to chikungunya virus infection. Virology Journal. 2012b;9:313.

Kumarasamy V, Prathapa S, Zuridah H, Chern YK, Norizah I, Chua KB. Re-emergence of chikungunya virus in Malaysia. Medical Journal of Malaysia. 2006;61:221-225.

Labadie K, Larcher T, Joubert C, Mannioui A, Delache B, Brochard P, Guigand L, Dubreil L, Lebon P, Verrier B, de Lamballerie X, Suhrbier A, Cherel Y, le Grand R, Roques P. Chikungunya disease in nonhuman primates involves long-term viral persistence in macrophages. Journal of Clinical Investigation. 2010;120:894-906.

Labrada L, Liang XH, Zheng W, Johnston C, Levine B. Age-dependent resistance to lethal alphavirus encephalitis in mice: analysis of gene expression in the central nervous system and identification of a novel interferon-inducible protective gene, mouse *ISG12*. Journal of Virology. 2002;76:11688-11703.

Lam SK, Chua KB, Hooi PS, Rahimah MA, Kumari S, Tharmaratnam M, Chuah SK, Smith DW, Sampson IA. Chikungunya infection: an emerging disease in Malaysia. Southeast Asian Journal Tropical Medicine and Public Health. 2001;32:447-451.

Lanciotti RS, Kosoy OL, Laven JJ, Panella AJ, Velez JO, Lambert AJ, Campbell GL. Chikungunya virus in US travelers returning from India, 2006. Emerging Infectious Diseases. 2007;13:764-767.

Lang KS, Navarini AA, Recher M, Lang PA, Heikenwalder M, Stecher B, Bergthaler A, Odermatt B, Akira S, Honda K, Hengartner H, Zinkernagel RM. MyD88 protects from lethal encephalitis during infection with vesicular stomatitis virus. European Journal of Immunology. 2007;37:2434-2440.

Laoprasopwattana K, Kaewjungwad L, Jarumanokul R, Geater A. Differential diagnosis of chikungunya, dengue viral infection and other acute febrile illnesses in children. Pediatric Infectious Disease Journal. 2012;31:459-463.

Latz E. The inflammasomes: mechanisms of activation and function. Current Opinion in Immunology. 2010;22:28-33.

Lazear HM, Lancaster A, Wilkins C, Suthar MS, Huang A, Vick SC, Clepper L, Thackray L, Brassil MM, Virgin HW, Nikolich-Zugich J, Moses A, Gale Jr M, Früh K, Diamond MS. IRF-3, IRF-5, and IRF-7 coordinately regulate the type I IFN response in myeloid dendritic cells downstream of MAVS signaling. PLoS Pathogens. 2013;9:e1003118.

Lee VJ, Chow A, Zheng X, Carrasco LR, Cook AR, Lye DC, Ng LC, Leo YS. Simple clinical and laboratory predictors of chikungunya versus dengue infections in adults. PLoS Neglected Tropical Diseases. 2012;6:e1786.

Lemant J, Boisson V, Winer A, Thibault L, André H, Tixier F, Lemercier M, Antok E, Cresta MP, Grivard P, Besnard M, Rollot O, Favier F, Huerre M, Campinos JL, Michault A. Serious acute chikungunya virus infection requiring intensive care during the reunion island outbreak in 2005-2006. Critical Care Medicine. 2008;36:2536-2541.

Leparc-Goffart I, Nougairede A, Cassadou S, Prat C, de Lamballerie X. Chikungunya in the Americas. Lancet. 2014;383:514.

Levine B, Griffin DE. Persistence of viral RNA in mouse brains after recovery from acute alphavirus encephalitis. Journal of Virology. 1992;66:6429-6435.

Levine B, Hardwick JM, Trapp BD, Crawford TO, Bollinger RC, Griffin DE. Antibody-mediated clearance of alphavirus infection from neurons. Science. 1991;254:856-860.

Levine B, Huang Q, Isaacs JT, Reed JC, Griffin DE, Hardwick JM. Conversion of lytic to persistent alphavirus infection by the bcl-2 cellular oncogene. Nature. 1993;361:739-742.

Levitt NH, Ramsburg HH, Hasty SE, Repik PM, Cole Jr FE, Lupton HW. Development of an attenuated strain of chikungunya virus for use in vaccine production. Vaccine. 1986;4:157-162.

Lewis J, Wesselingh SL, Griffin DE, Hardwick JM. Alphavirus-induced apoptosis in mouse brains correlates with neurovirulence. Journal of Virology. 1996;70:1828-1835.

Lewthwaite P, Vasanthapuram R, Osborne JC, Begum A, Plank JLM, Shankar MV, Hewson R, Desai A, Beeching NJ, Ravikumar R, Solomon T. Chikungunya virus and central nervous system infections in children, India. Emerging Infectious Diseases. 2009;15:329-331.

Lin K-I, Lee S-H, Narayanan R, Baraban JM, Hardwick JM, Ratan RR. Thiol agents and bcl-2 identify an alphavirus-induced apoptotic pathway that requires activation of the transcription factor NF-kappa B. Journal of Cell Biology. 1995;131:1149-1161.

Logue CH, Bosio CF, Welte T, Keene KM, Ledermann JP, Phillips A, Sheahan BJ, Pierro DJ, Marlenee N, Brault AC, Bosio CM, Singh AJ, Powers AM, Olson KE. Virulence variation among isolates of western equine encephalitis virus in an outbred mouse model. Journal of General Virology. 2009;90:1848-1858.

Lohachanakul J, Phuklia W, Thannagith M, Thongsakulprasert T, Smith DR, Ubol S. Differences in response of primary human myoblasts to infection with recent epidemic strains of chikungunya virus isolated from patients with and without myalgia. Journal of Medical Virology. 2015;87:733-739.

Loiarro M, Gallo G, Fantò N, Santis RD, Carminati P, Ruggiero V, Sette C. Identification of critical residues of the MyD88 death domain involved in the recruitment of downstream kinases. Journal of Biological Chemistry. 2009;284:28093-28103.

Lumsden WHR. An epidemic of virus disease in Southern Province, Tanganyika territory, in 1952–1953 II. General description and epidemiology. Transactions of the Royal Society of Tropical Medicine and Hygiene. 1955;49:33-57.

Lum F-M, Teo T-H, Lee WWL, Kam Y-W, Rénia L, Ng LFP. An essential role of antibodies in the control of chikungunya virus infection. Journal of Immunology. 2013;190:6295-6302.

Mallilankaraman K, Shedlock DJ, Bao H, Kawalekar OU, Fagone P, Ramanathan AA, Ferraro B, Stabenow J, Vijayachari P, Sundaram SG, Muruganandam N, Sarangan G, Srikanth P, Khan AS, Lewis MG, Kim JJ, Sardesai NY, Muthumani K, Weiner DB. A DNA vaccine against chikungunya virus is protective in mice and induces neutralizing antibodies in mice and nonhuman primates. PLoS Neglected Tropical Diseases. 2011;5:e928.

Maulik N, Sasaki H, Galang N. Differential regulation of apoptosis by ischemia-reperfusion and ischemic adaptation. Annals of the New York Academy of Sciences. 2006;874:401-411.

Maysinger D, Berezovskaya O, Fedoroff S. The hematopoietic cytokine colony stimulating factor 1 is also a growth factor in the CNS: (II) Microencapsulated CSF-1 and LM-10 cells as delivery systems. Experimental Neurology. 1996;141:47-56.

McKimmie CS, Roy D, Forster T, Fazakerley JK. Innate immune response gene expression profiles of N9 microglia are pathogen-type specific. Journal of Neuroimmunology. 2006;175:128-141.

Mohan A, Kiran DHN, Manohar IC, Kumar DP. Epidemiology, clinical manifestations, and diagnosis of chikungunya fever: lessons learned from the re-emerging epidemic. Indian Journal of Dermatology. 2010;55:54-63.

Mohd Zim MA, Sam IC, Syed Omar SF, Chan YF, AbuBakar S, Kamarulzaman A. Chikungunya infection in Malaysia: comparison with dengue infection in adults and predictors of persistent arthralgia. Journal of Clinical Virology. 2013;56:141-145.

Moore KW, de Waal Malefyt R, Coffman RL, O'Garra A. Interleukin-10 and the interleukin-10 receptor. Annual Review of Immunology. 2001;19:683–765.

Morris MM, Dyson H, Baker D, Harbige LS, Fazakerley JK, Amor S. Characterization of the cellular and cytokine response in the central nervous system following Semliki Forest virus infection. Journal of Neuroimmunology. 1997;74:185-197.

Morrison TE, Oko L, Montgomery SA, Whitmore AC, Lotstein AR, Gunn BM, Elmore SA, Heise MT. A mouse model of chikungunya virus-induced musculoskeletal inflammatory disease: evidence of arthritis, tenosynovitis, myositis, and persistence. American Journal of Pathology. 2011;178:32-40.

Morrison TE, Whitmore AC, Shabman RS, Lidbury BA, Mahalingam S, Heise MT. Characterization of Ross River virus tropism and virus-induced inflammation in a mouse model of viral arthritis and myositis. Journal of Virology. 2006;80:737-749.

Musthafa AK, Abdurahiman P, Jose J. Case of ADEM following chikungunya fever. Journal of the Association of Physicians of India. 2008;56:473.

Muthumani K, Lankaraman KM, Laddy DJ, Sundaram SG, Chung CW, Sako E, Khan A, Sardesai N, Kim JJ, Vijayachari P, Weiner DB. Immunogenicity of novel consensus-based DNA vaccines against chikungunya virus. Vaccine. 2008;26:5128-5134.

Nagata LP, Hu W-G, Parker M, Chau D, Rayner GA, Schmaltz FL, Wong JP. Infectivity variation and genetic diversity among strains of Western equine encephalitis virus. Journal of General Virology. 2006;87:2353-2361.

Nakagawa TY, Brissette WH, Lira PD, Griffiths RJ, Petrushova N, Stock J, McNeish JD, Eastman SE, Howard ED, Clarke SRM, Rosloniec EF, Elliott EA, Rudensky AY. Impaired invariant chain degradation and antigen presentation and diminished collagen-induced arthritis in cathepsin S null mice. Immunity. 1999;10:207-217.

Nakanishi H. Neuronal and microglial cathepsins in aging and age-related diseases. Ageing Research Reviews. 2003;2:367-381.

Nakao E. Biological and immunological studies on chikungunya virus: a comparative observation of two strains of African and Asian origins. Kobe Journal of Medical Sciences. 1972;18:133-141.

Nakaya HI, Gardner J, Poo Y-S, Major L, Pulendran B, Suhrbier A. Gene profiling of chikungunya virus arthritis in a mouse model reveals significant overlap with rheumatoid arthritis. Arthritis and Rheumatism. 2012;64:3553-3563.

Nandi S, Gokhan S, Dai X-M, Wei S, Enikolopov G, Lin H, Mehler MF, Stanley ER. The CSF-1 receptor ligands IL-34 and CSF-1 exhibit distinct developmental brain expression patterns and regulate neural progenitor cell maintenance and maturation. Developmental Biology. 2012;367:100-113.

Nargi-Aizenman JL, Griffin DE. Sindbis virus-induced neuronal death is both necrotic and apoptotic and is ameliorated by n-methyl-d-aspartate receptor antagonists. Journal of Virology. 2001;75:7114-7121.

Nelson J, Waggoner JJ, Sahoo MK, Grant PM, Pinsky BA. Encephalitis caused by chikungunya virus in a traveler from the Kingdom of Tonga. Journal of Clinical Microbiology. 2014;52:3459-3461.

Newton K, Dugger DL, Wickliffe KE, Kapoor N, de Almagro MC, Vucic D, Komuves L, Ferrando RE, French DM, Webster J, Roose-Girma M, Warming S, Dixit VM. Activity of protein kinase RIPK3 determines whether cells die by necroptosis or apoptosis. Science. 2014;343:1357-1360.

Ng LFP, Chow A, Sun Y-J, Kwek DJ, Lim P-L, Dimatatac F, Lee-Ching Ng, Ooi E-E, Choo K-H, Her Z, Kourilsky P, Leo Y-S. IL-1 β, IL-6, and RANTES as biomarkers of chikungunya severity. PLoS ONE. 2009;4:e4261.

Noret M, Herrero L, Rulli N, Rolph M, Smith PN, Li RW, Roques P, Gras G, Mahalingam S. Interleukin 6, RANKL, and osteoprotegerin expression by chikungunya virus-infected human osteoblasts. Journal of Infectious Diseases. 2012;7:457-459.

Nougairede A, de Fabritus L, Aubry F, Gould EA, Holmes EC, de Lamballerie X. Random codon re-encoding induces stable reduction of replicative fitness of chikungunya virus in primate and mosquito cells. PLoS Pathogens. 2013;9:e1003172.

O'Keefe GM, Nguyen VT, Benveniste EN. Regulation and function of class II major histocompatibility complex, CD40, and B7 expression in macrophages and microglia: implications in neurological diseases. Journal of NeuroVirology. 2002;8:496-512.

Oliver KR, Fazakerley JK. Transneuronal spread of Semliki Forest virus in the developing mouse olfactory system is determined by neuronal maturity. Neuroscience. 1997;82:867-877.

Oliver KR, Scallan MF, Dyson H, Fazakerley JK. Susceptibility to a neurotropic virus and its changing distribution in the developing brain is a function of CNS maturity. Journal of Neurovirology. 1997;3:38-48.

Oliver M, Grandadam M, Marimoutou C, Rogier C, Botelho-Nevers E, Tolou H, Moalic J-L, Kraemer P, Morillon M, Morand J-J, Jeandel P, Parola P, Simon F. Persisting mixed cryoglobulinemia in chikungunya infection. PLoS Neglected Tropical Diseases. 2009;3:e374.

Osawa R, Williams KL, Singh N. The inflammasome regulatory pathway and infections: role in pathophysiology and clinical implications. Journal of Infection. 2011;62:119-129.

Ozden S, Huerre M, Riviere J-P, Coffey LL, Afonso PV, Mouly V, de Monredon J, Roger J-C, Amrani ME, Yvin J-L, Jaffar M-C, Frenkiel M-P, Sourisseau M, Schwartz O, Butler-Browne G, Desprès P, Gessain A, Ceccaldi P-E. Human muscle satellite cells as targets of chikungunya virus infection. PLoS ONE. 2007;2:e527.

Pais TF, Figueiredo C, Peixoto R, Braz MH, Chatterjee S. Necrotic neurons enhance microglial neurotoxicity through induction of glutaminase by a MyD88-dependent pathway. Journal of Neuroinflammation. 2008;5:43.

Pang IK, Iwasaki A. Inflammasomes as mediators of immunity against influenza virus. Trends in Immunology. 2011;32:34-41.

Panning M, Grywna K, van Esbroeck M, Emmerich P, Drosten C. Chikungunya fever in travelers returning to Europe from the Indian Ocean region, 2006. Emerging Infectious Diseases. 2008;14:416-22.

Park E, Griffin DE. The nsP3 macro domain is important for Sindbis virus replication in neurons and neurovirulence in mice. Virology. 2009;388:305-314.

Parola P, de Lamballerie X, Jourdan J, Rovery C, Vaillant V, Minodier P, Brouqui P, Flahault A, Raoult D, Charrel RN. Novel chikungunya virus variant in travelers returning from Indian Ocean islands. Emerging Infectious Diseases. 2006;12:1493-1499.

Patil DR, Hundekar SL, Arankalle VA. Expression profile of immune response genes during acute myopathy induced by chikungunya virus in a mouse model. Microbes and Infection. 2012;14:457-469.

Peiris JS, Dittus WP, Ratnayake CB. Seroepidemiology of dengue and other arboviruses in a natural population of toque macaques (*Macaca sinica*) at Polonnaruwa, Sri Lanka. Journal of Medical Primatology. 1993;22:240-245.

Plante K, Wang E, Partidos CD, Weger J, Gorchakov R, Tsetsarkin K, Borland EM, Powers AM, Seymour R, Stinchcomb DT, Osorio JE, Frolov I, Weaver SC. Novel chikungunya vaccine candidate with an IRES-based attenuation and host range alteration mechanism. PLoS Pathogens. 2011;7:e1002142.

Plaskon NE, Adelman ZN, Myles KM. Accurate strand-specific quantification of viral RNA. PLoS ONE. 2009;4:e7468.

Poeck H, Bscheider M, Gross O, Finger K, Roth S, Rebsamen M, Hannesschläger N, Schlee M, Rothenfusser S, Barchet W, Kato H, Akira S, Inoue S, Endres S, Peschel C, Hartmann G, Hornung V, Ruland J. Recognition of RNA virus by RIG-I results in activation of CARD9 and inflammasome signaling for interleukin 1β production. Nature Immunology. 2010;11:63-69.

Pothlichet J, Meunier I, Davis BK, Ting JP-Y, Skamene E, von Messling V, Vidal SM. Type I IFN triggers RIG-I/TLR3/NLRP3-dependent inflammasome activation in influenza A virus infected cells. PLoS Pathogens. 2013;9:e1003256.

Powers AM, Logue CH. Changing patterns of chikungunya virus: re-emergence of a zoonotic arbovirus. Journal of General Virology. 2007;88:2363-2377.

Priya R, Dhanwani R, Patro IK, Rao PVL, Parida MM. Differential regulation of TLR mediated innate immune response of mouse neuronal cells following infection with novel ECSA genotype of chikungunya virus with and without E1:A226V mutation. Infection, Genetics and Evolution. 2013;20:396-406.

Priya R, Patro IK, Parida MM. TLR3 mediated innate immune response in mice brain following infection with chikungunya virus. Virus Research. 2014;189:194-205.

Prosniak M, Hooper DC, Dietzschold B, Koprowski H. Effect of rabies virus infection on gene expression in mouse brain. Proceedings of the National Academy of Sciences. 2001;98:2758-2763.

Pulmanausahakul R, Roytrakul S, Auewarakul P, Smith DR. Chikungunya in Southeast Asia: understanding the emergence and finding solutions. International Journal of Infectious Diseases. 2011;15:e671-e676.

Rampal, Sharda M, Meena H. Neurological complications in chikungunya fever. Journal of the Association of Physicians of India. 2007;55:765-769.

Randall RE, Goodbourn S. Interferons and viruses: an interplay between induction, signalling, antiviral responses and virus countermeasures. Journal of General Virology. 2008;89:1-47.

Rathore APS, Ng M-L, Vasudevan SG. Differential unfolded protein response during chikungunya and Sindbis virus infection: CHIKV nsP4 suppresses eIF2α phosphorylation. Virology Journal. 2013;10:36.

Reed LJ, Muench H. A simple method of estimating fifth percentage endpoints. American Journal of Hygiene. 1938;27:493-497.

Renault P, Solet JL, Sissoko D, Balleydier E, Larrieu S, Filleul L, Lassalle C, Thiria J, Rachou E, de Valk H, Ilef D, Ledrans M, Quatresous I, Quenel P, Pierre V. A major epidemic of chikungunya virus infection on Réunion Island, France, 2005-2006. American Journal of Tropical Medicine and Hygiene. 2007;77:727-731.

Rezza G, Nicoletti L, Angelini R, Romi R, Finarelli AC, Panning M, Cordioli P, Fortuna C, Boros S, Magurano F, Silvi G, Angelini P, Dottori M, Ciufolini MG, Majori GC, Cassone A. Infection with chikungunya virus in Italy: an outbreak in a temperate region. Lancet. 2007;370:1840-1846.

Richardson J, Molina-Cruz A, Salazar MI, Black IV W. Quantitative analysis of dengue-2 virus RNA during the extrinsic incubation period in individual *Aedes aegypti*. American Journal of Tropical Medicine and Hygiene. 2006;74:132-141.

Riley JK, Takeda K, Akira S, Schreiber RD. Interleukin-10 receptor signaling through the Jak-STAT pathway: requirement for two distinct receptor-derived signals for anti-inflammatory action. Journal of Biological Chemistry. 1999;274:16513-16521.

Robin S, Ramful D, le Seach F, Jaffar-Bandjee MC, Rigou G, Alessandri JL. Neurologic manifestations of pediatric chikungunya infection. Journal of Child Neurology. 2008;23:1028-1035.

Robinson MC. An epidemic of virus disease in Southern Province, Tanganyika territory, in 1952-53. Transactions of the Royal Society of Tropical Medicine and Hygiene. 1955;49:28-32.

Ross RW. The Newala epidemic. III. The virus: isolation, pathogenic properties and relationship to the epidemic. Journal of Hygiene. 1956;54:177-191.

Rudd PA, Wilson J, Gardner J, Larcher T, Babarit C, Le TT, Anraku I, Kumagai Y, Loo Y-M, Gale Jr M, Akira S, Khromykh AA, Suhrbier A. Interferon response factors 3 and 7 protect against chikungunya virus hemorrhagic fever and shock. Journal of Virology. 2012;86:9888-9898.

Ryman KD, Gardner CL, Burke CW, Meier KC, Thompson JM, Klimstra WB. Heparan sulfate binding can contribute to the neurovirulence of neuroadapted and nonneuroadapted sindbis viruses. Journal of Virology. 2007a;81:3563-3573.

Ryman KD, Gardner CL, Meier KC, Biron CA, Johnston RE, Klimstra WB. Early restriction of alphavirus replication and dissemination contributes to age-dependent attenuation of systemic hyperinflammatory disease. Journal of General Virology. 2007b;88:518-529.

Ryman KD, Klimstra WB. Host responses to alphavirus infection. Immunological Reviews. 2008;225:27-45.

Ryman KD, Meier KC, Nangle EM, Ragsdale SL, Korneeva NL, Rhoads RE, MacDonald MR, Klimstra WB. Sindbis virus translation is inhibited by a PKR/RNase L-independent effector induced by alpha/beta interferon priming of dendritic cells. Journal of Virology. 2005;79:1487-1499.

Saha S, Rangarajan PN. Common host genes are activated in mouse brain by Japanese encephalitis and rabies viruses. Journal of General Virology. 2003;84:1729-1735.

Saijo K, Crotti A, Glass CK. Regulation of microglia activation and deactivation by nuclear receptors. Glia. 2013;16:104-111.

Sam I-C, AbuBakar S. Chikungunya virus infection. Medical Journal of Malaysia. 2006;61:264-269.

Sam I-C, Chan YF, Chan SY, Loong SK, Chin HK, Hooi PS, Ganeswrie R, AbuBakar S. Chikungunya virus of Asian and Central/East African genotypes in Malaysia. Journal of Clinical Virology. 2009;46:180-183.

Sam I-C, Loong SK, Michael JC, Chua CL, Sulaiman WYW, Vythilingam I, Chan SY, Chiam CW, Yeong YS, AbuBakar S, Chan YF. Genotypic and phenotypic characterization of chikungunya virus of different genotypes from Malaysia. PLoS ONE. 2012;7:e50476.

Samoilova EB, Horton JL, Chen Y. Acceleration of experimental autoimmune encephalomyelitis in interleukin-10-deficient mice: roles of interleukin-10 in disease progression and recovery. Cellular Immunology. 1998;188:118-124.

Samuel MA, Whitby K, Keller BC, Marri A, Barchet W, Williams BRG, Silverman RH, Gale Jr M, Diamond MS. PKR and RNase L contribute to protection against lethal West Nile virus infection by controlling early viral spread in the periphery and replication in neurons. Journal of Virology. 2006;80:7009-7019.

Scallan MF, Allsopp TE, Fazakerley JK. bcl-2 acts early to restrict Semliki Forest virus replication and delays virus-induced programmed cell death. Journal of Virology. 1997;71:1583-1590.

Schaible HG, von Banchet GS, Boettger MK, Bräuer R, Gajda M, Richter F, Hensellek S, Brenn D, Natura G. The role of proinflammatory cytokines in the generation and maintenance of joint pain. Annals of the New York Academy of Sciences. 2010;1193:60-69.

Schilte C, Couderc T, Chretien F, Sourisseau M, Gangneux N, Guivel-Benhassine F, Kraxner A, Tschopp J, Higgs S, Michault A, Arenzana-Seisdedos F, Colonna M, Peduto L, Schwartz O, Lecuit M, Albert ML. Type I IFN controls chikungunya virus via its action on nonhematopoietic cells. Journal of Experimental Medicine. 2010;207:429-442.

Schilte C, Staikovsky F, Couderc T, Madec Y, Carpentier F, Kassab S, Albert ML, Lecuit M, Michault A. Chikungunya virus-associated long-term arthralgia: a 36-month prospective longitudinal study. PLoS Neglected Tropical Diseases. 2013;7:e2137.

Schoggins JW, Rice CM. Interferon-stimulated genes and their antiviral effector functions. Current Opinion in Virology. 2011;1:519-525.

Schuffenecker I, Iteman I, Michault A, Murri S, Frangeul L, Vaney MC, Lavenir R, Pardigon N, Reynes JM, Pettinelli F, Biscornet L, Diancourt L, Michel S, Duquerroy S, Guigon G, Frenkiel MP, Bréhin AC, Cubito N, Desprès P, Kunst F, Rey FA, Zeller H, Brisse S. Genome microevolution of chikungunya viruses causing the Indian Ocean outbreak. PLoS Medicine. 2006;3:1058-1070.

Schwartz O, Albert ML. Biology and pathogenesis of chikungunya virus. Nature Reviews. 2010;8:491-500.

Sebastian MR, Lodha R, Kabra SK. Chikungunya infection in children. Indian Journal of Pediatrics. 2009;76:185-189.

Seymour RL, Bergren SLRNA, Plante KS, Weaver SC. The role of innate versus adaptive immune responses in a mouse model of o'nyong-nyong virus infection. American Journal of Tropical Medicine and Hygiene. 2013;88:1170-1179.

Sharma A, Bhattacharya B, Puri RK, Maheshwari RK. Venezuelan equine encephalitis virus infection causes modulation of inflammatory and immune response genes in mouse brain. BMC Genomics. 2008;9:1471-2164.

Sharma A, Maheshwari RK. Oligonucleotide array analysis of Toll-like receptors and associated signalling genes in Venezuelan equine encephalitis virus-infected mouse brain. Journal of General Virology. 2009;90:1836-1847.

Sharma S, Yang B, Xi X, Grotta JC, Aronowski J, Savitz SI. IL-10 directly protects cortical neurons by activating PI-3 kinase and STAT-3 pathways. Brain Research. 2011;1373:189-194.

Silverman RH. Viral encounters with 2',5'-oligoadenylate synthetase and RNase L during the interferon antiviral response. Journal of Virology. 2007;81:12720-12729.

Simizu B, Yamamoto K, Hashimoto K, Ogata T. Structural proteins of chikungunya virus. Journal of Virology. 1984;51:254-258.

Simon F, Javelle E, Oliver M, Leparc-Goffart I, Marimoutou C. Chikungunya virus infection. Current Infectious Disease Reports. 2011;13:218-228.

Singh SS, Manimunda SP, Sugunan AP, Sahina, Vijayachari P. Four cases of acute flaccid paralysis associated with chikungunya virus infection. Epidemiology and Infection. 2008;136:1277-1280.

Solignat M, Gay B, Higgs S, Briant L, Devaux C. Replication cycle of chikungunya: a re-emerging arbovirus. Virology. 2009;393:183-197.

Sorensen G, Medina S, Parchaliuk D, Phillipson C, Robertson C, Booth SA. Comprehensive transcriptional profiling of prion infection in mouse models reveals networks of responsive genes. BMC Genomics. 2008;9:114.

Sourisseau M, Schilte C, Casartelli N, Trouillet C, Guivel-Benhassine F, Rudnicka D, Sol-Foulon N, le Roux K, Prevost MC, Fsihi H, Frenkiel MP, Blanchet F, Afonso PV, Ceccaldi PE, Ozden S, Gessain A, Schuffenecker I, Verhasselt B, Zamborlini A, Saïb A, Rey FA, Arenzana-Seisdedos F, Desprès P, Michault A, Albert ML, Schwartz O. Characterization of reemerging chikungunya virus. PLoS Pathogens. 2007;3:e89.

Staikowsky F, Talarmin F, Grivard P, Souab A, Schuffenecker I, le Roux K, Lecuit M, Michault A. Prospective study of chikungunya virus acute infection in the Island of La Réunion during the 2005–2006 outbreak. PLoS ONE. 2009;4:e7603.

Steele KE, Twenhafel NA. Pathology of animal models of alphavirus encephalitis. Veterinary Pathology. 2010;47:790-805.

Strauss JH, Strauss EG. The alphaviruses: gene expression, replication, and evolution. Microbiological Reviews. 1994;58:491-562.

Suthar MS, Shabman R, Madric K, Lambeth C, Heise MT. Identification of adult mouse neurovirulence determinants of the Sindbis virus strain AR86. Journal of Virology. 2005;79:4219-4228.

Sweet MJ, Hume DA. CSF-1 as a regulator of macrophage activation. Archivum Immunologiae et Therapiae Experimentalis. 2003;51:169-177.

Szretter KJ, Daffis S, Patel J, Suthar MS, Klein RS, Gale Jr M, Diamond MS. The innate immune adaptor molecule MyD88 restricts West Nile virus replication and spread in neurons of the central nervous system. Journal of Virology. 2010;84:12125-12138.

Takeda K, Kaisho T, Akira S. Toll-like receptors. Annual Review of Immunology. 2003;21:335-376.

Tallóczy Z, Jiang W, Virgin IV HW, Leib DA, Scheuner D, Kaufman RJ, Eskelinen E-L, Levine B. Regulation of starvation- and virus-induced autophagy by the eIF2α kinase signaling pathway. Proceedings of the National Academy of Sciences. 2005;99:190-195.

Tarbatt CJ, Glasgow GM, Mooney DA, Sheahan BJ, Atkins GJ. Sequence analysis of the avirulent, demyelinating A7 strain of Semliki Forest virus. Journal of General Virology. 1997;78:1551-1557.

Taubitz W, Cramer JP, Kapaun A, Pfeffer M, Drosten C, Dobler G, Burchard GD, Löscher T. Chikungunya fever in travelers: clinical presentation and course. Clinical Infectious Diseases. 2007;45.

Taylor K, Kolokoltsova O, Patterson M, Poussard A, Smith J, Estes DM, Paessler S. Natural killer cell mediated pathogenesis determines outcome of central nervous system infection with Venezuelan equine encephalitis virus in C3H/HeN mice. Vaccine. 2012;30:4095-4105.

Teng T-S, Foo S-S, Simamarta D, Lum F-M, Teo T-H, Lulla A, Yeo NKW, Koh EGL, Chow A, Leo Y-S, Merits A, Chin K-C, Ng LFP. Viperin restricts chikungunya virus replication and pathology. Journal of Clinical Investigation. 2012;122:4447-4460.

Teo T-H, Her Z, Tan JJL, Lum F-M, Lee WWL, Chan Y-H, Ong R-Y, Kam Y-W, Leparc-Goffart I, Gallian P, Rénia L, de Lamballerie X, Ng LFP. Caribbean and La Réunion chikungunya virus isolates differ in their capacity to induce pro-inflammatory Th1 and NK cell responses and acute joint pathology. Journal of Virology. 2015;89:7955-7969.

Teo T-H, Lum F-M, Claser C, Lulla V, Lulla A, Merits A, Rénia L, Ng LFP. A pathogenic role for CD4+ T cells during chikungunya virus infection in mice. Journal of Immunology. 2013;190:259-269.

Thiberville SD, Moyen N, Dupuis-Maguiraga L, Nougairede A, Gould EA, Roques P, de Lamballerie X. Chikungunya fever: epidemiology, clinical syndrome, pathogenesis and therapy. Antiviral Research. 2013;99:345-370.

Thon-Hon VG, Denizot M, Li-Pat-Yuen G, Giry C, Jaffar-Bandjee M-C, Gasque P. Deciphering the differential response of two human fibroblast cell lines following chikungunya virus infection. Virology Journal. 2012;9:213.

Ting JPY, Duncan JA, Lei Y. How the noninflammasome NLRs function in the innate immune system. Science. 2010;327:286-290.

Tiwari M, Parida M, Santhosh SR, Khan M, Dash PK, Rao PVL. Assessment of immunogenic potential of Vero adapted formalin inactivated vaccine derived from novel ECSA genotype of chikungunya virus. Vaccine. 2009;27:2513-2522.

Tsetsarkin KA, Vanlandingham DL, McGee CE, Higgs S. A single mutation in chikungunya virus affects vector specificity and epidemic potential. PLoS Pathogens. 2007;3:1895-1906.

Tucker PC, Strauss EG, Kuhn RJ, Strauss JH, Griffin DE. Viral determinants of age-dependent virulence of Sindbis virus for mice. Journal of Virology. 1993;67:4605-4610.

Tuittila M, Hinkkanen AE. Amino acid mutations in the replicase protein nsP3 of Semliki Forest virus cumulatively affect neurovirulence. Journal of General Virology. 2003;84:1525-1533.

Tuittila M, Nygårdas P, Hinkkanen A. mRNA expression of proinflammatory cytokines in mouse CNS correlates with replication rate of Semliki Forest virus but not with the strain of viral proteins. Viral Immunology. 2004;17:287-297.

Tuittila MT, Santagati MG, Röyttä M, Määttä JA, Hinkkanen AE. Replicase complex genes of Semliki Forest virus confer lethal neurovirulence. Journal of Virology. 2000;74:4579-4589.

Ubol S, Tucker PC, Griffin DE, Hardwick JM. Neurovirulent strains of alphavirus induce apoptosis in bcl-2-expressing cells: role of a single amino acid change in the E2 glycoprotein. Proceedings of the National Academy of Sciences. 1994;91:5202-5206.

Valamparampil JJ, Chirakkarot S, Letha S, Jayakumar C, Gopinathan KM. Clinical profile of chikungunya in infants. Indian Journal of Pediatrics. 2009;76:151-155.

Van den Doel P, Volz A, Roose JM, Sewbalaksing VD, Pijlman GP, van Middelkoop I, Duiverman V, van de Wetering E, Sutter G, Osterhaus ADME, Martina BEE. Recombinant modified vaccinia virus Ankara expressing glycoprotein E2 of chikungunya virus protects AG129 mice against lethal challenge. PLoS Neglected Tropical Diseases. 2014;8:e3101.

Van de Veerdonk FL, Netea MG, Dinarello CA, Joosten LAB. Inflammasome activation and IL-1β and IL-18 processing during infection. Trends in Immunology. 2011;32:110-116.

Van Riel D, Verdijk R, Kuiken T. The olfactory nerve: a shortcut for influenza and other viral diseases into the central nervous system. Journal of Pathology. 2015;235:277-287.

Venter M, Myers TG, Wilson MA, Kindt TJ, Paweska JT, Burt FJ, Leman PA, Swanepoel R. Gene expression in mice infected with West Nile virus strains of different neurovirulence. Virology. 2005;342:119-140.

Vince JE, Wong WW-L, Gentle I, Lawlor KE, Allam R, O'Reilly L, Mason K, Gross O, Ma S, Guarda G, Anderton H, Castillo R, Häcker G, Silke J, Tschopp J. Inhibitor of apoptosis proteins limit RIP3 kinase-dependent interleukin-1 activation. Immunity. 2012;36:215-227.

Vitner EB, Salomon R, Farfel-Becker T, Meshcheriakova A, Ali M, Klein AD, Platt FM, Cox TM, Futerman AH. RIPK3 as a potential therapeutic target for Gaucher's disease. Nature Medicine. 2014;20:204-208.

Voss JE, Vaney MC, Duquerroy S, Vonrhein C, Girard-Blanc C, Crublet E, Thompson A, Bricogne G, Rey F. Glycoprotein organization of chikungunya virus particles revealed by X-ray crystallography. Nature. 2010;468:709-714.

Wallach D, Kovalenko A, Kang T-B. 'Necrosome'-induced inflammation: must cells die for it? Trends in Immunology. 2011;32:505-509.

Walsh CM, Edinger AL. The complex interplay between autophagy, apoptosis, and necrotic signals promotes T-cell homeostasis. Immunological Reviews. 2010;236:95-109.

Wang D, Suhrbier A, Penn-Nicholson A, Woraratanadharm J, Gardner J, Luo M, Le TT, Anraku I, Sakalian M, Einfeld D, Dong JY. A complex adenovirus vaccine against chikungunya virus provides complete protection against viraemia and arthritis. Vaccine. 2011;29:2803-2809.

Wang E, Volkova E, Adams AP, Forrester N, Xiao S-Y, Frolov I, Weaver SC. Chimeric alphavirus vaccine candidates for chikungunya. Vaccine. 2008;26:5030-5039.

Wang JQ, Jeelall YS, Ferguson LL, Horikawa K. Toll-like receptors and cancer: MYD88 mutation and inflammation. Frontiers in Immunology. 2014;5:367.

Wang Y, Tang X, Yu B, Gu Y, Yuan Y, Yao D, Ding F, Gu X. Gene network revealed involvements of Birc2, Birc3 and Tnfrsf1a in anti-apoptosis of injured peripheral nerves. PLoS ONE. 2012;7:e43436.

Wang Y-Q, Berezovska O, Fedoroff S. Expression of colony stimulating factor-1 receptor (CSF-1R) by CNS neurons in mice. Journal of Neuroscience Research. 1999;57:616-632.

Wang ZW, Sarmento L, Wang Y, Li X-Q, Dhingra V, Tseggai T, Jiang B, Fu ZF. Attenuated rabies virus activates, while pathogenic rabies virus evades, the host innate immune responses in the central nervous system. Journal of Virology. 2005;79:12554-12565.

Watanaveeradej V, Endy TP, Simasathien S, Kerdpanich A, Polprasert N, Aree C, Vaughn DW, Nisalak A. Transplacental chikungunya virus antibody kinetics, Thailand. Emerging Infectious Diseases. 2006;12:1770-1772.

Wauquier N, Becquart P, Nkoghe D, Padilla C, Ndjoyi-Mbiguino A, Leroy EM. The acute phase of chikungunya virus infection in humans is associated with strong innate immunity and T CD8 cell activation. Journal of Infectious Diseases. 2011;204:115-123.

Weaver SC. Arrival of chikungunya virus in the new world: prospects for spread and impact on public health. PLoS Neglected Tropical Diseases. 2014;8:e2921.

Weger-Lucarelli J, Chu H, Aliota MT, Partidos CD, Osorio JE. A novel MVA vectored chikungunya virus vaccine elicits protective immunity in mice. PLoS Neglected Tropical Diseases. 2014;8:e2970.

Wendt W, Lübbert H, Stichel CC. Upregulation of cathepsin S in the aging and pathological nervous system of mice. Brain Research. 2008;1232:7-20.

Werneke SW, Schilte C, Rohatgi A, Monte KJ, Michault A, Arenzana-Seisdedos F, Vanlandingham DL, Higgs S, Fontanet A, Albert ML, Lenschow DJ. ISG15 is critical in the control of chikungunya virus infection independent of UbE1L mediated conjugation. PLoS Pathogens. 2011;7:e1002322.

White A, Berman S, Lowenthal JP. Comparative immunogenicities of chikungunya vaccines propagated in monkey kidney monolayers and chick embryo suspension cultures. Applied and Environmental Microbiology. 1972;23:951-952.

White E. Autophagic cell death unraveled: pharmacological inhibition of apoptosis and autophagy enables necrosis. Autophagy. 2008;4:399-401.

White JD. Electron microscopy of chikungunya virus infection in the nervous system of suckling mice. Fort Detrick, Maryland: Department of the Army, USA. 1969. 10 p. Technical manuscript No.: 525.

White LK, Sali T, Alvarado D, Gatti E, Pierre P, Streblow D, de Filippis VR. Chikungunya virus induces IPS-1-dependent innate immune activation and protein kinase R-independent translational shutoff. Journal of Virology. 2011;85:606-620.

Wikan N, Sakoonwatanyoo P, Ubol S, Yoksan S, Smith DR. Chikungunya virus infection of cell lines: analysis of the East, Central and South African lineage. PLoS ONE. 2012;7:e31102.

Wong AH, Tam NW, Yang YL, Cuddihy AR, Li S, Kirchhoff S, Hauser H, Decker T, Koromilas AE. Physical association between STAT1 and the interferon-inducible protein kinase PKR and implications for interferon and double-stranded RNA signaling pathways. EMBO Journal. 1997;16:1291-1304.

Xin J, Wainwright DA, Mesnard NA, Serpe CJ, Sanders VM, Jones KJ. IL-10 within the CNS is necessary for CD4+ T cells to mediate neuroprotection. Brain, Behavior, and Immunity. 2011;25:820-829.

Yang Y, Ye J, Yang X, Jiang R, Chen H, Cao S. Japanese encephalitis virus infection induces changes of mRNA profile of mouse spleen and brain. Virology Journal. 2011;8:80.

Zhang G, Ghosh S. Toll-like receptor–mediated NF-κB activation: a phylogenetically conserved paradigm in innate immunity. Journal of Clinical Investigation. 2001;107:13-19.

Zhou Z, Peng X, Insolera R, Fink DJ, Mata M. Interleukin-10 provides direct trophic support to neurons. Journal of Neurochemistry. 2009;110:1617-1627.

Ziegler SA, Lu L, da Rosa APAT, Xiao SY, Tesh RB. An animal model for studying the pathogenesis of chikungunya virus infection. American Journal of Tropical Medicine and Hygiene. 2008;79:133-139.

LIST OF PUBLICATIONS AND PAPERS PRESENTED

Research articles related to thesis:

Chiam CW, Chan YF, Ong KC, Wong KT, Sam IC. Variation in neurovirulence and gene expression profiles in mice infected with different chikungunya genotypes. Journal of General Virology. 2015. doi: 10.1099/jgv.0.000263.

Chiam CW, Chan YF, Loong SK, Yong SSJ, Hooi PS, Sam IC. Real-time polymerase chain reaction for diagnosis and quantification of negative strand of chikungunya virus. Diagnostic Microbiology and Infectious Disease. 2013;77:133-137.

Other research articles:

Lani R, Hassandarvish P, **Chiam CW**, Moghaddam E, Chu JJH, Rausalu K, Merits A, Higgs S, Vanlandingham D, AbuBakar S, Keivan Z. Antiviral activity of silymarin against chikungunya virus. Scientific Reports. 2015;5:11421.

Sam IC, Loong SK, Michael JC, Chua CL, Wan Sulaiman WY, Vythilingam I, Chan SY, **Chiam CW**, Yeong YS, AbuBakar S, Chan YF. Genotypic and phenotypic characterization of chikungunya virus of different genotypes from Malaysia. PLoS One. 2012;7:e50476.

Chan YF, Wee KL, **Chiam CW**, Khor CS, Chan SY, Wan Nor Amalina WMZ, Sam IC. Comparative genetic analysis of VP4, VP1 and 3D gene regions of enterovirus 71 and coxsackievirus A16 circulating in Malaysia between 1997-2008. Tropical Biomedicine. 2012;29:451-466.

Chiam CW, Chan YF, Sam IC. 2010. Changing trends of genital herpes in Kuala Lumpur, Malaysia, 1982-2008. International Journal of STD & AIDS. 2010;21:450-451.

Poster presentations:

Chiam CW, Chan YF, Ong KC, Wong KT, Sam IC. Variation in neurovirulence and gene expression profiles in mice infected with different chikungunya genotypes. Chikungunya 2013. Langkawi, Malaysia, 28-30th October 2013.

Chiam CW, Loong SK, Yong SSJ, Chan YF, Sam IC. Development of strand-specific quantitative real-time polymerase chain reaction chikungunya virus. 9th Asian Pacific Congress of Medical Virology. Adelaide, Australia, 6-8th June 2012. (Awarded travel grant)

Chiam CW, Chan YF, Ong KC, Wong KT, Sam IC. Neurovirulence variation of different chikungunya virus genotypes in ICR newborn mice. 16th Biological Sciences Graduate Congress. National University of Singapore, Singapore, 12-14th December 2011. (Awarded travel grant)

Loong SK, Wan Sulaiman WY, **Chiam CW**, Chan YF, Sam IC. *In vitro* and *in vivo* chikungunya virus replication kinetics in *Aedes albopictus*. Colloquium on Updates on Dengue and Arbovirus Research in Malaysia. University of Malaya, Kuala Lumpur, Malaysia, 12-13th April 2010. (Third prize poster)

APPENDICES

Appendix 1: pGEM-T Vector

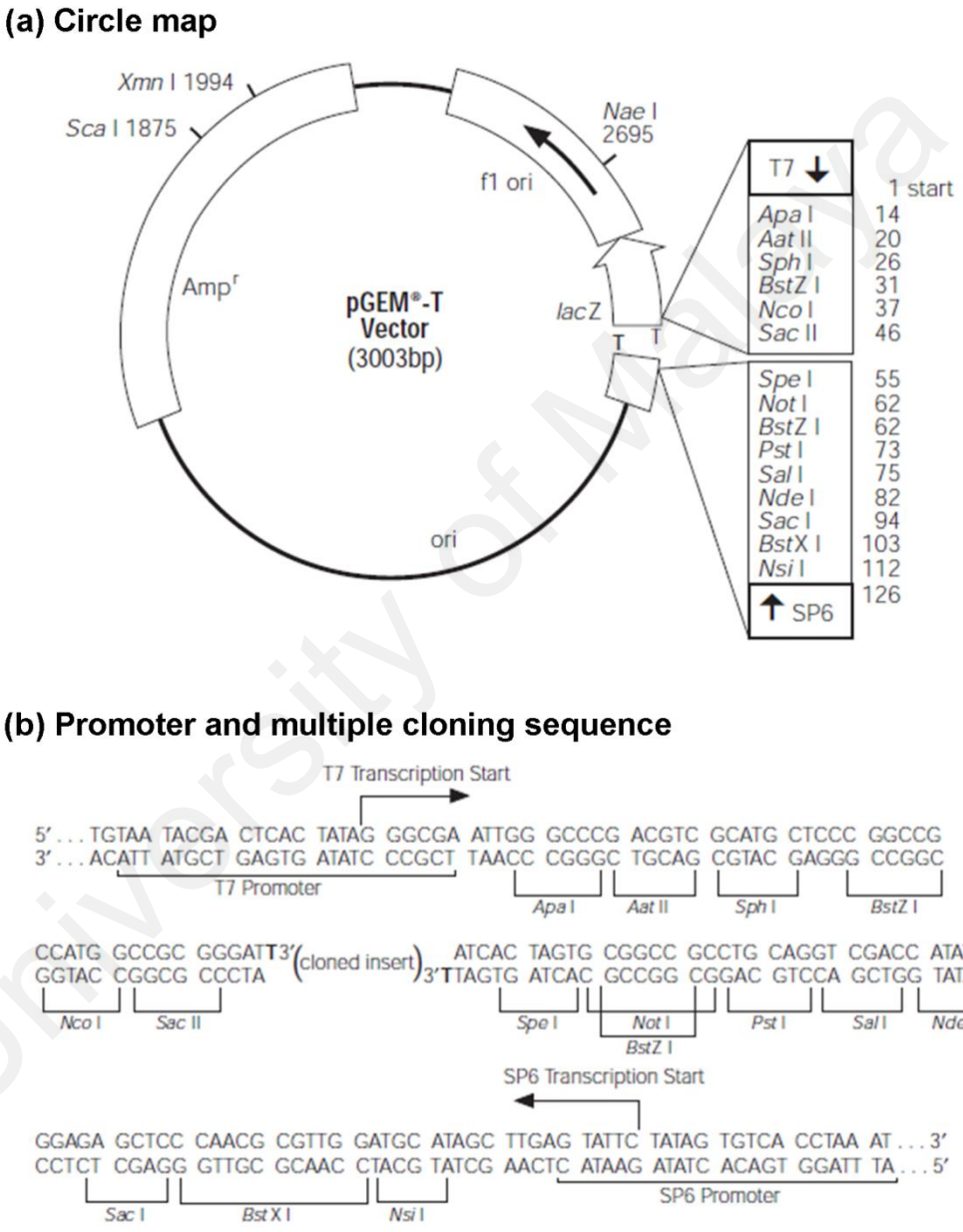

Appendix 2: Immune-related genes which were differentially expressed in the microarray analysis

GenBank accession no.	Gene symbol	Description	Fold change	
			MY/06/37348	MY/08/065
a) Upregulated at 1 dpi only in MY/06/37348-infected suckling mouse brains				
NM_009735	B2M	beta-2 microglobulin	3.771	2.180
NM_001001892	H2-K1	histocompatibility 2, K1, K region	5.432	2.058
NM_013819	H2-M3	histocompatibility 2, M region locus 3	5.547	2.981
NM_010392	H2-Q2	histocompatibility 2, Q region locus 2	4.766	3.018
NM_010393	H2-Q5	histocompatibility 2, Q region locus 5	4.998	2.490
NM_010394	H2-Q7	histocompatibility 2, Q region locus 7	4.502	1.675
NM_029803	IFI27L2A	interferon, alpha-inducible protein 27 like 2A	3.389	2.261
b) Upregulated at 1 dpi in both MY/06/37348- and MY/08/065-infected suckling mouse brains				
NM_013484	C2	complement component 2 (within H-2S)	2.557	1.638
NM_007609	*Casp4	caspase 4	6.496	4.705
NM_011331	CCL12	chemokine (C-C motif) ligand 12	15.247	8.658
NM_008176	CXCL1	chemokine (C-X-C motif) ligand 1	31.926	10.309
NM_021274	*CXCL10	chemokine (C-X-C motif) ligand 10	103.691	64.669
NM_172689	DDX58	DEAD (Asp-Glu-Ala-Asp) box polypeptide 58	30.937	20.474
NM_030150	*DHX58	DEXH (Asp-Glu-X-His) box polypeptide 58	7.934	6.216
NM_011163	*eIF2αK2	eukaryotic translation initiation factor 2-alpha kinase 2	11.509	8.081
NM_030711	ERAP1	endoplasmic reticulum aminopeptidase 1	3.745	2.495
NM_001039647	GDP11	guanylate-binding protein 11	6.772	6.332
NM_018734	GDP3	guanylate binding protein 3	20.631	14.318
NM_194336	GDP6	guanylate binding protein 6	18.168	9.993
NM_145545	GDP7	guanylate binding protein 6	19.457	13.287
NM_172777	GDP9	guanylate-binding protein 9	4.561	3.319
NM_010395	H2-T10	histocompatibility 2, T region locus 10	9.696	6.33
NM_010399	H2-T9	histocompatibility 2, T region locus 9	6.261	6.364
NM_008329	IFI204	interferon activated gene 204	9.01	5.681
BC010546	IFI204	interferon activated gene 204	11.665	7.076
NM_008330	IFI47	interferon gamma inducible protein 47	16.484	11.932
NM_027835	IFIH1	interferon induced with helicase C domain 1	20.755	11.809
NM_016850	IRF7	interferon regulatory factor 7	13.812	10.448
NM_001159417	*IRF9	interferon regulatory factor 9	6.792	6.595
NM_008326	*IRGM1	immunity-related GTPase family M member 1	19.151	15.339
NM_015783	*ISG5	ISG15 ubiquitin-like modifier	20.186	14.234
NM_001025208	LOC547349	MHC class I family member	6.111	5.881
NM_010846	Mx1	myxovirus (influenza virus) resistance 1	34.187	22.629
NM_013606	Mx2	myxovirus (influenza virus) resistance 2	44.688	34.317
NM_145211	OAS1A	2'-5' oligoadenylate synthetase 1A	16.932	10.966
NM_001083925	OAS1B	2'-5' oligoadenylate synthetase 1B	7.849	6.11
NM_033541	OAS1C	2'-5' oligoadenylate synthetase 1C	5.007	4.466
NM_145153	OAS1F	2'-5' oligoadenylate synthetase 1F	12.789	9.252
NM_145227	*OAS2	2'-5' oligoadenylate synthetase 2	10.423	66.926
NM_145209	OASL1	2'-5' oligoadenylate synthetase-like 1	21.744	15.584
NM_011854	OASL2	2'-5' oligoadenylate synthetase-like 2	44.423	26.156
NM_178087	PML	promyelocytic leukemia	3.248	2.39
NM_011190	PSME2	proteasome activator complex subunit 2 (Proteasome activator 28-beta subunit) (PA28beta)	2.933	2.215
NM_021384	RSAD2	radical S-adenosyl methionine domain containing 2	58.206	31.339
NM_018851	SAMHD1	SAM domain and HD domain, 1	2.923	2.393
NM_009251	SERPINA3G	serine (or cysteine) peptidase inhibitor, clade A, member 3G	11.855	9.433
NM_025858	Shisa5	shisa homolog 5 (Xenopus laevis)	3.247	2.753
NM_175397	Sp110	Sp110 nuclear body protein	6.079	5.724
NM_001025313	TAPBP	TAP binding protein	4.869	3.395
NM_001145164	TGTP2	T-cell specific GTPase 2; T-cell specific GTPase	27.242	19.666
NM_126166	*TLR3	toll-like receptor 3	29.704	21.762
NM_009425	TNFSF10	tumor necrosis factor (ligand) superfamily, member 10	10.296	10.281
NM_023738	UBA7	ubiquitin-activating enzyme E1-like	6.265	5.178
NM_019949	UBE2L6	ubiquitin-conjugating enzyme E2L 6	3.544	2.771
NM_011909	USP18	ubiquitin specific peptidase 18	50.544	39.06

GenBank accession no.	Gene symbol	Description	Fold change	
			MY/06/37348	MY/08/065
NM_001037713	*XAF1	XIAP associated factor 1	12.21	8.31
NM_028864	ZC3HAV1	zinc finger CCCH type, antiviral 1	9.831	9.063
c) Upregulated at 6 dpi only in MY/08/065-infected suckling mouse brains				
NM_007913	*EGR1	early growth response 1	1.248	3.591
NM_007987	*Fas	Fas (TNF receptor superfamily member 6)	2.811	8.359
d) Upregulated at 6 dpi in both MY/06/37348- and MY/08/065-infected suckling mouse brains				
NM_012054	AOAH	acyloxyacyl hydrolase	4.25	5.277
NM_031159	APOBEC1	apolipoprotein B mRNA editing enzyme, catalytic polypeptide 1	6.707	8.89
NM_009735	B2M	beta-2 microglobulin	12.031	11.952
NM_007535	*BCL-2A1c	B-cell leukemia/lymphoma 2 related protein A1c	6.272	14.574
NM_007536	*BCL-2A1d	B-cell leukemia/lymphoma 2 related protein A1d	7.256	16.162
NM_007464	*BIRC3	baculoviral IAP repeat-containing 3	3.432	5.282
NM_033601	BLC3	B-cell leukemia/lymphoma 3	3.852	8.699
NM_007572	C1qA	complement component 1, q subcomponent, alpha polypeptide	3.159	3.621
NM_009777	C1qB	complement component 1, q subcomponent, beta polypeptide	2.378	3.078
NM_007574	C1qC	complement component 1, q subcomponent, C chain	3.014	4.075
NM_013484	C2	complement component 2 (within H-2S)	6.28	7.055
NM_009778	C3	complement component 3	5.78	7.016
NM_009780	C4B	complement component 4B (Childo blood group)	4.49	5.014
NM_009807	*Casp1	caspase 1	3.761	5.592
NM_007609	*Casp4	caspase 4	10.485	20.935
NM_013653	*CCL5	chemokine (C-C motif) ligand 5	128.077	217.76
NM_021443	CCL8	chemokine (C-C motif) ligand 8	19.3	66.074
NM_145634	CD300LF	CD300 antigen like family member F	76.726	235.849
NM_001169153	CD300LF	CD300 antigen like family member F	39.437	115.444
NM_007645	CD37	CD37 antigen	1.815	1.798
NM_013487	CD3D	CD3 antigen, delta polypeptide	9.532	31.056
NM_009850	CD3G	CD3 antigen, gamma polypeptide	6.654	22.057
NM_009851	CD44	CD44 antigen	3.042	3.865
NM_007649	CD48	CD48 antigen	4.7	6.642
NM_019388	CD86	CD86 antigen	1.797	3.05
NM_001111099	CDKN1A	cyclin-dependent kinase inhibitor 1A (P21)	2.622	1.834
NM_008198	CFB	complement factor B	80.031	133.782
NM_009805	*CFLAR	Casp8 and FADD-like apoptosis regulator	1.461	2.063
NM_019948	CLEC4e	C-type lectin domain family 4, member e	25.817	79.679
NM_020001	CLEC4n	C-type lectin domain family 4, member n	3.247	5.112
NM_001113530	*CSF1	colony stimulating factor 1 (macrophage)	2.105	2.166
NM_018866	CXCL13	chemokine (C-X-C motif) ligand 13	38.342	52.631
NM_008599	CXCL9	chemokine (C-X-C motif) ligand 9	48.038	172.466
NM_007829	DAXX	Fas death domain-associated protein	1.35	2.101
NM_172689	DDX58	DEAD (Asp-Glu-Ala-Asp) box polypeptide 58	10.577	14.348
NM_030150	*DHX58	DEXH (Asp-Glu-X-His) box polypeptide 58	18.348	37.789
NM_010070	DOK1	docking protein 1	2.303	2.543
NM_011163	*eIF2αK2	eukaryotic translation initiation factor 2-alpha kinase 2	8.028	13.772
NM_030711	ERAP1	endoplasmic reticulum aminopeptidase 1	2.833	4.98
NM_010185	FCER1G	Fc receptor, IgE, high affinity I, gamma polypeptide	3.171	4.374
NM_010186	FCGR1	Fc receptor, IgG, high affinity I	2.315	2.918
NM_010208	FGR	Gardner-Rasheed feline sarcoma viral (Fgr) oncogene homolog	3.969	5.818
NM_011815	FYB	FYN binding protein	5.242	6.592
NM_011817	GADD45g	growth arrest and DNA-damage-inducible 45 gamma	1.511	2.043
NM_001039647	Gbp11	guanylate-binding protein 11	3.927	12.098
NM_010260	GBP2	guanylate binding protein 2	17.488	45.647
NM_018734	GBP3	guanylate binding protein 3	23.755	39.075
NM_145545	GBP6	guanylate binding protein 6	8.446	19.008
NM_029509	Gbp8	guanylate-binding protein 8	22.545	68.784
NM_172777	GBP9	guanylate-binding protein 9	5.701	12.52
NM_008102	GCH1	GTP cyclohydrolase 1	2.7	4.527
NM_010275	GDNF	glial cell line derived neurotrophic factor	1.464	3.133
NM_194336	GDP6	guanylate binding protein 6	8.446	19.008
NM_008175	Grn	granulin	2.214	2.345
NM_010370	GzmA	granzyme A	12.78	37.424

GenBank accession no.	Gene symbol	Description	Fold change	
			MY/06/37348	MY/08/065
NM_013542	GzmB	granzyme B	9.113	46.316
NM_207105	H2-AB1	histocompatibility 2, class II antigen A, beta 1	7.688	14.079
AY533667	H2-Bl	histocompatibility 2, blastocyst; predicted gene 8810	14.656	15.946
NM_010380	H2-D1	histocompatibility 2, D region locus 1	16.516	9.385
NM_010382	H2-EB1	histocompatibility 2, class II antigen E beta	3.36	9.716
NM_001001892	H2-K1	histocompatibility 2, K1	19.369	16.175
NM_177635	H2-M11	histocompatibility 2, M region locus 11	8.902	5.3
NM_013819	H2-M3	histocompatibility 2, M region locus 3	8.548	10.273
NM_008206	H2-OA	histocompatibility 2, O region alpha locus	4.062	4.016
NM_010391	*H2-Q10	histocompatibility 2, Q region locus 10	13.38	12.599
NM_010392	H2-Q2	histocompatibility 2, Q region locus 2	17.637	13.644
NM_010393	H2-Q5	histocompatibility 2, Q region locus 5	18.268	12.309
NM_207648	H2-Q6	histocompatibility 2, Q region locus 6	21.311	14.145
NM_010394	H2-Q7	histocompatibility 2, Q region locus 7	17.772	10.768
NM_023124	H2-Q8	histocompatibility 2, Q region locus 8	18.608	17.401
NM_010395	H2-T10	histocompatibility 2, T region locus 10	11.41	13.613
NM_010398	H2-T23	histocompatibility 2, T region locus 23	16.428	17.736
NM_010399	H2-T9	histocompatibility 2, T region locus 9	8.689	15.85
NM_001172117	HCK	hemopoietic cell kinase	3.038	3.607
NM_008225	HCLS1	hematopoietic cell specific Lyn substrate 1	4.12	4.393
NM_010493	*ICAM1	intercellular adhesion molecule 1	5.331	8.601
BC010546	IFI204	interferon activated gene 204	48.522	104.249
NM_008329	IFI204	interferon activated gene 204	48.522	104.2486
NM_029803	IFI27L2A	interferon, alpha-inducible protein 27 like 2A	67.907	65.585
NM_008330	IFI47	interferon gamma inducible protein 47	27.657	72.721
NM_027835	IFIH1	interferon induced with helicase C domain 1	16.437	22.895
NM_025378	IFITM3	interferon induced transmembrane protein 3	10.097	12.577
NM_010510	IFNB1	interferon beta 1, fibroblast	20.071	61.489
NM_010531	*IL-18BP	interleukin 18 binding protein	3.105	5.207
NM_008368	IL-2RB	interleukin 2 receptor, beta chain	2.813	6.571
NM_008390	*IRF1	interferon regulatory factor 1	66.596	17.149
NM_016850	IRF7	interferon regulatory factor 7	129.024	143.179
NM_008320	IRF8	interferon regulatory factor 8	3.584	6.973
NM_001159417	*IRF9	interferon regulatory factor 9	6.303	8.52
NM_008326	*IRGM1	immunity-related GTPase family M member 1	18.349	34.788
NM_015783	*ISG15	ISG15 ubiquitin-like modifier	94.187	122.446
NM_008400	ItgAL	integrin alpha L	3.464	4.047
NM_008404	ItgB2	integrin beta 2	3.5	5.02
NM_183390	Klhl6	kelch-like 6 (Drosophila)	2.139	1.975
NM_020044	LAT2	linker for activation of T cells family, member 2	2.939	4.613
NM_008879	LCP1	lymphocyte cytosolic protein 1	3.656	6.513
NM_011095	LILRB3	leukocyte immunoglobulin-like receptor, subfamily B (with TM and ITIM domains), member 3	13.319	27.97
NM_013532	LILRB4	leukocyte immunoglobulin-like receptor, subfamily B, member 4	16.853	40.571
NM_001025208	LOC547349	MHC class I family member	10.299	24.222
NM_019391	LSP1	lymphocyte specific 1	2.574	3.362
NM_010734	LST1	leukocyte specific transcript 1	2.215	2.28
NM_001111096	LYN	Yamaguchi sarcoma viral (v-yes-1) oncogene homolog	1.98	2.32
NM_013590	Lyz1	lysozyme 1	4.148	5.938
NM_017372	Lyz2	lysozyme 2	5.406	5.614
NM_010846	Mx1	myxovirus (influenza virus) resistance 1	101.089	259.456
NM_013606	Mx2	myxovirus (influenza virus) resistance 2	28.229	43.492
NM_010851	*MyD88	myeloid differentiation primary response gene 88	2.477	3.753
NM_053214	Myo1F	myosin IF	4.772	3.479
NM_010872	*NAIP2	NLR family, apoptosis inhibitory protein 2	5.93	7.182
NM_010871	NAIP6	NLR family, apoptosis inhibitory protein 4; NLR family, apoptosis inhibitory protein 7; NLR family, apoptosis inhibitory protein 1; baculoviral IAP repeat-containing 1f	2.339	3.264
NM_010876	NCF1	neutrophil cytosolic factor 1	2.933	4.503
NM_028728	NFAM1	Nfat activating molecule with ITAM motif 1	2.148	2.603
NM_019408	*NF-κB2	nuclear factor of kappa light polypeptide gene enhancer in B-cells 2	1.829	2.992
NM_010907	NF-κBIA	nuclear factor of kappa light polypeptide gene enhancer in B-cells inhibitor, alpha	1.311	2.074
NM_181547	NOSTRIN	nitric oxide synthase trafficker	1.836	2.214

GenBank accession no.	Gene symbol	Description	Fold change	
			MY/06/37348	MY/08/065
NM_145211	OAS1A	2'-5' oligoadenylate synthetase 1A	92.221	105.141
NM_001083925	OAS1B	2'-5' oligoadenylate synthetase 1B	3.834	6.767
NM_033541	OAS1C	2'-5' oligoadenylate synthetase 1C	3.317	4.022
NM_145153	OAS1F	2'-5' oligoadenylate synthetase 1F	58.192	78.861
NM_145227	*OAS2	2'-5' oligoadenylate synthetase 2	43.251	45.348
NM_145226	OAS3	2'-5' oligoadenylate synthetase 3	13.677	18.007
NM_145209	OASL1	2'-5' oligoadenylate synthetase-like 1	162.122	303.328
NM_011854	OASL2	2'-5' oligoadenylate synthetase-like 2	142.191	186.725
NM_172285	PLCG2	phospholipase C, gamma 2	2.175	2.154
NM_019549	Plek	pleckstrin	1.946	3.027
NM_021451	PMAIP1	phorbol-12-myristate-13-acetate-induced protein 1	2.272	3.145
NM_178087	PmL	promyelocytic leukemia	1.995	2.459
NM_010724	PSMB8	proteasome (prosome, macropain) subunit, beta type 8 (large multifunctional peptidase 7)	29.538	46.781
NM_013585	PSMB9	proteasome (prosome, macropain) subunit, beta type 9 (large multifunctional peptidase 2)	26.25	37.818
NM_011190	PSME2	proteasome activator complex subunit 2 (Proteasome activator 28-beta subunit) (PA28beta)	2.422	3.23
NM_001077705	PTPN6	protein tyrosine phosphatase, non-receptor type 6	3.67	5.669
NM_001111316	PTPRC	protein tyrosine phosphatase, receptor type, C	3.512	4.806
NM_023258	*PYCARD	PYD and CARD domain containing	2.579	3.604
NM_009008	RAC2	RAS-related C3 botulinum substrate 2	3.398	4.487
NM_009046	RELB	avian reticuloendotheliosis viral (v-rel) oncogene related B	1.307	2.32
NM_019955	*RIPK3	receptor-interacting serine-threonine kinase 3	3.356	4.352
NM_021384	RSAD2	radical S-adenosyl methionine domain containing 2	13.85	28.601
NM_001111022	RUNX1	runt related transcription factor 1	3.655	5.767
NM_010101	S1PR3	sphingosine-1-phosphate receptor 3	1.454	2.259
NM_018851	SAMHD1	SAM domain and HD domain, 1	3.295	6.006
NM_028773	SASH3	SAM and SH3 domain containing 3	3.211	3.471
NM_009121	SAT1	spermidine/spermine N1-acetyl transferase 1	1.639	2.523
NM_009251	SERPINA3G	serine (or cysteine) peptidase inhibitor, clade A, member 3G	28.009	70.06
NM_008871	SERPINE1	serine (or cysteine) peptidase inhibitor, clade E, member 1	2.729	6.821
NM_025858	Shisa5	shisa homolog 5 (Xenopus laevis)	3.36	3.883
NM_001002898	SIRPB1A	signal-regulatory protein beta 1A	16.335	50.915
NM_013612	*SlC11A1	solute carrier family 11 (proton-coupled divalent metal ion transporters), member 1	7.331	8.1
NM_011407	Slfn1	schlafen 1	13.338	25.171
NM_011408	Slfn2	schlafen 2	26.113	57.281
NM_009896	SOCS1	suppressor of cytokine signaling 1	2.449	6.181
NM_007707	SOCS3	suppressor of cytokine signaling 3	1.685	3.745
NM_175397	Sp110	Sp110 nuclear body protein	8.781	16.36
NM_009259	Spn	sialophorin	3.127	3.828
NM_013683	TAP1	transporter 1, ATP-binding cassette, sub-family B (MDR/TAP)	18.971	18.652
NM_001025313	TAPBP	TAP binding protein	4.198	7.316
NM_145391	TAPBPL	TAP binding protein-like	2.513	3.721
NM_009371	TGFBR2	transforming growth factor, beta receptor II	2.604	2.781
NM_011579	TGTP1	T-cell specific GTPase 1; T-cell specific GTPase	4.29	7.015
NM_205820	TLR13	toll-like receptor 13	3.142	3.961
NM_011905	TLR2	toll-like receptor 2	6.94	11.473
NM_011604	TLR6	toll-like receptor 6	2.496	3.457
NM_133211	*TLR7	toll-like receptor 7	2.788	3.592
NM_028261	TMEM173	transmembrane protein 173	2.192	3.478
NM_013693	*TNF	tumor necrosis factor	8.546	14.813
NM_009397	TNFAIP3	tumor necrosis factor, alpha-induced protein 3	1.846	3.047
NM_027206	TNFAIP8L2	tumor necrosis factor, alpha-induced protein 8-like 2	3.127	3.648
NM_011609	TNFRSF1A	tumor necrosis factor receptor superfamily, member 1a	1.731	2.414
NM_011610	TNFRSF1B	tumor necrosis factor receptor superfamily, member 1b	3.016	4.428
NM_023738	UBA7	ubiquitin-like modifier activating enzyme 7	10.1072	12.778
NM_019949	UBE2L6	ubiquitin-conjugating enzyme E2L 6	9.406	11.282
NM_019449	Unc93B1	unc-93 homolog B1 (C. elegans)	2.452	2.963
NM_011909	USP18	ubiquitin specific peptidase 18	123.816	209.737
NM_011691	Vav1	vav 1 oncogene	3.274	4.304
NM_011693	VCAM1	vascular cell adhesion molecule 1	2.121	2.192

GenBank accession no.	Gene symbol	Description	Fold change	
			MY/06/37348	MY/08/065
NM_009515	WAS	Wiskott-Aldrich syndrome homolog (human)	2.08	2.848
NM_001037713	*XAF1	XIAP associated factor 1	42.756	58.171
NM_028864	ZC3HAV1	zinc finger CCCH type, antiviral 1	16.263	22.759

* indicates genes selected for validation by qRT-PCR